CORROSION FATIGUE OF WELDED JOINTS

Papers presented at the Conference
on 'Steels in Marine Structures'
Delft, Holland 1987

FATIGUE PAR CORROSION DE JOINTS SOUDÉS

Documents présentés à la Conférence
'Steels in Marine Structures' qui s'est tenue à
Delft, Hollande, en 1987

The research work described here
was funded by the Interdepartmental
Panel on Energy Research and Development

Les travaux de recherche présentés dans ce rapport
ont été subventionnés par le Comité interministériel
de recherche et développement énergétiques

99pp

CANMET Special Publication
SP 87-12E

Publication spéciale de CANMET
SP 87-12E

Available in Canada through

Associated Bookstores
and other booksellers

or by mail from

Canadian Government Publishing Centre
Supply and Services Canada
Ottawa, Canada K1A 0S9

Catalogue No. M38-15/87-12E
ISBN 0-660-12895-0

Price subject to change without notice

FOREWORD

When the Department initiated its Offshore Steels program in 1983, funded by the Federal Panel on Energy Research and Development, twin objectives were set: to develop, with industry, the technology to supply steel, fabricate platforms and caissons, and inspect and maintain rigs; and to document the protection technology, in terms of design and performance guidelines, rules and specifications, which would ensure the safe operation and performance of rigs in the aggressive environments of the East Coast and the Arctic. The main component of the protection technology program is the study of fatigue crack initiation and growth from the toes of welds, directed at the translation of experimentally measured effects of environment and geometry into a complete fracture mechanics treatment of the fatigue process. This compendium of papers marks the extensive progress of the team of industry, government and university researchers towards that goal, and constitutes the Canadian contribution to the 1987 "Steels in Marine Structures" Conference sponsored by our colleagues of the European Coal and Steel Community and of the United Kingdom Offshore Steels Project. The cooperation of those trans–Atlantic researchers, formalized by a Canada–ECSC letter of agreement, is gratefully acknowledged.

AVANT–PROPOS

Lorsque le Ministère a instauré le Programme canadien de recherche sur les aciers destinés à des ouvrages offshore en 1983, subventionné par le groupe fédéral de Recherche et Développement de l'Énergie, deux objectifs ont été définis: développer, avec l'industrie, la technologie pour produire l'acier, construire les plates–formes et les caissons, entretenir et inspecter les installations; et établir les données de base d'une technologie de protection, en termes de design et lignes directrices de performance, de règles et spécifications, pour s'assurer de la sécurité d'opération et du rendement adéquat des installations dans les environnements agressifs de la côte Est et de l'Arctique. L'étude de l'initiation et de la croissance des fissures en fatigue dans les cordons de soudure constitue l'élément principal de l'établissement des données technologiques pour la protection. Cette étude traduit les observations expérimentales de l'effet de l'environnement et de la géométrie mécanique de la rupture. Ce recueil de publications indique la progression considérable du groupe de chercheurs de l'industrie, du gouvernement et des universités vers ce but, et constitue la contribution canadienne à la conférence de 1987 "L'Acier dans les Structures Marines", commandité par nos collègues européens de la Communauté Européenne du Charbon et l' "Offshore Steel Project" du Royaume–Uni. Nous remercions sincèrement de leur coopération, officialisée par un accord Canada–CECA, ces chercheurs outre–Atlantique.

TABLE OF CONTENTS

TABLE DES MATIÈRES

AN OVERVIEW OF THE NATIONAL CANADIAN OFFSHORE STEELS RESEARCH PROGRAM

GRANDES LIGNES DU PROGRAMME NATIONAL DE RECHERCHE SUR LES ACIERS DESTINÉS À DES OUVRAGES OFFSHORES

GRANDES LIGNES DU PROGRAMME NATIONAL DE RECHERCHE SUR LES ACIERS DESTINÉS À DES OUVRAGES OFFSHORES

R. Thomson et W. Tyson

Laboratoires de recherche en métallurgie physique
Centre canadien de la technologie des minéraux et de l'énergie
Ministère de l'Énergie, des Mines et des Ressources
Ottawa (Ontario)

RÉSUMÉ

Le Programme canadien de recherche sur les aciers destinés à des ouvrages offshore est relativement récent. Il englobe l'approvisionnement en acier, la fabrication de l'acier et l'évaluation de sa ténacité et de son comportement en fatigue. Il touche également l'élaboration des normes de ténacité en vue de normaliser la fabrication des aciers devant être utilisés dans des températures pouvant atteindre −30 °C dans l'Est canadien et −50 °C dans l'Arctique. Le rapport donne un aperçu des recherches relatives aux effets de la microstructure sur la résistance à la rupture des soudures et des zones affectées par la chaleur. Les résultats des projets portant sur la fatigue–corrosion sont présentés avec une attention spéciale à l'effet correctif limité de la protection cathodique, aux prédictions de l'effet de l'épaisseur des sections à partir d'essais menés sur des joints soudés, et à la modélisation de la forme de croissance des fissures. Le rapport fait état des recherches en cours sur les joints tubulaires rigides et les joints tuyau–plaque simulant les joints tubulaires, et donne un aperçu des activités futures du programme de recherche.

AN OVERVIEW OF THE NATIONAL CANADIAN OFFSHORE STEELS RESEARCH PROGRAMME

R. THOMSON AND W. TYSON

Physical Metallurgy Research Laboratories
Canada Centre for Mineral and Energy Technology
Dept. of Energy, Mines and Resources
Ottawa, Ontario

ABSTRACT

The offshore steels programme in Canada is of fairly recent origin, and includes steel supply, fabrication, fatigue and toughness evaluation and standards formulation for design temperatures of -30°C in Eastern Canada and -50°C in the Arctic. Work on the contribution of microstructure to the fracture toughness of HAZ and weld metal is described. The results of corrosion fatigue projects are reviewed, with attention being drawn specifically to the limited corrective effect of cathodic protection, and the prediction of the section-thickness effect by experiments on plate welded joints, and modelling crack growth shape. Ongoing work on stiffened tubulars and pipe-to-plate joints (simulating tubulars) is referenced, and the thrust of future programme activities mentioned.

1. INTRODUCTION

Canada's two major offshore oil and gas fields present unique environmental conditions which affect the design, materials selection, fabrication and inspection of marine structures such as platforms, undersea pipelines, icebreakers etc [1]. In the Beaufort Sea and Arctic Islands fields, bottom-founded rigs and caissons operate at design temperatures of -45° to -50°C, and are subject to large, fairly static loads from current- and storm-driven ice packs. Of somewhat greater relevance to this forum, the Hibernia and Scotian Shelf fields on Canada's East Coast present North Atlantic marine conditions similar, but not identical, to the relatively well-known environment of the North Sea. The fixed and semi-submersible production platforms on the East Coast will experience a different wave climate [2,3], and air design temperatures 10 to 20 Celcius degrees colder than the -10°C level used in North Sea practice; and of course the presence of icebergs requires the consideration of impact and/or avoidance for platforms, and of the sea-bed scouring hazard for undersea pipelines.

To address some of the materials problems engendered by these severe conditions, a programme of research and development was initiated in 1981 by the Department of Energy, Mines and Resources, knitting together the resources of Canadian industry, universities, and Federal government laboratories [4] in a series of fully funded and cost-shared contracts. The twin objectives of the programme are to ensure that appropriate regulations, standards and design data are generated to govern the selection and performance of welded steel structures; and to simultaneously equip Canadian industry with the technology base needed to maximise its share of the material supply aspects of offshore resource development.

In moving toward these objectives, the specific problems addressed to this point, and reviewed briefly here, are related to East coast applications (design temperatures between -20°C and -30°C). The span of activities ranges from the supply of offshore grades of steel plate from Canadian mills, with the attendant considerations of cleanliness and HAZ toughness; through weld process and consumable selection; corrosion fatigue performance; to a consideration of a probabilistic approach to fracture control. These main programme thrusts are summarised and referenced in Table 1 with selected areas being detailed below.

2. WELDING TECHNOLOGY AND FRACTURE

Given the lower service temperatures found in Canada, assurance of adequate toughness after welding receives due attention in the national programme. Much effort has been focussed on the measurement of the fracture initiation resistance of weldments (HAZ and weld metal) and its dependence on weld process, heat input, and microstructure (notably inclusion size distribution). Support of weld process development has led to an automated FCAW system for welding tubulars [10], and a promising assessment of pulsed GMAW of thick section 350 MPa offshore steel grades [11]. The advantages of lower heat

input and elimination of lack of fusion defects in the pulsed system may be further enhanced by ongoing work aimed at modifying weldment properties through optimisation of gas compositional variants.

The ability of commercial consumables for the SMAW, FCAW and SAW welding processes to deliver adequate fracture toughness in the weldment has been examined in detail [12]. 16 FCAW, 20 SMAW and 12 SAW consumables have been evaluated by full thickness (20 mm) CTOD tests at -10° and -30°C. A Charpy transition curve was also developed for each weldment, permitting the interim Charpy/CTOD correlation depicted in Figure 1. About three quarters of the SMAW electrodes showed poor toughness performance in both Charpy and CTOD tests and would not be acceptable for offshore structures experiencing -30°C. The remaining SMAW consumables had marginal performance relative to the proposed CTOD value for the 20 mm specimen thickness. Similar conclusions were reached for the FCAW consumables. There were, however, several SAW wire-flux combinations which gave good Charpy and CTOD values at -30°C. This observation is ascribed to improvements in weld cleanliness, i.e. inclusion type, size distribution, and volume fraction [13,16]. Current work has linked cleavage initiation sites to weld metal inclusions of 1μ m or greater, and has prompted closer attention to weld pool deoxidation and arc atmosphere control.

The interpretation of weld toughness and microstructure after post-weld heat treatment has produced, thus far, a less clear picture [17]. C-Mn and C-Mn-Ni SMAW welds have been evaluated by both Charpy and CTOD testing. While the C-Mn weldment response to PWHT is predictably acceptable, giving increased fracture initiation toughness, the presence of Ni produces some anomalous effects believed to be related to retained MA phase, resulting in larger carbide particles (Fig. 2) which may themselves act as cleavage initiation sites. Current work is exploring this area further by varying N_i content in the weld metal and heat input to alter the retained MA volume fraction.

While the work referenced above has concentrated on the resistance of plate, HAZ and weld metal to crack initiation, one of the key problem areas being addressed in the Canadian programme is that of specifying fracture toughness evaluation methodology for low design temperatures [18], and developing standards for materials selection and fabrication [19,20]. It has been deemed appropriate at this time to draft specific toughness requirements for highly stressed and critical members for design temperatures no lower than -30°C (i.e. East coast applications), thus permitting a conservative extrapolation of test procedures and acceptance levels from the well documented history of North Sea experience. The treatment of the -30°C to -50°C regime remains sub judice, and will require a greater elaboration of the relationships between small scale Charpy and CTOD results and the results of dynamic tear and wide plate testing [21]. Experience with structures existing in the Arctic will also be used. Throughout these studies, the problem of variability of toughness test results and its relation to defect population, inclusion size distribution and local brittle zones, has been given some attention. A weakest-link model of cleavage fracture has been used to demonstrate fracture toughness dependence on thickness and yield strength [22], and the model further verified by extensive testing of offshore grade plate steel [23]. As an extension of this approach, probabilistic fracture mechanics is being explored as a means of quantifying the reliability of a structure under load against brittle fracture in material with a known distribution of defect size and fracture toughness [20].

3. FATIGUE AND STRESS ANALYSIS

Benefitting greatly from the experience of the ECSC corrosion fatigue programme, and the continued collaboration of the countries and scientists in it, the Canadian activity in corrosion fatigue first sought to confirm European results on plate T-joints, enhancing the data using extensive crack monitoring. The programme subsequently expanded, as summarised in Table 2, to include work on the effect of internal ring stiffeners in tubular joints on fatigue behaviour in air and seawater; on the development of a pipe-to-plate configuration as a low cost alternative to large scale tubular testing; and on the use of computed stress intensity factors for weld toe cracks to model multiple crack initiation and coalescence and so predict fatigue life using fracture mechanics. Details of many of the results achieved to date are presented in the four technical papers from Canada included in these Proceedings [26-28,33], so that only the principal features need be highlighted in this overview.

To corroborate early ECSC and UKOSRP work on the detrimental effect of plate thickness on fatigue life, plate T-joints 16 to 103 mm thick were tested in 3-point bending under constant amplitude loading. The steels used were those offshore grade mill products produced in the earlier part of the national programme [6-8]. The reduction in fatigue life with thickness in air and seawater reported herein [26,27] will be further evaluated under variable amplitude loading using the COLOS sequence. The same T-joint geometries were used to study the effects of

cathodic protection in seawater at 5°C. In these tests, it was noted that impressed voltages do not restore corrosion fatigue lives to those levels obtained in air testing. This effect is illustrated in Figure 3 in which air, free corrosion and two levels of cathodic protection are compared. The effect of thickness in seawater was found to be the same as in air i.e. life reduced linearly with increasing thickness. This trend will be confirmed under conditions of variable amplitude loading.

The testing of large scale stiffened tubulars, the specimen geometry of which is shown in Figure 4, is being undertaken to complement and extend previous European work on tubulars. The project is under way at this time, with ten of the twelve fabricated joints having internal ring stiffeners. The effect of the stiffeners on stress distribution and fatigue crack development will be documented in tests in air under axial, in-plane bending, and out-of-plane bending loads. Further tests in seawater, using optimum cathodic protection, will be done using axial loading only.

As previously mentioned, one of the novel aspects of the Canadian programme is the pipe-to-plate simulation of a brace/chord connection, as depicted in Figure 5. As discussed later [28] this configuration, to be referred to as the "Scotch Tubular", can be placed under variable plate restraint to alter stress distribution and subsequent fatigue crack development.

All of the tests referred to above have been extensively instrumented. Strain gauges are used to determine stress distribution, notably in hot spot regions and around the stiffeners in tubular joints; and both AC and DC potential drop probes monitor crack growth from initiation to test completion. From these data has emerged a more complete picture of the crack initiation and growth process, enabling the use of fracturé mechanics methods to describe propagation [30]. The experimental work has been actively supported by stress analysis and modelling [30-33], leading to the succéssful use of da/dN data to predict crack growth in T-joints. An example of the output of this work is shown in Figure 6, in which the crack propagation life of plate T-joints as a function of thickness is predicted using three models of crack behaviour, viz. single (nearly elliptical) crack growth, single straight-fronted crack growth, and multiple crack coalescence and growth. The experimental points are those for total life, i.e. they include a contribution of about 0.3 N for initiation. It may be noted also that the multiple coalescence model predicts a linearly inverse relationship between propagation life and thickness.

4. FUTURE WORK

In addition to the ongoing projects on the development of consumables yielding welds with lower inclusion content and improved fracture initiation toughness, and studies of microconstituent behaviour in Gleeble simulated HAZ's, closer attention will be given to weld metal slag and weld metal gas interactions during pool formation. In fatigue projects, the effects of variable amplitude loading will receive appropriate attention, and experiments will be designed to study initiation, short crack growth phenomena, and the influence of electrochemical parameters. Fracture control activities will include further studies on the statistics of fracture, with the objective of setting toughness criteria that ensure an acceptable survival probability without imposing excessive economic penalties.

The future direction of large tubular testing, the pipe-to-plate experiments, and the smaller scale plate T-joint tests must await the outcome of the ongoing projects, and will no doubt be greatly influenced by the deliberations of this assembly.

4.1 Acknowledgements

The Canadian researchers whose work is referred to above are greatly appreciative of the advice and support given by their European colleagues, and acknowledge that help with gratitude.

4.2 REFERENCES

[1] Van Hee, G., Mclntosh, 1., and SendÇll, K.: "Engineering Systems for Offshore and Arctic Hydrocarbon Development", presented at 23rd Conference of Metallurgists (C.I.M.) Quebec City, August 1984.

[2] Baird, W.F.: "Comparison of Wave Data from Hibernia and Venture with North Sea Wave Climate", Marine Environmental Data $ervice, Dept. of Fisheries and Oceans, Ottawa, July 1984.

[3] Maes, M.A.: "Variability and Occurrence of Offshore Wind and Waves", Federal Govt. Report No. DSS 23004-6-5000/5Z-01 (Det norske Veritas (Canada) Ltd).

[4] Braid, J.E.M.: "Offshore Structures Materials, Research: Ongoing Programmes at CANMET S Physical Metallurgy Research Laboratories", Marine Engineering Digest, 6, (1) (August 1986), 23-30.

[5] "Inclusions and Residuals in Steels", edited by Boyd, J.D. and Champion, C.S., Conference Proceedings CANMET/CSIRA, CANMET/EMR PMRL 85-75(OP-J).

[6] McCutcheon, D.B.: "Determination of the Ability of Stelco Ingot and Strand Cast Structural Plate to Meet Mechanical Property Requirements for Canadian Offshore Structures and Ships", Federal Govt. Report No. DSS OSQ82-00211 (Stelco Inc.).

[7] Kay, J.D., Ackert, R.J., and McLean, M.K.: "Fabrication of Steels for Use in Offshore Structures and Arctic Vessels", Federal Govt. Report DSS OSQ82-00230 (Algoma Steel Corp.).

[8] McCutcheon, D.B.: "Controlled Rolled Grade 350 Plate for Arctic Applications", presented at 23rd Conference of Metallurgists (C.I.M.), Quebec City, August 1984.

[9] Bala, S.R. and Pond, S.: "Weldability and Formability of Two Candidate Steels for Offshore Structures and Arctic Vessels", Federal Govt. Report No. DSS OSQ82-00212 (AMCA International Ltd).

[10] Dorling, D.V., Huntly, R.M. and Rothwell, A.B.: "Development of All-Position Mechanical and Automatic FCAW Systems for the Fabrication of Offshore Structures and Arctic Vessels", Federal Gov't. Report No. DSS O$Q82-00250 (NOVA, an Alberta Corporation).

[11] Dorling, D.V., Huntley, R.M. Gerlings, J., and Rothwell, A.B.: "Pulsed Gas Metal Arc Welding of Thick Section Steels for Low Temperature Application", Federal Gov't. Report No. DSS OSQ84-00042 (NOVA, an Alberta Corporation).

[12] Braid, J.E.M., and Gianetto, J.A.: "Toughness of Weld Metals for Fabrication Of Cold Marine Structures and Vessels", CANMET/EMR Reports Nos. PMRL 86-99 and 86-100 (TR).

[13] Bala, S.R., Chin, C., Morrison, K., and Santyr, S.: "Evaluation of HAZ and Weld Metal Toughness in Selected Steels", Federal Gov't. Report No. DSS OSQ84-00137 (AMCA International).

[14] Shehata, M.T., Chandel, R.S., Braid, J.E.M., and McGrath, J.T.: "Characterisation of Non-Metallic Inclusions in Weld Metals", ASM Microstructural Science, vol. 14, (1987), 65-76.

[15] Braid, J.E.M., and McGrath, J.T.: "Influence of Microstructure and Strain on the Toughness of Welded Joints in Structural Steels for Offshore Applications", Canadian Metallurgical Quarterly, 25 (2), (1986), 131-143.

[16] Braid, J.E.M.: "Charpy-CTOD Correlations for Weld Metals Used in the Fabrication of Cold Marine Structures", CANMET/EMR FMRL report to be published.

[17] Braid, J.E.M. and Gianetto, J.A.: "Effects of Post Weld Heat Treatment on the Toughness of Shielded Metal Arc Welds for Use in Canadian Offshore Structure Fabrication", presented at Welding for Challenging Environments, Permagon Press, Toronto (1986), 145-155.

[18] "Fracture Toughness Evaluation of Steel for Arctic Marine Use", edited by Thomson, R., and Champion, C.S., EMR/CANMET PMRL 83-72(OP-J).

[19] Tomin, M.: "Development of Steel Plate Requirements for Fixed Offshore Structures", Federal Gov't Report No. DSS OST83-00427 (Det norske Veritas (Canada) Ltd.).

[20] Tomin, M., and Lantos, S.L.: "Evaluation of Fracture Toughness Data with Respect to the Reliability of Sub-Arctic and Arctic Structures", Federal Gov't Report No. DSS ISQ85-00206, (Det norske Veritas (Canada) Ltd.).

[21] Glover, A.: "Wide Plate Testing of the Heat-Affected Zone of LT60 ,and A710 Plate Material", Federal Gov t. Report No. DSS OSQ84-00032 (Welding Institute of Canada).

[22] Tyson, W.R., and Marandet, B.: "Cleavage Toughness Variability and Inclusion Size Distribution of a Weld Metal", CANMET/EMR PMRL 85-22(OP-J).

[23] Faucher, B. and Tyson, W.R.: "Factors Affecting the Fracture Toughness of an Arctic Grade Steel Plate", CANMET/EMR PMRL 85-29(OP-J)

[24] Lotsberg, I., Rengaard, O. and Nasseri, T.: "Assessment of Fatigue Design of Large Welded Joints, in Offshore Structures", Federal Gov't Report No. DSS OSQ83-00110 (Det norske Veritas (Canada) Ltd.).

[25] Vosikovsky, O. and Tyson W.R.: "Effects of Cathodic Protection on Fatigue Life of Steel Welded Joints in Seawater", CANMET/EMR PMRL 86-73(OP-J).

[26] Vosikovsky, O., Bell, R., Burns, D.J. and Mohaupt, U.H.: "Effects of Cathodic Protection and Thickness on Corrosion Fatigue Life of Welded Plate T-joints:, Paper No. TS 44, ibid.

[27] Mohaupt, U.H., Burns, D.J., Vosikovsky, O., Bell, R., and Kalbfleisch, J.: Fatigue Crack Development and Thickness Effects in Welded Plate to Plate Connections, Paper No. TS 3 ibid.

[28] Lambert, S., Mohaupt, U.H., Burns, D.J., and Vosikovsky, O.: "Simulation of Fatigue Behaviour of Tubular Joints Using a Pipe to Plate Specimen", Paper No. TS 18, ibid.

[29] Bell, R.: "Offshore Structures: Design and Analysis by the Finite Element Method", CANMET/EMR PMRL 82-41(TR).

[30] Vosikovsky, O., Bell, R., Burns, D.J. and Mohaupt, U.H.: "Fracture Mechanics Assessment of Fatigue Life of Welded Plate T-Joints, Including Size Effect", Proc. 4th International Conference on Behaviour of Offshore Structures (BOSS 1985), Delft, 157-168.

[31] Bell, R., and Vosikovsky, O.: "3 D Stress Intensity Factors for Weld Toe Cracks and Fatigue Life Prediction of Plate T-Joints, Proceedings of the 4th Irish Durability and Fracture Conference, Belfast, Sept. 1986, 214-225.

[32] Bhuyan, C.S., Arockiasamy, M., Muneswamy, K., Vosikovsky, O.: "Finite Element Analysis of Cracked and Un-cracked Tubular T-joints", Canadian Journal of Civil Engineering, 13 (3) 1986, 261-269.

[33] Bell, R., Vosikovsky, O., Burns, D.J., Mohaupt, U.H.: "A Fracture Mechanics Model for Life Prediction of Welded Plate Joints", Paper No. TS 53, ibid.

[34] Brigham, R.G.: "Corrosion of Welds in Ice-Breaking Ships", CANMET/EMR PMRL 86-66(OP-J).

[35] "Assessment of Non-Destructive Technology Required for Inspecting Offshore Structures", edited by Mak, D. CANMET/EMR ERP/PMRL 84-56(TR).

[36] Braid, J.E.M.: "Draft CSA Standard for Repair of Fixed Steel Offshore Structures", CANMET/EMR ERP/PMRL 84-72(TR).

Table 1 Principal Activities in the Canadian Offshore Steel Programme

Technology	Activity	References
Steel plate production	350 MPa plate 15-100 mm norm. and controlled rolled; HAZ toughness evaluation	5-9
Welding processes	Weld metal CTOD at -30°C from FCAW, SMAW, SAW related to structure, inclusions	10-17
Fracture evaluation	CTOD, Charpy, drop weight and wide plate test correlations	18-22
Corrosion fatigue	Plate to plate, pipe-to-plate, and stiffened tubular tests with multi-probe P.D. data	23-27
Stress analysis	2D amd 3D modelling for fatigue life prediction; tables of K data	28-32
Corrosion	Tank simulation of HAZ and weld metal corrosion in marine ice	33
NDE	3D defect characterisation by transducer arrays and acoustic imaging	34
Codes, regulations	Interim standards for Arctic icebreaker hulls; CSA design and repair code for fixed offshore structures	35

Table 2 Canadian Projects in Corrosion Fatigue and Stress Analysis

Topic	Performer	Ref.
Fatigue in air and seawater		
- plate T-joints	AMCA, CANMET, Waterloo Univ.	25, 26, 28
- pipe-to-plate	AMCA, Waterloo Univ.	27
- large tubulars	AMCA, Arctec Ltd., Memorial Univ., Waterloo Univ.	ongoing
- crack electro-chemistry	Memorial Univ.	ongoing
Stress analysis		
- stress concentration in tubulars	Memorial Univ.	32
- stress intensity in T-joints	Carleton Univ.	29,30,31,33

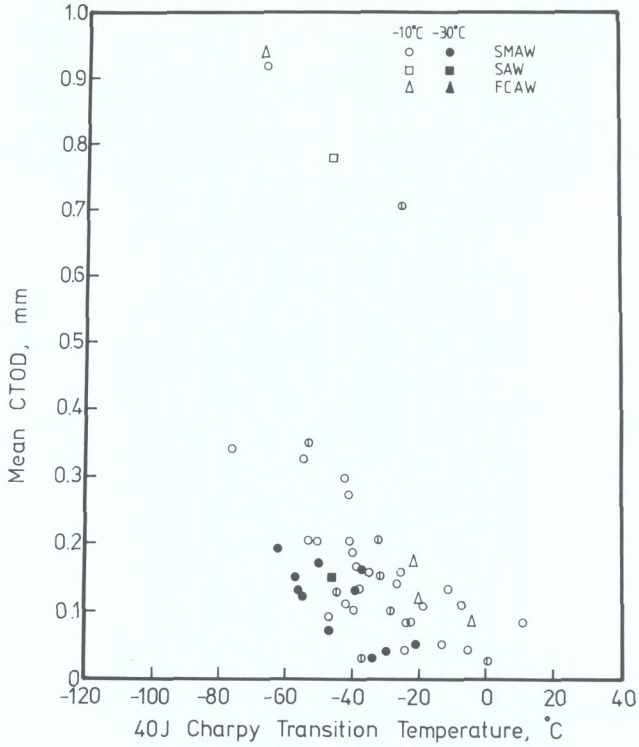

Figure 1 Interim correlation of CTOD at -10 and -30°C with 40 J Charpy transition temperature for various consumables and weld processes. CTOD specimens full thickness B x 2B with B = 20 mm for all welds (except circles with vertical bars B = 40 mm); CVN results from weld root region (Courtesy J.E.M. Braid, PMRL/CANMET).

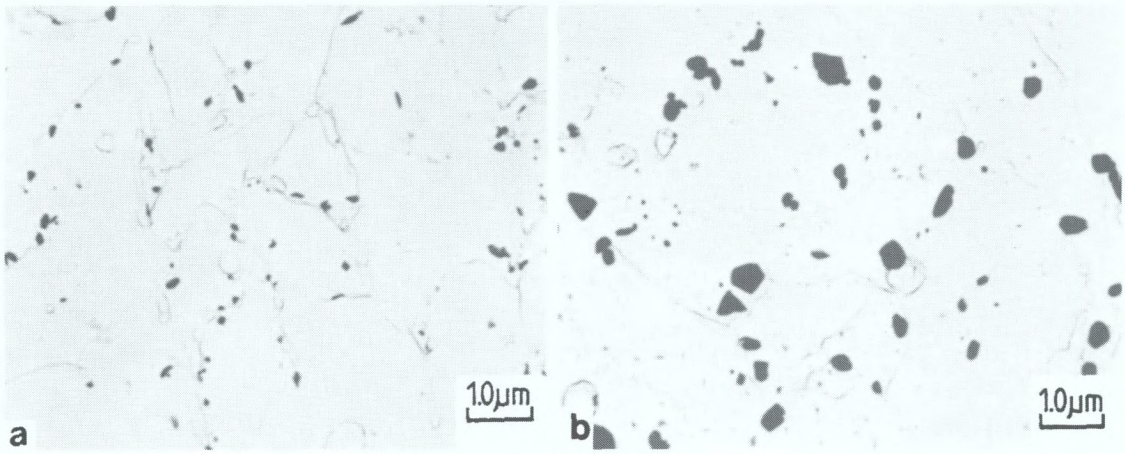

Figure 2 Carbon extraction replicas of carbides in a C-Mn-Ni SMAW weldment (a) as welded and (b) after PWHT. (Ref. 17).

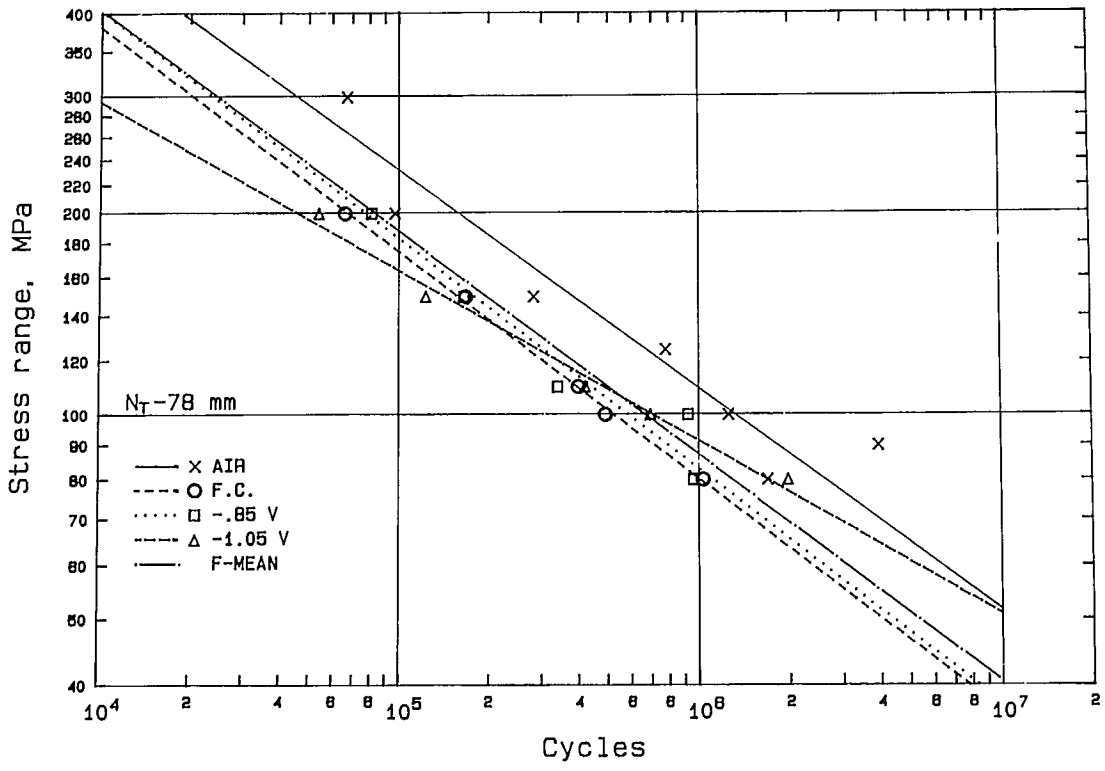

Figure 3 S-N curves showing total life N_T for 78 mm plate T-joints in air and seawater under free corrosion (F.C.), optimum C.P. (-0.85v) and overprotection (- 1.05V). Also shown is the F-Mean line for air (Courtesy O. Vosikovsky PMRL/CANMET).

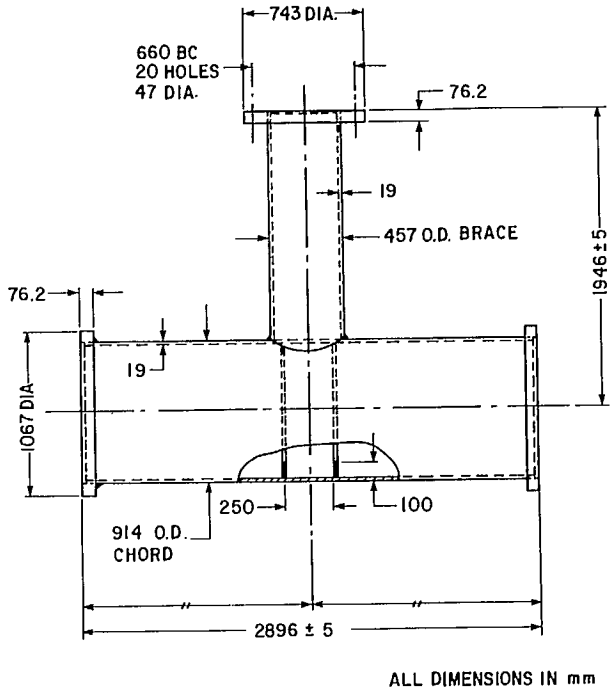

Figure 4 Geometry and dimensions of tubular T-joint with internal ring stiffeners. (Courtesy University of Waterloo).

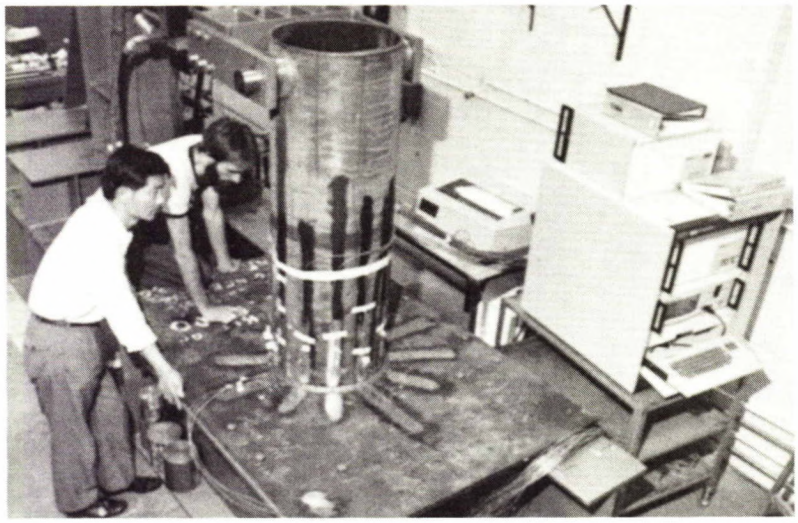

Figure 5 View of pipe-to-plate assembly being prepared for fatigue testing. (Courtesy University of Waterloo).

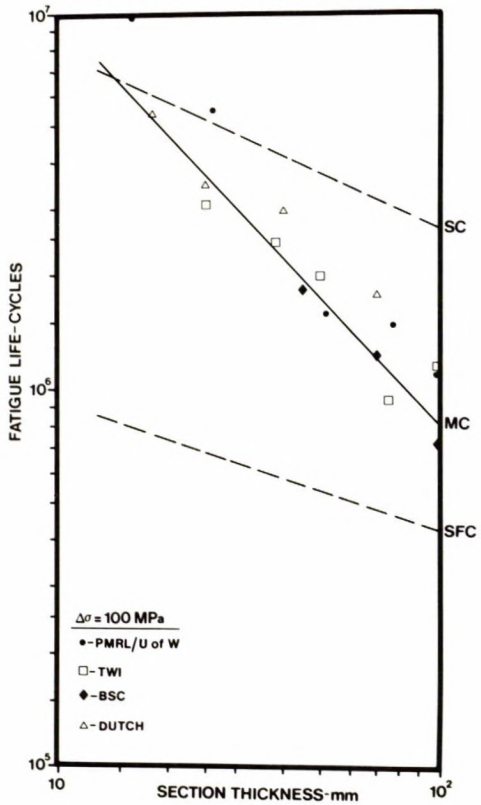

Figure 6 Fracture mechanics predictions of propagation life of plate T-joints in air at 100 MPa stess range as a function of plate thickness.
SC - single (semi-elliptical) crack
MC - multiple crack
SFC - straight-fronted crack

Experimental points are total life versus model's propagation life only. (Courtesy O. Vosikovsky PMRL/CANMET and R. Bell, Carleton Univ.).

CRACK GROWTH BEHAVIOUR AND FRACTURE MECHANICS APPROACH

ÉTUDE DE LA VITESSE DE CROISSANCE DES FISSURES ET DES MÉCANISMES DE RUPTURE

ÉTUDE DE LA VITESSE DE CROISSANCE DES FISSURES ET DES MÉCANISMES DE RUPTURE

D.J. Burns, S.B. Lambert et U.H. Mohaupt

Génie mécanique, Université de Waterloo, Waterloo (Ontario) Canada

RÉSUMÉ

Le rapport fait état des techniques de mesure de la mécanique linéaire de rupture qui sont utilisées pour prédire la croissance des fissures en fatigue dans des cordons de soudure. Les données concernant les soudures de deux plaques, d'un tuyau et d'une plaque, et de sections de tubes (joints tubulaires) sont présentées afin de démontrer les effets de la coalescence sur le développement de la forme de la fissure. Quelques mécanismes permettant de discerner jusqu'à quel point la coalescence influe sur le calcul de la vitesse de croissance des fissures sont passés en revue. Les analyses qui ont été effectuées en vue de déterminer et prédire l'endurance des matériaux et les risques de rupture dans diverses applications sont également présentées.

CRACK GROWTH BEHAVIOUR AND FRACTURE MECHANICS APPROACH

D.J. BURNS, S.B. LAMBERT and U.H. MOHAUPT

Mechanical Engineering, University of Waterloo, Waterloo, Ontario, Canada

ABSTRACT

Some Linear Elastic Fracture Mechanics (LEFM) methods for predicting the growth of fatigue cracks at welded toes are reviewed. Data is presented for plate-to-plate, pipe-to-plate and pipe-to-pipe (tubular) joints to illustrate the influence that coalescence has on crack shape development; some mechanisms for recognizing this influence in growth calculations are discussed. Deterministic and probabilistic LEFM analyses of fatigue life and/or risk of failure for various applications are reviewed.

1. INTRODUCTION

In his plenary paper in 1981, Professor Radenkovic [1] discussed the problems encountered when attempting to use fracture mechanics concepts to predict the life or residual life of tubular or other welded joints. Then and now the normal basis for a fracture mechanics analysis of fatigue crack growth is the assumption that the rate of fatigue crack growth, da/dN, is a function of the range of crack tip stress intensity factor, ΔK. Most authors assume that the relationship proposed by Paris-Erdogan [2] is applicable i.e.

$$\frac{da}{dN} = C(\Delta K)^m \qquad \ldots \quad (1)$$

This equation can be used in three ways. For some specimen geometries, there are very well established solutions for the crack tip stress intensity factor, K_I, so observations of fatigue crack growth in such specimens are used to determine material "constants", C and m and the limitations of equation (1) when considering environmental, mean stress, threshold and other effects.

A second use for this equation, when C and m are known, is to make measurements of crack growth rate, da/dN, in specimens of more complex geometry, e.g. a tubular joint, and to use the equation to predict values of ΔK for comparison with values obtained by theoretical methods [3].

A third use for this equation is life prediction. By assuming initial crack depths, a_i, that are small, 0.1 to 0.5 mm, compared to the sizing capabilities of structural non-destructive inspection techniques for welds [4], authors attempt to predict S-N curves for typical joints. The success of this approach depends very much on the method used to model crack shape development [1] and the relative magnitude of initiation life, N_i (for crack depth less than a_i), and propagation life, N_p (for crack depth greater than a_i). If crack depth and shapes are measured during in-service inspection, then equation (1) can be used to predict residual life (N_{RES}) which is one indicator that should be considered when scheduling repairs.

All of these uses for equation (1) will be discussed herein. Three types of welded connections will be considered. Plate-to-plate joints, particularly T-plate, full penetration welded specimens, have been used extensively in the fatigue programs discussed at this conference. In some cases the attachment plate has been load-carrying, Figure 1(b), and in others non-load-carrying, Figure 1(a); in most cases the mode of loading has been bending.

Pipe-to-pipe joints, Figure 1(d), particularly unstiffened T-tubular joints, must obviously be discussed, since this has been a basic geometry for most fatigue programs. In addition, some attention will be given to pipe-to-plate joints, Figure 1(c), since these appear to be a reasonable model of a low β-ratio tubular joint [5] and much cheaper for assessing the usefulness of

fracture mechanics methods proposed for predicting N_p or N_{RES} for tubular joints.

2. RELATIONSHIP BETWEEN da/dN AND ΔK

Most texts use a schematic similar to Figure 2 (inset) to illustrate the relationship that often exists between da/dN and ΔK. Equation (1) is valid in region B, mean stress effects and fracture toughness are important in region C, and various threshold effects come into play in region A.

In his plenary paper in 1981, E.F. Walker [6] discussed the influence that environment, mean stress (R ratio) and threshold effects have on fatigue crack growth rate. In his plenary paper in 1981, W. Schütz [7] mentioned how equation (1) was modified in 1967 by Forman et al [8] to include mean stress (R) and fracture toughness (K_c), i.e.

$$\frac{da}{dN} = \frac{C^* (\Delta K)^{m^*}}{(1-R)\, K_c - \Delta K} \quad \ldots \quad (2)$$

Equations (1) and (2) can be used for life prediction for variable amplitude loading by using a counting technique such as the Rainflow method [9] and calculating the crack propagation per cycle. This ignores interaction effects, which are often beneficial and are the basis for many variants of equations (1) and (2) [7]. An indication of the effect of periodic overloads on crack growth rates in BS 4360-50D steel is given in Figure 6 of paper TS 50 by Austen and Walker [10]. In their paper they rewrite equation (1) as

$$\frac{da}{dN} = C(\Delta K_{eff})^m \quad \ldots \quad (3)$$

where the effective range of stress intensity factor accounts for closure, overloads, and static fracture. Their outline of the factors affecting crack closure/thresholds indicates the complexity of the problem and why many analylsts still use the much simpler equations (1) and (2) and ignore interaction effects.

Equation (2) accounts for the trends in region C but ignores the threshold effects in region A. To account for regions A, B and C, Saxena, Hudak and Jouris [11] proposed a three component model for representing wide range fatigue crack resistance (inverse of da/dN) for regions A, B and C to obtain

$$\frac{1}{da/dN} = \frac{C_1}{\Delta K^{m_1}} + \frac{C_2}{\Delta K^{m_2}} - \frac{C_2}{[(1-R)K_c]^{m_2}} \quad \ldots \quad (4)$$

where C_1, m_1, C_2 and m_2 are empirical constants defined in Figure 2. When $C_1 = 0$ and $K_c \to \infty$, equation (4) reduces to equation (1). In a recent paper, Hudak, Burnside and Chan [12] tabulate these constants for various mean stress and environmental conditions for welded steels in marine applications. For details see their report to the Ship Structures Committee [13].

In their paper [12] they emphasize that "Although equation (4) is capable of representing low growth rate data, it is not dependent on a threshold stress intensity for fatigue crack growth (ΔK_{th})--a parameter which is arbitrarily defined, as well as dependent on test technique and measurement sensitivity. Thus, incomplete data at low growth rates are given by a power-law extrapolation of available data, thereby resulting in conservative life prediction. In contrast, asymptotic-type models which contain ΔK_{th} can result in significant nonconservatisms in life when low growth rate data are inadequate--as is often the case."

As mentioned earlier, the problem of defining behaviour in region A is addressed by Austen and Walker [10] in paper TS 50. Their program of threshold testing on BS 4360-50D steel includes constant amplitude (CA) and variable amplitude (VA) loading, see Table 3 in TS 50. The effects of test frequency, stress ratio, and environment are being evaluated. To compare constant amplitude and narrow band random fatigue data, the authors use an equivalent range of crack tip stress intensity, ΔK_h. They emphasize that ΔK_h is not very different from the root mean square value, ΔK_{RMS}, sometimes used for such comparisons.

Figure 2 (Figure 2 from TS 50) compares corrosion fatigue crack growth data for BS 4360-50D steel in sea water for three types of narrow band random loading with constant amplitude data. The correlation is reasonable considering the scatter normally seen in such plots. The transition from region B to region A is obvious, but the figure does not illustrate the difficulty inherent in defining a threshold value, ΔK_{th}, at a cutoff growth rate of 10^{-11} m/cycle. The considerable scatter in ΔK_{th} values reported by Austen and Walker, provides some support for the argument of Hudak et al for a power law extrapolation defined by C_1 and m_1, without a cutoff at 10^{-11} m/cycle. Also, Austen and Walker point out that it may be more meaningful to define the cutoff rate as 10^{-11} m/block length, which

for constant amplitude loading reduces to 10^{-11} m/cycle.

Equation (4) will not model the plateau observed in crack growth rates for BS 4360-50D under cathodic protection at high R. Hudak et al note that this plateau can be included by adding a constant to equation (4); this constant is the reciprocal of the plateau velocity, a value of 10^6 cycles/m for 0.1 Hz data. This and other curve-fitting decisions made by Hudak et al [12,13] provide the analyst with a mathematical model that fits the data but does not further our understanding of the processes operating. This understanding will only be obtained by developing crack growth equations such as the environmental and global models proposed by Austen and Walker [10]. Until it is shown that such models are more reliable than equations (1), (2) or (4) most analysts are likely to continue to use equations (1), (2) or (4) and to ignore interaction effects.

To use any of these equations to predict life, N_p or N_{RES}, one must estimate how ΔK will change with increase in crack depth and crack shape. Some methods for estimating crack tip stress intensity factors will now be reviewed.

3. PREDICTION OF CRACK TIP STRESS INTENSITY FACTOR (K_I)

To illustrate the general problem, Figure 3(a) shows a crack developing from the hot-spot in a T-tubular joint. The crack has an irregular shape, Figure 3(b), with a surface length, 2c, and maximum depth, a_{max}. Before the crack develops, the stress field, Figure 3(b), can be described by $\sigma_r(x)$ and $\sigma_r(t)$, where r is the direction normal to the expected crack plane, t is the circumferential direction around the weld, and x is the distance through the chord wall.

In most analyses it is usual to ignore any crack curvature in the t or x directions and the variations in σ_r in the t direction. It is also usual to bound the irregular crack by a semi-ellipse [14]. This bounding recognizes the difficulty of using non-destructive inspection techniques to size cracks and the need for a crack shape that is mathematically tractable. These approximations reduce the problem to that shown in Figure 4. Here the "no crack" stress field, $\sigma_r(x)$, has been normalized by dividing by the nominal stress at the weld toe, σ_o, and the crack depth, a, or the distance, x, has been divided by the chord thickness T. The inset diagrams on Figure 4 show the semi-elliptical crack (a, 2c) and the next level of simplification--an edge crack of depth a. The latter is also of interest because various authors at this conference discuss the behaviour of cracks in T-plate specimens, which by design or by natural development to the free edges become edge cracks [15-17].

Various numerical methods are available for calculating the crack tip stress intensity factor for the semi-elliptic or edge cracks and the type of stress field shown in Figure 4. The dominant method is to model the cracked component with finite elements [15, 18-20].

For edge or semi-elliptic surface cracks in flat plates it is convenient to present estimates of K_I as

$$K_I = M\ \sigma(\pi a)^{1/2} \qquad \ldots \quad (5)$$

where σ is nominal stress and M is a stress intensity correction factor.

For a plate-to-plate welded joint such as that shown in Figure 1(a) it is usual to present estimates of K_I as

$$K_I = M_k\ M\ \sigma(\pi a)^{1/2} \qquad \ldots \quad (6)$$

For very small cracks in this type of joint, it is usual to argue that the magnification factor, M_k, will tend to a value equal to the elastic stress concentration factor, K_t.

In general, the "no crack" stress field normal to the expected crack plane has the shape shown in Figure 4 and the nominal stress at the weld toe, σ_o, can be split into membrane (σ_m) and bending (σ_b) components, i.e.

$$\sigma_o = \sigma_m + \sigma_b \qquad \ldots \quad (7)$$

For the general case, equation (6) can be rewritten as

$$K_I = M_{km}\ M_m\ \sigma_m(\pi a)^{1/2} + M_{kb}\ M_b\ \sigma_b(\pi a)^{1/2} \qquad \ldots \quad (8)$$

where M_{km} and M_m are magnification and correction factors respectively for pure membrane stressing and M_{kb} and M_b are corresponding factors for pure bending.

3.1 Theoretical Estimates of Correction and Magnification Factors

Paper TS 52 in this conference by Dijkstra, Snijder, Overbeeke and Wildschut [15] presents expressions for M_{km} and M_{kb} for an edge crack at the toe of a stub on a flat plate. This stub is equivalent to the non-load carrying attachment plate shown in Figure 1(a). Five weld geometries were analysed using a finite element method; Table 1 (Table 4 from TS 52) lists the geometric parameters and estimates of M_k.

In their paper, ϕ is the weld toe angle, ρ is the weld toe radius, and T is the base plate thickness. In all geometries, the width of the top of the weld stub was equal to the plate thickness, T. In other words the "attachment" plate and base plate had the same thickness.

The values of M_k shown in Table 1 for a/T of zero are their estimates of K_t. Estimates of M_k for very small cracks are always less than K_t; the difference between M_k and K_t is small when the toe radius is 5 mm. In all cases M_{kb} is larger than M_{km}. The sets of data for 70° toe angle stubs indicates that M_k decreases with increase in ρ/T at very small values of a/T. A similar study by Niu and Glinka (to be published this year [21,22]) for an edge crack in a T-butt welded joint, with 45° weld angle, under bending load shows the same trends; for a/T values less than 0.04, increasing ρ/T decreases M_{kb}.

Several other aspects of this study by Niu and Glinka merit some discussion in this section. The weight function method was used to estimate K_I for edge and semi-elliptic cracks in T-joints. The usual way to define the weight function for a given geometry is to find or derive a reference stress intensity factor for any stress system, together with the corresponding crack opening displacement field [23]. Niu and Glinka used the Petroski and Achenbach appoximation for the crack opening displacement function [32]. For edge cracks they assumed that the effect of the corner (weld) angle on the weight function does not depend on the plate thickness, T, and that it can be determined by solving the problem of a crack emanating from an angular corner in a semi-infinite plate with a step, see inset diagram on Figure 5. For a semi-elliptic crack they derived a weight function for flat plates, using Newman and Raju solutions [24], as the reference stress intensity. Then they assumed that the effect of weldment geometry on K_I at the deepest point of the semi-elliptic crack is the same as in the case of an edge crack. This enabled them to define a correction factor to apply to their weight function solutions for flat plates. In particular the correction factor is the ratio of K_I for an edge crack in the weld geometry to K_I for an edge crack in a flat plate.

Figure 5 shows Niu and Glinka's estimates for K_I for an edge crack in a T-butt welded joint under bending load [21]. In all cases the ratio ρ/T was 0.04 and the weld toe angle was either 30, 45 or 60°. These authors chose an ordinate axis of $K_I/\sigma_o(\pi a)^{1/2}$, which equation (6) shows is equivalent to M_{kb} M. This data shows that weld toe angle has a significant effect for a/T values less than about 0.2.

In their paper, Dijkstra et al [15] also discuss the effect of weld toe angle. Comparing specimens C-2-3(ϕ=45°) and C-1-1(ϕ=70°), see Table 1, they argue that reducing the weld angle had a positive and a negative effect. Reducing the angle reduced M_k at very small a/T. However, reducing the angle also increased the stub width at the plate surface, thereby tending to increase M_k. For these particular cases, these counteracting effects have approximately cancelled each other when a/T is only 0.025.

This dependence of M_k on stub width at the plate surface has been examined by Smith [18] and by Burdekin, Chu, Chan and Manteghi [25]. Some of Smith's finite element results for edge cracks are shown in Table 2. Four different attachment sizes were investigated, in particular t/T of 0.3, 0.4, 0.5 and 0.6. In all cases a weld leg length of 0.2T was assumed and the data in Table 2 is for pure bending, Figure 1(a). Table 2 shows that M_k increases with increase in stub width at the plate surface and that the weld has little or no effect for a/T values higher than 0.2.

Burdekin et al [25] do not list their values for M_k but note that "they found that a major factor influencing the fatigue strength...was the distance between the two weld toes on the surface". This conclusion will be discussed in a later section; here attention will be given to the method they used to calculate K_I since they and others [26] have also used it to calculate K_I values for cracks in tubular joints.

This approach to the problem of determining stress intensity factors for cracks in gradient stress fields is to use the integral technique developed by Oore and Burns [27]. Their approach was to examine the structure of weight functions for three dimensional embedded cracks for which there are known solutions, and to surmise that in general these weight functions, $W_{QQ'}$, could be rewritten as or approximated by

$$W_{QQ'} = \frac{\sqrt{2}}{\pi \ell_{QQ'}^2} \frac{1}{\int \left[\frac{ds}{\rho_Q^2}\right]^{1/2}} \quad \ldots (9)$$

where, as shown in Figure 3(c), Q' is the point on the crack front at which K_I must be computed, and Q is the point on the crack surface at which $P_{Q'}$, a pair of symmetric opening forces, act. Here $\ell_{QQ'}$ and ρ_Q denote, respectively, the distances between Q and Q', and between Q and a point S at the

centroid of an elemental length ds of the crack front. The resulting stress intensity factor K_I at Q' is given by

$$K_{Q'} = P_Q W_{QQ'}$$

Therefore, for an arbitrary normal stress field, σ_Q, Oore and Burns argued that an estimate of the stress intensity factor, $K_{Q'}$, at point Q' should be given by the integral

$$K_{Q'} = \iint \frac{\sqrt{2}}{\pi \ell_{QQ'}^2} \frac{\sigma_Q dA_Q}{\int \left[\frac{ds}{\rho_Q^2}\right]^{1/2}} \quad \ldots (10)$$

where A is the area of the crack surface, Figure 3(c).

It has been shown [27] that this integral satisfactorily predicts K_I for a variety of normally loaded, embedded cracks for which there are published solutions. In particular, solutions have been derived for a circular crack with a pair of opening, symmetrical, point loads at any location in the crack area, for an elliptical crack under uniform or linear varying stress field, for an annular circular crack in a uniform stress field, for a parabolic crack in a uniform stress field, and for a straight-through tunnel crack of constant width with line or uniform loading.

Another paper [28] shows that this integral also gives satisfactory results for embedded rectangular defects and for an embedded irregular defect, which had changes from convex to concave curvature along the defect front. For these defect shapes the integral estimates of K_I were in good agreement with estimates obtained by stress-freezing photoelasticity.

For two of the aforementioned test cases, it was possible to obtain a closed-form solution for equation (10); for other test cases it was necessary to develop numerical procedures to solve equation (10). It should be noted that the numerical procedure outlined in reference [27] has been replaced by a much more sophisticated procedure which is detailed in another paper [29].

One of the authors [30] and others [31] have also shown how the integral equation (10) can be used with correction factors to predict stress intensity factors for surface cracks of semi-elliptical shape. In studies at Interatom [31], they have developed their own numerical procedures for evaluatiing equation (10) and for determining correction factors for free surfaces.

To use equation (10) to estimate K_I values along the front of a surface crack in a tubular joint, e.g. Figure 3(b), one must first analyse the equivalent embedded crack. The imaginary "mirror image" part of this embedded crack, see Figure 3(b), is subjected to an imaginary mirror image of the "no crack" stress field, i.e. $\sigma_r(x)$ and $\sigma_r(t)$. K_I values are then corrected for free surface effects [30,31].

As mentioned, equation (10) has been used successfully to predict K_I for embedded irregular defects in plates [28] and to predict K_I for surface semi-elliptic defects in plates. Burdekin et al [25], and Dover and Connolly [26] have used equation (10) to predict K_I values for semi-elliptic cracks in tubular joints. Both groups have used an appropriate bending/membrane combination to describe $\sigma_r(x)$ and considered the variation in surface stress distribution around the brace, i.e. $\sigma_r(t)$.

In their paper, Dover and Connolly compare their O-integral (equation (10)) estimates of K_I with estimates obtained from experimental observations of crack growth in tubulars having Y or K joints. They conclude that the O-integral provides good estimates of K_I for tubular joints over most of the crack growth range. They also show very clearly the need to consider the variation in $\sigma_r(t)$ around the intersection. This influences K_I at the deepest point, a_{max}, and the rate of growth along the surface.

So far attention has been focussed on K_I for edge cracks or K_I for the deepest point in a semi-elliptic or irregular crack. For edge cracks the effect of the weld (M_k) is insignificant where $a/T > 0.2$. For semi-elliptic cracks one needs to consider M_k at two locations, deepest point and free surface, to correctly assess the effect of the weld on fatigue crack shape development. Although accuracy diminishes as one approaches the free surface, it is possible to use finite element methods to obtain surface magnification factors, M_{ks} [20].

Paper TS 53 in this conference by Bell, Vosikovsky, Burns and Mohaupt [17] presents stress intensity factors for the deepest point of a semi-elliptic crack in a T-plate, subjected to bending as shown in Figure 1(b). Nui and Glinka [21] have analysed the same specimen using their weight function method and report excellent agreement with Bell's finite element results for K_I at the deepest point. Bell's contract reports [19,20] also contain estimates of K_I for the surface of the semi-elliptic cracks. These surface values are compared in Figure 6 with values for the deepest point. They have been normalized by dividing by Newman and Raju solutions for semi-elliptic cracks in flat plates [24] so the ordinate axis in

Figure 6 is M_k or M_{ks}. As would be expected at small values of a/T, M_{ks} is much larger than M_k. Also M_{ks} does not approach unity until the normalized crack depth is about 0.4 whereas, as mentioned before, M_k approaches unity as a/T tends to 0.2. These differences have important implications when considering the development of fatigue cracks at weld toes; this will now be considered.

4. SHAPE DEVELOPMENT OF FATIGUE CRACKS

Vosikovsky, Bell, Burns and Mohaupt [33] monitored the development of fatigue cracks from the toes of full penetration welds on T-joints subjected to bending as shown in Figure 1(b). Ink staining, beach marks and potential drop techniques were used to monitor crack development. Crack depth and surface length information obtained from fracture surfaces has been used to prepare Figure 7. Although there is considerable scatter, the trend is very clear; as the crack depth increases the aspect ratios tend to about 0.1. Also, as the surface crack length increases in this type of specimen, the crack eventually reaches one or both free edges (sides in the width direction) and the aspect ratio drops to zero.

As crack length increases, the observed aspect ratios tend to 0.1 because of coalescence. This coalescence phase can be split into three parts [34]. Microcracks exist or are formed by fatigue along the weld toe at micro geometrical discontinuities and inclusions. Some of these microcracks coalesce to form very small semi-ellipses of low aspect ratio. As these microcracks grow their aspect ratios tend to increase; when these single cracks are about 0.5 mm deep the aspect ratios may be as high as 0.5. Linear elastic fracture mechanics analysis of fatigue crack growth in welds when crack depth is less than 0.5 mm is either complicated by "short crack" problems or not valid because the microcracks are not planar [35,36]. Therefore, 0.5 mm is a convenient choice for initial crack depth in life calculations.

Vosikovsky et al [33] developed a so-called multiple crack model for coalescence; two predictions of the model are shown on Figure 7. In both examples the free edge effect mentioned earlier is assumed to occur when a/2c equals 0.1. This multiple crack (MC) model gives much more realilstic estimates of fatigue life (N_P) than modelling based on the growth of a single crack (SC) model. Bell [37] has used equataion (1) and his estimates of M_k and M_{ks} for a single semi-elliptic crack in a T-plate weld, see Figure 6, to predict how the shape of a single crack changes as crack depth increases. This prediction is shown on Figure 7 for an initial aspect ratio of 0.5. At very small values of a/T, the single crack model and the empirical multiple crack model agree; thereafter the single crack model predicts an aspect ratio development that is very different from the experimental observations of Vosikovsky et al [33] and others [38,39].

The aspect ratio development predicted by the single crack model is compared on Figure 8 with equivalent predictions for semi-elliptic cracks in flat plates subjected to pure bending. These flat plate predictions are based on the K_I solutions of Newman and Raju [24]. Five flat plate cases are shown; the starting points for the calculations being A, B, C, D or E. Starting at A, there is a steady reduction in a/2c and the B, C, D and E solutions tend to the "A" solution.

It will be noticed that Bell's T-plate solutions also tend to the "A" solution for a flat plate as a/T tends to 0.6. In other words, the effect on K_I of the welded attachment is very small when a/T is 0.5 to 0.6. Between a/T of 0.1 to 0.4, the welded attachment influences M_{ks} but has little effect on M_k, see Figure 6. Therefore, in this region the aspect ratios may peak as in a flat plate (cases B, C and D) but M_{ks} increases surface growth and keeps the aspect ratios below the flat plate predictions. For a/T values less than 0.1, M_k and M_{ks} are both significant but surface growth dominates so the aspect ratio drops from 0.5 at a high rate compared to the flat plate "A" solution.

Also shown on Figure 8 are some experimental data from paper TS 51 of this conference by Wildschut, Overbeeke, Snijder and Dijkstra [16]. To obtain the geometrical effect of a weld attachment without the complication of multiple crack initiation and coalescence, these authors machined a specimen (type D) from base metal. A semi-elliptic defect was spark machined at the toe of the stub on this T-specimen and grown in fatigue. The aspect ratio values shown on Figure 8 were obtained from beachmarks. The spark machined defect was 0.5 mm deep and 10 mm long; the plate thickness, T, was 40 mm. Again the effect of the "weld" geometry is to produce a very rapid change in aspect ratio for a/T values less than 0.1. In this case the initial aspect ratio was very small (0.05) and the effect of the "weld" geometry was to increase the aspect ratio with a peak at a/T of about 0.1 and a steady decline thereafter. It is not clear why the experi-

mental data tends to lie below and parallel to the "A" solution at high a/T values. A possible explanation for this is that both the "A" solution and Bell's results do not adequately model the surface length development in a real specimen. At the surface, the local stress concentration produced by the weld toe geometry causes local surface damage or microcrack initiation along the entire length. This damage will accelerate crack growth along the surface relative to virgin material and result in lower aspect ratios.

Figure 8 also shows the empirical multiple crack model proposed by Vosikovsky et al [33]. Clearly, single crack development is very different from that observed at weld toes of T-plates by Vosikovsky et al. Observations have also been made on the development of fatigue cracks in T-butt welded joints by Morgan [38] and Webster et al [39]. Their data, Figure 9(a), shows very similar trends to that on Figure 7.

Figures 9(a) and 9(b) show T-plate data and data for fatigue cracks in pipe-plate specimens, PP1 and PP2, and a tubular joint, TB1, subjected to in-plane bending. Details for these specimens are given in paper TS 18 by Lambert, Mohaupt, Burns and Vosikovsky [5]. In all cases, the aspect ratio was at or below about 0.2 when a/T reached 0.2. As mentioned earlier, the usefulness of T-plate specimens for studying crack shape development is limited by the tendency of the cracks to propagate to the free edges (sides). In pipe-plate and pipe-pipe (tubular) joints free edges are not a factor and the surface length of the crack is influenced by weld geometry and stress variation around the intersection.

A general indication of the relationship between aspect ratios and a/T for cracks in tubular joints was recently published by Topp and Dover [4]. From 22 sets of fatigue data they derived 253 values of (a/2c, a/T). These values were used by them to prepare a distribution plot that is compared on Figure 10 with the pipe-plate and tubular data shown previously on Figure 9. Here no attempt is made to distinguish between modes of loading or the geometry of the tubular joints. At a/T values below 0.2, Topp and Dover's aspect ratios are small compared to observations from [5]. This difference is probably a reflection of differences in measurement technique. In [5], a/2c values at a/T less than 0.1 are based on ink stains and beachmarks. If Topp and Dover's a/2c values are only based on ACPD measurements, the accuracy is questionable at small crack depths because of uncertainty about probe locations relative to the deepest point and a tendency to average when sizing semi-elliptic defects [40].

For a/T values greater than 0.2, Figure 10 indicates that a/2c is likely to be less than 0.1. However the distribution plots have wide bounds and Topp and Dover point out that "in the extreme one could, for example, measure a crack length of 200 mm and this could have a depth of anything from 1 to 26 mm. This shows clearly that it is dangerous to try to infer crack depth from crack length and also that crack length is not closely related to remnant (residual) life".

A much less pessimistic view of surface crack length as an indicator of residual life is taken by Tweed [41] in paper TS 49 of this conference. In many of the UKOSRP and ECSC tubular tests the development of fatigue cracking was recorded as surface crack length versus number of cycles. Clayton [42] and Tweed and Freeman [43] have reviewed this surface length data and developed some indicators for assessing residual life.

In total, data for 105 fatigue cracks are analysed. By considering lower bounds to plots of 2c/T versus N/N_3, Tweed and Freeman [43] show that residual life (N_{RES}) is likely to be at least 50% of N_3 for a 0.5T surface crack length, 25% of N_3 for a 2T crack, and 10% for a 4T crack. This lower bound approach makes no distinction between modes of loading and variations in joint geometry. However, categories proposed by Tweed and Freeman [43] for simple T-joints as a function of geometry and loading are given as Table 1 of TS 49. They say that "this systematic surface crack growth behaviour can be understood [43] in terms of the ratio of membrane to bending stress at the tubular joint hot spot and the extent (strictly the rate of decline) of the highly stressed weld toe region around the hot spot; high bending components and extensive, relatively highly stressed regions favouring enhanced surface crack growth". This is a reasonable argument but it is complicated by the scatter introduced by the random nature of the "initiation" mechanism for fatigue cracks at weld toes. Identifying the lower bound for a particular category is obviously a difficult problem and there are many other factors which are likely to render their joint categorization more or less conservative [41]. However, their basic argument concerning the importance of the ratio of membrane/bending stress and the extent of the highly stressed weld toe region merits further discussion here.

Figures 11, 12 and 13 present data obtained by J. Forbes [44] for a T-tubular joint having a 457 mm diameter brace welded at right angles to a 914 mm chord. The

brace and chord of the tubular joint, TB1 on Figures 9 and 10, were 19 mm thick. Strain gauges, inside and outside, were used to determine the radial stress distributions plotted in Figures 11, 12 and 13 for axial, out-of-plane and in-plane bending respectively. This tubular was fatigued in in-plane bending; the development of the fatigue crack was monitored by ink-staining, beach marks, and DCPD measurements. A sample of the crack profiles are shown on Figure 13. The interruptions in the profiles near one end of the crack indicate where a step developed in the crack so it went behind the probe pairs on that part of the weld.

Figure 13 shows that the fatigue crack had almost reached its full surface length when $(a/T)_{max}$ was about 0.2 and N/N_3 was 162,700/240,000 cycles. This and the gradual increase in aspect ratio thereafter has been reported by others. For example, Figure 14 shows one of the aspect ratio vs a/T plots obtained in the French program; this tubular had a 685 mm chord, 345 mm brace, 41.6 mm chord thickness, α of 5.84, β of 0.5, γ of 8.2 and τ of 0.53 [45].

A comparison of Figures 11, 12 and 13 emphasizes that the extent of the highly stressed zone is much larger for in-plane bending than for axial or out-of-plane bending for this geometry. In all three cases there is a location around the weld toe at which the stress field starts to decay rapidly. Although one would expect fatigue cracks to grow beyond these "stress decay" points, one would also expect to see a decay and end to surface growth not too far beyond the "decay" locations. For the in-plane bending example shown in Figure 13, surface growth ended at locations where the radial stresses were 64% and 92% of the hot spot stress.

Van Delft, Dijkstra and Snijder [46] have published crack growth data for a tubular joint, B3, tested in the second phase of the ECSC program. This T-tubular had a chord of 914 mm diameter and 32 mm thickness with a brace of 457 mm diameter and 16 mm thickness. The crack shape development for this axially loaded tubular is compared on Figure 14 with that for the in-plane bending tubular mentioned earlier [45]. The differences in crack development are noticeable. When a/T is 0.3 or less the aspect ratio is smaller for the bending case. Beyond a/T of 0.3 to 0.4, the aspect ratio for the bending case increases with a/T whereas the axial case shows a steady decline with increase in a/T. These observations and the previously discussed differences between axial and in-plane bending stress fields are the basis for the crack growth model shown schematically in Figure 15. This figure follows the development of a weld toe crack as it grows around the brace and through the chord wall.

As a result of micro-crack coalescence and growth, assume that a small semi-elliptic crack of high aspect ratio (about 0.5) has formed and is not immediately next to another small semi-ellipse. At this stage the differences between axial and bending are not important and the single crack develops along the line 0-1. At this point interaction and coalescence with a like crack occurs and the crack develops along the line 1-2. At 2 it has a semi-elliptic shape and develops as a single crack until 3 when interaction and coalescence occurs again. At 4 it has a semi-elliptic shape and it again develops as a single crack. During this next phase of single crack growth, the difference between bending and axial loading becomes apparent. The extent of the highly stressed weld toe region around the brace is much larger for the in-plane bending case so the probability of further interaction and coalescence is higher for in-plane bending. This occurs from 5-6; at 6 the crack has a semi-elliptic shape but by now its aspect ratio is low so growth of this single crack increases the aspect ratio (Wildshut observed this type of growth in his single crack tests [16]). At 7, interaction and coalescence start again; this ends at 8 and the sequence of single crack growth and coalescence continues along the path 8, 9, 10, 11, 12, 13, 14, 15 and 16. After 16, coalescence is no longer a significant event and the aspect ratio gradually increases.

Since the extent of the highly stressed weld toe region around the brace is smaller for axial loading the path followed is 4-5', 5-6', 6-7', etc. After 13', coalescence is no longer a significant event and the aspect ratio gradually reduces.

The behaviour between 13' and 14' (axial load) and between 16 and 17 (in-plane bending) is not easily explained. For example Figure 14 shows two flat plate solutions for semi-elliptic cracks in a membrane/bending stress field where $\sigma_m/(\sigma_m + \sigma_b)$ is 0.25. The starting points for these solutions are on the experimental curves at a/T of 0.3. These starting points were chosen because Figure 6 indicates that M_k is not changing when $a/T \geq 0.3$. However, M_{ks}/M_k is greater than unity so the weld is still having some effect on surface growth. This effect must explain some of the difference between the flat plate solutions and the experimental curves. For both types of loading the surface growth rates along the surface should be higher than those predicted for the flat plate so the flat plate

solutions should lie above the sets of experimental data. This is the case, but the differences are such that it is tempting to argue that load redistribution is the factor not considered! Since load redistribution is easily invoked but very difficult to quantify or handle in life predictions, it is expedient to try to empirically define a forcing function for aspect ratio. Some of the options are shown schematically on the inset diagram on Figure 15.

The relationship between a/2c and a/T should be AB'C' for axial loading and ABC for in-plane bending. However these paths do not recognize that coalescence may occur very rapidly in a bad weld bead, so lower bound relationships D'B'C' or DBC may be more appropriate when using LEFM analyses to generate S-N curves for tubulars. Defining these lower bound relationships would avoid the need to calculate M_{ks}, which as mentioned earlier is likely to be much less accurate than M_k. Also, as shown on Figure 8, single crack models, experimental or theoretical, that do not allow coalescence, have aspect ratio changes that are unlikely to model reality.

If single crack solutions are used without a forcing function for aspect ratio, their predictions of aspect ratio development should always be checked. Too often a comparison of predicted and experimental life is the only measure of performance for a model and this can be very misleading since scatter always clouds the experimental picture.

Applications will now be considered. It will be convenient to start with deterministic models; then discuss two papers on probabilistic models and conclude with a very brief discussion on fracture.

5. FATIGUE CRACK PROPAGATION LIFE -- DETERMINISTIC APPROACH

5.1 Plate-Plate Joints

These have been used extensively in the fatigue programs discussed at this conference. LEFM analyses have been used to interpret and supplement experimental studies of the effect of plate thickness on fatigue life. Most of these experiments have used specimens with the same thickness for the 'base' plate and welded attachments. A survey by Bainbridge [47] of 19,494 tubular brace-to-chord intersections in North Sea structures shows that the trend is for the brace to chord thickness ratio to decrease with increasing chord thickness. Several authors have used LEFM models to investigate the effect of this thickness ratio on fatigue performance.

5.1.1 Edge Crack Models

Dijkstra et al [15] have used their estimates of M_k, see Table 1, in LEFM analyses of the effect of plate thickness on propagation life, N_p, for a T-plate geometry with plates of equal thickness. They conclude that their M_k estimates and equation (1) give life predictions in good agreement with their experiments on T-plates with edge notches. Their calculations show a decrease in N_p with increase in plate thickness but the thickness effect is less pronounced than the experimental effect reported by others. They say that this is probably due to the 3-D crack growth in real specimens and due to initiation (N_i) effects.

These authors also discuss the influence of initial crack size and weld toe radius on life predictions. As mentioned earlier, life predictions based on initial crack sizes less than 0.5 mm are suspect because they ignore crack closure; it is not clear from our preliminary copy of TS 52 whether their comments on weld toe radius effects are based on a_i values smaller or larger than 0.5 mm.

As mentioned earlier I.J. Smith [18] has used finite element techniques to estimate K_I for edge cracks in single-sided transverse attachments of varying thickness made with full penetration welds. In other words, the specimen geometry was that shown in Figure 1(a). Estimates of M_k, eg. Table 2, were used to asess the influence of 1) variation in attachment thickness for a fixed thickness of the load-carrying plate or 2) variation in thickness of the load-carrying plate for a fixed attachment thickness. An initial defect depth of 0.2 mm was assumed. This arbitrary assumption is not likely to mirror the real problem; there is ample evidence that fatigue cracks of this depth at weld toes are likely to be semi-elliptic and dispersed randomly along the weld, eg. see Figure 3 in paper TS 3. Models based on semi-elliptic cracks will now be discussed.

5.1.2 Semi-Elliptic Cracks

As mentioned earlier, Burdekin et al [25] have used the O-integral, equation (10), to determine stress intensity factors for semi-elliptic surface flaws in various specimens. One phase of their work was to determine crack growth development in flat plates with different combinations of bending and membrane stress, using equation (1) with equation (10) or with Newman and Raju solutions [24]. Another phase of their work was to use the integral equation (10) to determine K_I for cracks in T-butt weld

geometries having a range of attachment to main plate thickness ratios. Fatigue lives, N_p, were calculated for various initial flaw sizes, often less than 0.5 mm, with a sensitivity study on the effects of the constants assumed in the Paris equation (1); they assumed that these constants were linked by the equation suggested by Gurney [49]. These authors present theoretical and experimental data for crack development in flat plates but do not include any details of the theoretical crack development predicted for semi-elliptical cracks in T-butt welds. It would be very interesting to superimpose their predictions on Figures 7 and 8.

As discussed earlier, the experimental data on Figure 7 is the basis for a so-called multi-crack model developed by Vosikovsky et al [33] for predicting N_p for T-butt welds loaded as shown in Figure 1(b). In this conference, Bell et al [17] used this model with equation (1) to predict the effect of thickness on T-joints having attachment and main plates of the same thickness. In these predictions, any effects of weld toe radius were ignored, the initial defect size was 0.5 mm, and the initial crack shape was semi-circular. As mentioned earlier, this multiple crack model recognizes that T-plate fatigue specimens have a finite width and that the crack eventually reaches one or both free edges (sides). In paper TS 3, Mohaupt et al [34] point out that this free edge effect may exaggerate (confuse) the effect that plate thickness has on fatigue life. Table 2 in paper TS 3 shows the incidence of this edge cracking; it is clearly a problem for the thicker specimens. Figure 16 shows the crack growth versus cycles data for one of these thicker specimens, tested with a hot spot stress range of 100 MPa. The approximate end of the coalescence phase is shown by a^*, N^* and the onset of edge cracking by a_E, N_E. Equation (1) and three simple models, (1), (2) and (3) on Figure 16, have been used by R. Yee [61] to quantify the difference between the actual edge crack growth and the semi-elliptic growth that would likely have occurred beyond a_E if the same crack had developed in a much wider plate. In the semi-elliptic model (2) the aspect ratio was held constant; in the semi-elliptic model (3) the surface length was held constant. In all cases the calculations were terminated at a/T of 0.5.

For all three specimens analysed, see Table 3, the agreement between model (1) growth beyond a_E and experimental growth was very good. The predictions of growth beyond a_E using models (1), (2) and (3) have been used to correct the measured values of propagation, N_p, and total, N_T, life. The corrected values, N_{p1}, N_{p2}, N_{p3}, N_{T1}, N_{T2}, N_{T3} have been used to calculate corrected ratios of initiation/total life and propagation/total life for comparison with the experimental ratios N_i/N_T and N_p/N_T, see Table 3. These calculations indicate that using a wider specimen (i.e. reducing the chance of the crack propagating to the free edges) might have raised the ratio of N_p/N_T by about 4 to 6 points above the measured values of 68.6 to 79.6%.

These experimental and corrected experimental estimates of propagation/total life for 52 and 78 mm thick T-plate specimens can be compared to the data obtained by Berge et al [50] for 20, 100 and 150 mm T-plate specimens. In their paper, TS 45, they report that they used an ACPD technique to monitor crack growth, after crack initiation had been detected by applying soap water. For their 20 mm thick specimens, N_p/T_T ranged from 64 to 81%. For their 100 mm specimens, N_p/N_T ranged from 67 to 96%. For their 150 mm specimens, N_p/N_T ranged from 81 to 90%. Overall, with the exception of one specimen, their values of N_p/N_T ranged from 64 to 90% compared to Vosikovsky et al's [33,34] uncorrected values of about 69 to 80%. In other words this small set of data, uncorrected or corrected, lies within the range measured by Berge et al [50], using a somewhat wider specimen and a different technique to detect initiation.

All of this data emphasizes the dominance of the crack propagation phase. To interpret this phase Berge et al assumed an initial defect size of 0.5 mm and initial aspect ratio of 0.6. These assumptions and the change of aspect ratio with crack depth were based on experimentally measured shapes. No details are given in TS 45 other than that the aspect ratio after coalescence was in the range of 0.1 to 0.2; it seems likely that they used a multiple crack model similar to that used by Bell et al [17] except that it was not necessary with their wider specimens to allow for propagation to the free edges.

Their stress intensity factors were calculated using the solutions of Newman and Raju [24] for plates with a magnification factor. This magnification factor was calculated using the weight function technique of Petroski and Achenbach [32], a 2-D finite element analysis of the uncracked weld and K_t values based on parametric formulae derived from photoelastic results. Few details are given in TS 45 but it would be interesting to compare their values of M_k with those predicted by the more rigorous K_I analysis of Niu and Glinka for like geometries [21,22].

Berge et al [50] assumed that weld root

radius is independent of the weld size or plate thickness so K_t increases with plate thickness. To account for operation in seawater rather than in air they changed the constants in the Paris equation from m=3.1, $C = 5 \times 10^{-12}$ to m = 3.5, $C = 6.0 \times 10^{-12}$ (units of MPa and m). For both environments, their numerical results are somewhat conservative but correctly predict the effect of increasing plate thickness on the fatigue of these full penetration welded T-joints.

A paper by Eide and Berge [51] in this conference (TS 7) discusses the fatigue performance of large scale plate girders with thicknesses of 20, 40 and 60 mm. Paper TS 7 includes a brief outline of a fracture mechanics analysis of the fatigue cracks that developed along the toe of the stiffener plate welds, close to the end of the stiffeners. A detailed description of the growth of these fatigue cracks through the thickness of the weld plate is given in another recent paper by these authors [52]. Since this stage of growth occupied about 90% of the total fatigue life of these girders and smaller scale girders tested by others, their LEFM analysis only considered this stage of growth. Fatigue cracks initiated at various sites along the weld toe with coalescence occurring at a crack depth of 5 mm, independent of plate thickness. The semi-elliptic crack produced by coalescence became slightly unsymmetrical as it grew through the web thickness because of the stress gradient along the stiffener weld.

The crack shape development was described by two equations

$$2c = 3.0\,a + 0.97 \quad \text{for} \quad a < 5 \text{ mm} \quad (11)$$

and

$$2c = 2.34a + 10.76 \quad \text{for} \quad a > 5 \text{ mm} \quad (12)$$

The physical surface length of deep cracks was somewhat larger than described by equation (12) due to the unsymmetrical shape. The authors argue that the important measure of ellipticity is the curvature of the crack front at the deepest point so equation (12) is adequate.

The stress intensity factor was calculated by an influence function methd using

$$K_I = \sigma(\pi a)^{1/2} F_S F_T F_W F_E F_G \quad \ldots \quad (13)$$

where F_S is a free surface correction factor
F_T is a finite thickness correction factor
F_W is a finite width correction factor
F_E is an ellipticity correction factor
and F_G is a stress gradient correction factor

It appears that the factors F_S, F_T, F_W and F_E were derived in a manner akin to that used by Maddox [53] and by Albrecht and Yamada [54]. The stress gradient correction factor, F_G, was calculated from the stress distribution (no crack) across the crack plane by means of an influence function method based on a point load model [55]. The 'no crack' stress distribution was calculated using a 2-D finite element method.

The girders were subjected to a block loading program resembling the general shape of stress spectra for marine structures. Variable amplitude fatigue lives were predicted by numerical integration using the equivalent constant amplitude stress range approach, i.e. interaction and threshold effects were ignored.

The authors found that scatter in experimental data could be accounted for in LEFM predictions by assuming mean values of weld geometry parameters and a scatter in initial defect size in the range 0.05 to 0.4 mm. A significant effect of plate thickness on fatigue life was found experimentally and predicted by LEFM analyses. An examination of their LEFM predictions (see Figures 8-10 in [52]), shows that assuming an initial defect size of 0.4 mm produced close to a lower bound for the 40 and 60 mm plate results. This and our previously mentioned concerns about closure effects for weld cracks smaller than about 0.5 mm suggests that an initial defect size of about 0.5 mm might be a wise choice for LEFM calculations based on the Paris equation (1).

So far all of the applications reviewed have been for non-load-carrying or load-carrying attachment plates transverse to the main load-carrying plate. A recent paper by I.F.C. Smith and T.R. Gurney [56] discusses how attachment height, length, and width influence the fatigue life of fillet welded, longitudinal stiffeners on plates in tension. A 3-D elastic finite element method was used to calculate the "no crack" stress field and the influence function method of Albrecht and Yamada [54] was used to calculate K_I. It should be mentioned here that this method is akin to deriving a weight function for a plate containing a central through-thickness crack and adding correction factors equivalent to F_S, F_T, F_W and F_E in equation (13), to obtain K_I for a semi-elliptic crack.

In their LEFM calculations they used equation (1) and the following equations to describe crack shape development

$$2c = 9.29\,a \quad \text{for} \quad a \leq 1 \text{ mm} \quad \ldots \quad (14)$$

and

$$2c = 6.71 + 2.58\,a \quad \text{for} \quad a > 1 \text{ mm} \quad (15)$$

An initial crack depth of 0.15 mm was assumed. They say that this LEFM procedure

predicted total lives that were well below experimentally observed values. The authors say that "it is probable that this is largely due to the fact that the Paris law (equation (1)) overestimates the very slow growth rates that occur in welded joints with cracks that are very small [57]". In other words one must either develop an equation such as equation (3), see paper TS 50, or start with a larger initial defect, say 0.5 mm; use equation (1) to calculate N_p and accept that N_i must be calculated by other means [63] or assumed to be some percentage of N_p for different classes of joint.

For tubular joints it is often argued that N_i is very small and attention is focussed on N_p; however analysts often use very small initial defects for their calculations without using a more sophisticated form of the crack growth equation. Some methods for assessing N_p for tubular joints will now be reviewed.

5.2 Tubular Joints

As mentioned earlier, Van Delft et al [47] have published crack growth data for a T-tubular joint, B3, tested in the second phase of the ECSC program. To model the observed crack growth behaviour, see Figure 14, they modified formulae for semi-elliptical cracks in an infinite plate subjected to tension or bending [58]. The influence of the weld toe geometry was taken into account by applying magnification factors, M_k, derived by Maddox [59] for an edge crack in a non-load carrying T-joint with tension in the main plate. These values of M_k were applied to both the membrane and the bending solutions for flat plates. In addition it was assumed that the extrapolated value of M_k at a=0 (nominally equal to K_t) could be used to obtain K_I values at the free surface of the semi-elliptic crack i.e. $M_k(a=0) = M_{ks}$.

To allow for the small crack problem mentioned earlier, the depth (length) correction factor (ℓ_o) developed by El Haddad and Topper [60] was applied to equation (6) i.e.

$$K_I = M_k \, M\sigma(\pi(a+\ell_o))^{1/2} \quad \ldots \quad (16)$$

where

$$\ell_o = \frac{1}{\pi}\left(\frac{\Delta K_{th}}{\Delta \sigma_e}\right)^2 \quad \ldots \quad (17)$$

and $\Delta\sigma_e$ is the fatigue limit of the material in the unnotched situation.

Equations (16) and (1) were then used to calculate increments of crack growth along the free surface and at the deepest point for a semi-elliptic crack. In some calculations the surface growth rates were reduced by 10% to conform with observations reported for semi-elliptic cracks by Newman and Raju [24].

The membrane and bending stress components of the hot spot stress range were obtained assuming that σ_m/σ_b was 1/3; a value supported by finite element and photoelastic tests for this type of joint. These membrane and bending components of the hot spot stress range were used in the calculation of K_I, see equations (7) and (8). The authors argue that the reduction in $\sigma_m + \sigma_b$ that occurs away from the hot spot tends to negate an effect of the finite width so they did not include a finite width correction factor.

Their approach appears to correctly predict the experimentally observed crack shape development, see Figure 11 in [47], and propagation life. The effect of excluding the correction factor, ℓ_o, and the 10% reduction in surface growth is not very significant. Their decision to set $M_{ks} = M_k(a=o)$ for an edge crack was prompted by a lack of information on magnification factors (M_{ks}) for the free surface. This decision is probably responsible for the apparent success of this single crack model, which does not recognize coalescence. Figure 6 shows that it is not reasonable to assume that M_{ks} is a fixed value so it would be unwise to assume that their approach would work for other modes of loading and geometries. This should be checked.

In our opinion a forcing function should be used for aspect ratio since this allows for coalescence and avoids the need to calculate the magnification factor, M_{ks}. This is the approach adopted by Connolly and Dover in a very recent paper [62]. Their forcing functions for all modes of loading and geometries considered are based on experimental observations. All of the forcing functions have the same general shape as DBC on the inset diagram on Figure 15.

These forcing functions are used in [62] with equation (1) and the weight function equation (10) to predict N_p. Stress intensity factors predicted by equation (10) were corrected for free surface effects using the method described earlier [30] but a finite width correction was also included. This correction was calculated assuming the crack in a tubular joint is analogous to a crack in a flat plate of width equal to half the tube circumference. For large a/T this finite width correction tends to increase K_I. However, it must be emphasized that these authors considered the stress distribution around and through the intersection when using equation (10), and this will tend

to reduce K_I below estimates based only on hot spot stresses [26].

Their results and the work of Burdekin et al [25] emphasize the significance of the ratio of membrane to bending stress when calculating N_p. This significance has not been recognized by Hudak et al [12] in their model for estimating N_p. Their equation for estimating the 'no crack' stress field gives a distribution that is not representative of distributions in tubular joints. Their equation is

$$\sigma_r(x=a) = S_{rHS}\{1+(K_t-1)\exp[-35(K_t-1)a/T]\} \quad \ldots (18)$$

This equation for $\sigma_r(x=a)$ tends to the hot spot stress value (S_{rHS}) as a/T increases. This effectively ignores bending; it appears that values of $\sigma_r(x=a)$ are substituted as σ_m in the Newman and Raju equation [24]. For most values of a/T, this approach will seriously overestimate K_I as these authors found, see Figure 11 in [12].

Although Hudak et al [12] did not include coalescence in their model, they do discuss it and present a schematic in their paper that is very similar to ABC on the inset figure on Figure 15. This figure and the previous discussion emphasizes the random nature of the fatigue initiation process and the transition from micro-cracks by coalescence to a dominant semi-elliptic crack. This and the uncertainty about the wave loading that a structure will experience naturally leads to a probabilistic approach for determination of fatigue life. This will now be briefly considered.

6. FATIGUE CRACK PROPAGATION LIFE -- PROBABILISTIC APPROACH

6.1 Plate-Plate Joints

Engesvik and Moan [55] have published a probabilistic analysis of the uncertainty in the fatigue capacity of welded joints. Their predictions are for the weld and crack geometry of non-load-carrying fillet welded, cruciform joints that had been subjected to constant amplitude loading with tension in the main plate. A Monte Carlo simulation procedure was used to reflect the uncertainties associated with the parameters in a fracture mechanics model of fatigue. This fracture mechanics model was based on equation (1), i.e. no threshold and crack closure effects were considered. For the cruciform joint considered, the weld toe angle (θ), radius of curvature at the weld toe (ρ), and the initial crack depth, a_i, were the significant geometrical parameters.

Measurements of weld geometry for their test specimens were analysed using four distribution functions. Of these a three parameter Weibull and a two parameter log normal distribution gave the best fit to the data for weld toe angle. The same four distribution functions were fitted to the data on weld toe radius; a two parameter Weibull distribution gave the best fit. In the simulation studies, a two parameter log normal distribution was used for weld angle and a conditional, two parameter Weibull distribution was used for weld toe radius.

Two models for the variability in a_i were used in the simulations: a two parameter log normal distribution or a shifted exponential distribution. The authors emphasize that the data base used to determine statistical parameters for a_i is far from ideal and so the choice of distribution is uncertain.

Measurements of the crack growth parameters, m and C, for the Paris equation were obtained from three-point bending tests for stress-relieved HAZ material. A log normal distribution was used to fit data for m. For a particular value of m, the other parameter, C, was obtained from a deterministic equation

$$\log C = -6.177 - 1.603\, m \quad \ldots (19)$$

In some of the Monte Carlo simulations all but one of the base variables, θ, ρ, a_i and m were held constant, i.e. given mean values, and a random sample of 500 was used to investigate the effect of the other variable on fatigue life. In some of the simulations, all basic variables were allowed to vary randomly and a sample size of 1000 was used to assess the variability in fatigue life.

Failure was defined as the crack depth, a_f, at which net section yielding was predicted. K_I was estimated using equation (13) with one additional factor; a plasticity correction factor. They say that in their computations, "crack coalescence was synonymous with the transition from surface crack ($a/2c > 0$) to edge crack ($a/2c = 0$)". Their forcing function for growth of a semi-elliptic crack was based on experimental observations. The maximum observed depth of surface (semi-elliptic) cracks was about 3 mm with an aspect ratio of about 0.16. Their model for crack shape development can be considered to be a 'worst case' form of the 'single crack' and 'multiple crack' models shown on Figure 7. Single cracks with initial aspect ratios of 0.3 to 0.4 develop and become single cracks with aspect ratios of 0.16. At a small ratio of a/T (about 0.1), without prior interaction, the single cracks coalesce to form an edge

crack.

In this study the experimental lives, N_T, varied from 323,960 to 1,191,670 cycles in a sample of 42 specimens. The simulated lines, N_p, varied from 56,280 to 22,469,216 cycles in a sample of 1000 specimens. The simulated mean life was 609,153 which was 8% less than the experimental mean. The simulation studies also showed that the likely order of importance of the basic variables is weld geometry, initial crack size and then material properties, C and m.

This study only considered constant amplitude loading; the next section considers the much more complex problem of spectrum loading of tubular joints.

6.2 Tubular Joints

In paper TS 57 Bergez, Lebas and Samier [63] outline a method for computing the probability of failure of a tubular node. The method considers fatigue crack initiation, fatigue crack propagation and instability. The boundary between initiation and propagation is defined as the appearance of a visual crack.

They first consider the probability of initiation of a fatigue crack at points 1, 2, 3, etc. along the weld at the intersection of a brace and chord. This probability is based on a Monte Carlo simulation, which in turn is based on a statistical study of the scatter of results for tests on cruciform joints and a damage summation for variable amplitude loading [64].

They assume that a crack will appear at a point when the probability of initiation at that point reaches a critical value. Their choice of a value for the depth of these initial cracks, a_i, is based on observations made during the French program of tests on tubular joints [45] and the recommendations of Amiot, Putot and Radenkovic [65]; in particular, a_i of 1 mm for small tubulars (nodes), 2 mm for medium nodes and 3 mm for large nodes. They admit the need for a distribution function to describe a_i but don't have the necessary information.

Once a crack has initiated at a point, n, its growth through the chord thickness is predicted using a variation of equation (1) for a 'plane strain' slice through the wall at point n.

The Paris equation is not used to simulate surface growth. Instead it is assumed that surface growth from slice n will occur when a crack is initiated at slice n-1 or n+1. This mixture of initiation and propagation will generate an irregular crack along the wall. As this irregular crack develops, 'stress redistribution' is assumed to occur. A redistribution function is proposed [65] which, as the crack propagates, will tend to reduce the irregularity along the front. This redistribution function has the same effect as a weight function but it defines an "effective" stress acting on a particular slice, thereby changing K_I along the irregular front. Particular values of K_I are calculated using this effective slice stress and a line-spring method.

During the propagation analysis for slice n it is assumed that 'slice' instability will occur when net section yield occurs (plastic instability) or when $K_{Imax} > K_{Ic}$. Since K_{Imax} is a function of the wave distribution, it is possible to define a probability of instability in the through thickness direction.

This scheme for surface growth does not permit unstable growth along the weld. Only when the crack is through the thickness is it likely that general instability will occur so this phase is handled separately but no details are given.

This scheme for surface growth could be modified to consider smaller sizes for the initiated crack (at present a_i/T varies from 0.05 to 0.13), and the growth and coalescence of semi-elliptic cracks. The initiated crack could be assumed semi-elliptic as in other models. Independent growth within a slice could be calculated using equation (1) and values for M_k and M_{ks}. Coalescence could be invoked when any single crack reaches its slice boundaries and there is another semi-elliptic crack in an adjacent slice. This local coalescence will produce a bounding semi-ellipse with surface length equal to two slices. This modification would also permit consideration of surface growth when coalescence is no longer a significant event, i.e. when a/T is about 0.4 in our experience. This modification would also avoid the need to consider the growth of an irregular crack front using a stress redistribution function.

Paper TS 57 concludes with a sample calculation for a T node on a platform subjected to North Sea wave spectra. Another paper in this conference, TS 56 by Snijder, Dijkstra and ter Avest [66], describes a probabilistic approach for assessing the risk of fatigue failure leading to brittle fracture in tubular nodes. In their case the sample calculation is for a tubular joint in the Eastern Scheldt Storm Surge Barrier, since the steel used in some joints has a coarse grain structure and brittle fracture due to a peak load is a risk that must be assessed.

Their reliability function for fatigue followed by brittle fracture is defined as the difference between the crack depth at which brittle fracture occurs (a_{bf}) and the crack depth caused by fatigue, (a_{fat}) i.e.

$$z = a_{bf} - a_{fat} \quad \ldots \quad (20)$$

Their LEFM approach for determining a_{fat} has already been discussed herein; see discussion of paper by Van Delft et al [47] in section 5.2. For this risk assessment, the factors m and C in the Paris equation (1) are assumed to have mean values of 2.8 and 0.8833×10^{-12} (N, mm). The factor m is assumed deterministic and a log-normal distribution is used for C.

The stress spectrum is represented using an equivalent constant amplitude stress range which is calculated from the spectrum using Miner's rule. Two classes of initial defect are considered using an equation

$$c_i = F_{ac}\, a_i \quad \ldots \quad (21)$$

For undercut defects it is assumed that the initial crack depth, a_i, is uniformly distributed between 0 and 1 mm and that F_{ac} is normally distributed. For slag inclusions the initial defect is assumed normally distributed and F_{ac} is deterministic. The crack depth, a_N, of this semi-ellipse after N cycles is then transformed into an equivalent 'constant depth' surface crack which is a_{fat} required for equation (20).

The model for determining a_{bf} is based on the CTOD approach. The crack depth, a_{bf}, at which brittle fracture occurs depends on the strain level at the hot spot in the tubular joint and on the fracture toughness expressed as a critical CTOD. Some reservations about the design curve from BSI PD6493 (1980) are expressed because the results of some full scale fracture tests on cracked tubulars lie very close to the design curve whereas wide plate tests indicate that the design curve is conservative. For their probabilistic approach, a mean line through a collection of test results is used with an uncertainty factor and a correction which considers all CTOD values rather than minimum values.

The hot spot strain, ε, is the sum of two components. One (ε_1) is caused by wave loads and water level differences across a gate; the other, (ε_2), is an assessment of residual stresses due to welding.

Their level II reliability calculations for an undercut defect indicate that the failure probability per year is 1.9×10^{-5}. It is important to note that 90% of the variance of z is determined by the brittle fracture model, see Table 1 in TS 56. For a slag inclusion defect, assuming a 1% probability of occurence of such a defect at the hot spot, the probability of failure is 1.6×10^{-5}. It is shown that not using material with CTOD values below 0.1 mm leads to a factor of ten reduction in these failure probabilities.

In a recent paper [67], Burdekin and Thurlbeck present another methodology for 1) determining the acceptability of a surface, semi-elliptic defect at the weld toe of a T-tubular joint under axial load or 2) determining the toughness requirements for a material for a particular design. Three test results for a large scale tubular are analysed using their so-called unit K method. The authors point out that the existing methods in BSI PD6493 calculate critical CTOD or K values based on tension stress only whereas their unit K method incorporates bending and will tend to reduce toughness requirements.

Paper TS 55 by Denys [68] considers another major aspect that must be considered when setting toughness requirements -- the control and design of the laboratory tests used to determine the material CTOD or other toughness parameters.

Denys considers the problem of assessing the significance of the local brittle zone (LBZ) revealed in CTOD testing of welded low alloyed, low C-Mn steels. In particular Denys addresses the problem of fatigue precracking of wide plate test specimens so that the fatigue crack samples a representative amount of the LBZ regions. He argues that the chance of success of sampling these regions can be enhanced by using a multiple, zig-zag starter notch. This zig-zag recognizes that the weld-bead contour and consequently the position of the coarse grained HAZ varies considerably along the weld length. He reports that variations of more than 1 mm are not uncommon and discusses the tendency of fatigue cracks to curve away from the LBZ regions.

In writing this paper, we have concentrated on sub-critical growth due to fatigue loading. The papers on probabilistic assessment of life of tubular joints introduce the problem of defining final failure because of plastic instability and/or fracture. The paper by Denys introduces one of the current concerns about defining the toughness of the material. It is beyond the scope of this paper to delve more deeply into the 'final failure' area. However some of the issues are addressed in a recent report of the Ship Structures Committee [69] on fracture control for fixed offshore structures.

7. CONCLUSIONS

In the interim since the 1981 Paris conference, more information has become available on the initiation and coalescence of fatigue cracks at weld toes of plate-to-plate and tubular joints. LEFM models developed to predict the propagation or residual life of such joints are based on variants of the Paris-Erdogen crack growth equation. All except one of the models reviewed herein consider the development of a semi-elliptic defect, with some mechanism that allows for aspect ratio changes produced by crack growth and coalescence. This mechanism and the effects on K_I of stress variation around a tubular intersection require more study. Nevertheless the results of deterministic and probabilistic assessments of fatigue life and/or risk of failure indicate that existing models are already useful aids when assessing the significance of defects.

8. ACKNOWLEDGEMENTS

Drs. Bell, Vosikovsky, Glinka and Dover very kindly provided advance copies of papers and/or data to be published elsewhere. J. Forbes, R. Yee and J. Otegui provided data from research projects that will eventually be summarized in theses. The kind efforts of L. Lingard, E. Spike and J. Wright in the preparation of this manuscript are gratefully acknowledged.

9. REFERENCES

[1] Radenkovic, D.: "Stress Analyses in Tubular Joints", International Conference: Steel in Marine Structures, 5-8 October 1981, Paris, Plenary Session PS 1.

[2] Paris, P. and Erdogan, F.: "A Critical Analysis of Crack Propagation Laws", Joun. Basic Engng., Dec. 1963, pp. 528-534.

[3] Connolly, M.P.: "A fracture mechanics approach to the fatigue assessment of tubular welded Y and K-joints", Ph.D. Thesis, University of London, 1985.

[4] Topp, D.A. and Dover, W.D.: "Validation of Crack Sizing and Detection Techniques for Offshore Structures", BINDT (British Institute for Non-Destructure Testing), Annual Conference, September 1986, Newcastle.

[5] Lambert, S.B., Mohaupt, U.H., Burns, D.J., and Vosikovsky, O.: "Simulation of Fatigue Behaviour of Tubular Joints Using a Pipe-to-Plate Specimen", Proc. of this Intnl. Offshore Conf. Steel in Marine Structures, Delft, 1987, paper TS 18.

[6] Walker, E.F.: "Effect of Marine Environment", Ibid 1, Plenary Session PS 4.

[7] Schütz, W.: "Procedures for the Prediction of Fatigue Life of Tubular Joints", Ibid 1, Plenary Session PS 5.

[8] Forman, F.G., Kearney, V.E. and Engle, R.M.: "Numerical Analysis of Crack Propagation in Cyclic Loaded Structures", Journal of Basic Engineering, Sept. 1967, pp. 459-564.

[9] "Fatigue Handbook: Offshore Structures", Almar-Naess, A. editor, Tapir 1985, pp. 204-207.

[10] Austen, I.M., and Walker, E.F.: "Corrosion Fatigue Crack Growth Rate Information for Offshore Life Prediction", Ibid 5, paper TS 50.

[11] Saxena, A., Hudak, S.J. and Jouris, G.M., "A Three Component Model for Represdenting Wide Range Fatigue Crack Growth Data", Engineering Fracture Mechanics, Vol. 12, 1979, pp. 103-115.

[12] Hudak, S.J., Burnside, O.H., and Chan, K.S.: "Analysis of Corrosion Fatigue Crack Growth in Welded Tubular Joints", Transactions of the ASME, Vol. 107, June 1985, pp. 212-219.

[13] Burnside, O.H., Hudak, S.J., Oelkers, E., Chan, K., and Dexter, R.J.: "Long-Term Corrosion Fatigue of Welded Marine Steels", Ship Structure Committee report SSC-326, 1984.

[14] Maccary, R.R., "A Technical Basis for Characterizing Flaws Detected by preservice and inservice examinations of Nuclear Power Plant Components", ASME Journal of Pressure Vessel Technology, Nov. 1975, pp. 322-326.

[15] Dijkstra, O.D., Snijder, H.H., Overbeeke, J.L., and Wildschut, H.: "Prediction of Fatigue Crack Growth for Welded Joints Using Stress Intensity Factors Determined by FEM Calculations", Ibid 5, paper TS 52.

[16] Wildshut, H., Overbeeke, J.L., Snijder, H.H., and Dijkstra, O.D.: "Fatigue Crack Development and Stress Intensity Factors in Specimens with the Shape of Weldments", Ibid 5, paper TS 51.

[17] Bell, R., Vosikovsky, O., Burns, D.J. and Mohaupt, U.H.: "A Fracture Mechanics Model for Life Prediction of Welded Plate Joints", Ibid 5, paper TS 53.

[18] Smith, I.J.: "Stress Intensity Factors for Toe Defects in Single-Sided Transverse Attachments of Varying Thickness made with fully penetrating Welds", International Institute of Welding. Document No. XIII-1177-85.

[19] Bell, R. and Kirkhope, J.: "Determina-

tion of Stress Intensity Factors for Weld Toe Defects", Phase I, DSS Contract OSU82-00233 Report, April 1984.
[20] Bell, R.: "Determination of Stress Intensity Factors for Weld Toe Defects", Phase II, DSS Contract OST 84-00125 Report, October 1985.
[21] Niu, X. and Glinka, G.: "The Effect of Weld Geometry on Stress Intensity Factors and Fatigue Crack Growth in Welded Joints", Intl. Conf. on Fatigue of Welded Constructions, Brighton, U.K., 7-9 April 1987.
[22] Niu, X. and Glinka, G.: "The Weld Profile Effect on Stress Intensity Factors in Weldments", Submitted to International Journal of Fracture, 1986.
[23] Mattheck, C., Morawietz, P., and Munz, D.: "Stress Intensity Factor at the Surface and at the Deepest Point of a Semi-Elliptical Surface Crack in Plates Under Stress Gradients", International Journal of Fracture, Vol. 23, No. 2, 1983, pp. 201-212.
[24] Newman, J.C., Jr. and Raju, I.S.: "An Empirical Stress Intensity Factor Equation for the Surface Crack", Engineering Fracture Mechanics, Vol. 15, No. 2, 1981, pp. 185-192.
[25] Burdekin, F.M., Chu, W.H., Chan, W.T.W. and Manteghi, S.: "Fracture Mechanics Analysis of Fatigue Crack Propagation in Tubular Joints", Intnl. Conf. on Fatigue and Crack Growth in Offshore Structures, 7-8, April 1986, I Mech E C133/86.
[26] Dover, W.D. and Connolly, M.: "Fatigue Fracture Mechanics Assessment of Tubular Welded Y and K-joints", Ibid 25, I Mech E C141/86
[27] Oore, M, and Burns, D.J.: "Estimation of Stress Intensity Factors for Embedded Irregular Cracks Subjected to Arbitrary Normal Stress Fields", ASME Journal of Pressure Vessel Technology, Vol. 102, May 1980, pp. 202-211.
[28] Khattab, M.A.A., Burns, D.J., Pick, R.J. and Thompson, J.C.: "Opening Mode Stress Intensity Factors for Embedded Rectangular and Irregular Planar Defects", ASME Journal of Pressure Vessel Technology, Vol. 108, Feb. 1986, pp. 41-49.
[29] Khattab, M.A.A., Burns, D.J., Thompson, J.C., and Pick, R.J.: "An Integral Technique to Evaluate Opening Mode Stress Intensity Factors for Embedded Planar Cracks of Arbitrary Shape", Canadian Society for Mechanical Engineering, 1985, Vol. 9, No. 1, pp. 1-10.
[30] Oore, M., and Burns, D.J.: "Estimation of Stress Intensity Factors for Irregular Cracks Subjected to Arbitrary Normal Stress Fields", Proceedings of the 4th International Conference on Pressure Vessel Technology, London, I Mech E 1980, Vol. 1, pp. 139-147.
[31] Grueter, L., Huget, W., and Kylla, H.: "Weight Functions and Stress Instensity Magnification Factors for Elliptical and Semi-Elliptical Cracks under Variable Normal Stress," Interatom Report INTAT No. 32.05095.0, May 1981
[32] Petroski, H.J. and Achenbach, J.D.: "Computation of the Weight Function from a Stress Intensity Factor", Engineering Fracture Mechanics, Vol. 10, No. 2, 1978, pp. 257-266.
[33] Vosikovsky, O., Bell, R., Burns, D.J., and Mohaupt, U.H.: "Fracture Mechanics Assessment of Fatigue Life of Welded Plate T-Joints Including Thickness Effect", 4th Intnl. Conf. on Behaviour of Offshore Structures, BOSS 85, J.A. Battjes editor, Elsevier Science Publishers B.V., Amsterdam, 1985, pp. 453-464.
[34] Mohaupt, U.H., Burns, D.J., Kalbfleisch, J.G. Vosikovsky, O., and Bell, R.: "Fatigue Crack Development, Thickness and Corrosion Effects in Welded Plate to Plate Joints", Ibid 5, paper TS 3.
[35] Verreman, Y., Bailon, J.P., and Masounave, J.: "Fatigue Short Crack Propagation and Plasticity-Induced Crack Closure at the Toe of a Fillet Welded Joint", 1st Intnl. Symposium on the Behaviour of Short Fatigue Cracks, University of Sheffield (U.K.), Sept. 26-28, 1985.
[36] Otegui, J.: private communication.
[37] Bell, R.: private communication.
[38] Morgan, H.G.: "Fatigue Crack Shape Development in Cracked Plates and Welded Joints", Ibid. 25, I Mech E C142/86.
[39] Webster, S., Austen, I.M., and Rudd, W.J.: Draft final report on ECSC agreement 7210 KG/801, ECSC, April 1984.
[40] Aboutorabi, A.A. and Cowling, M.J.: "Measurement of Crack Profile of Semi-Elliptical Surface Cracks Using the AC Potential Technique", NDT International, Vol. 16, No. 3, June 1983 pp. 139-143.
[41] Tweed, J.H.: "Surface Crack Growth Behaviour of UKOSRP-II Joints and Implications for Prediction of Remaining Life of Defective Tubular Joints", Ibid 5, paper TS 49.
[42] Clayton, A.M.: "Assessment of UKOSRP

Crack Growth Data to Investigate the Remaining Life of Offshore Structures after Inspection", UKAEA, Northern Division Report, ND-R-852(R), HMSO, November 1982.
[43] Tweed, J.H. and Freeman, J.H.: "Remaining Life of Defective Tubular Joints - An Assessment Based on Surface Crack Growth in Tubular Joint Fatigue Tests", Offshore Technology Report OTH 87 259, HMSO, 1987.
[44] Forbes, J: private communication.
[45] Gerald, J.: "Interpretation des Essais sur les Noeuds IRSID", Ecole Polytechnique, Paris, ANMT: Rapport No. 15, Decembre 1981.
[46] Bignonnet, A., Lieurade, H.P., Sixou, Y., and Lebrun, J.L., "Experimental Study of Fatigue Crack Propagation in Welded Tubular Connections", Second Intnl. Conf. on Fatigue and Fatigue Thresholds, 3-7 September 1984, Birmingham, U.K., 1505-1513.
[47] Van Delft, D.R.V., Dijkstra, O.D. and Snijder, H.H.: "The Calculation of Fatigue Crack Growth in Welded Tubular Joints Using Fracture Mechanics", OTC 5352, 1986, pp. 573-582.
[48] Bainbridge, C.A.: "Strength and Fatigue Analyses: The North Sea Experience", presented to the Institute of Marine Engineers, October 8, 1985, published as a Lloyd's Register Technical Reprint No. 92.
[49] Gurney, T.R.: "Fatigue of Welded Structures", Second Edition, Cambridge University Press, 1979, pp. 61.
[50] Berge, S., Eide, O.I., Astrup, O.C., Palm, S., Wastberg, S., Gunleiksrud, A., and Lian, B.: "Effect of Plate Thickness in Fatigue of Welded Joints in Air and in Sea Water", Ibid 5, paper TS 45.
[51] Eide, O.I. and Berge, S.: "Fatigue of Large Scale Plate Girders with Plate Thickness 20, 40 and 60 mm", Ibid 5, paper TS 7.
[52] Eide, O.I. and S. Berge: "Fracture Mechanics Analysis of Welded Girders in Fatigue", Ibid 21.
[53] Maddox, S.J.: "An Analysis of Fatigue Cracks in Fillet Welded Joints", Intnl. Journal of Fracture, Vol. 11, No. 2, April 1975, pp. 221-243.
[54] Albrecht, P. and Yamada, K.: "Rapid Calculation of Stress Intensity Factors", Journal of Structural Division Proc. ASCE, Vol. 103, No. 2, pp. 377-389.
[55] Engesvik, K. and Moan, T.: "Probabilistic Analysis of the Uncertainty in Fatigue Capacity of Welded Joints", Engng, Fract. Mech., Vol. 8, No. 4, 1983.
[56] Smith, I.F.C. and Gurney, T.R.: "Changes in the Fatigue Life of Plates with Attachments Due to Geometrical Effects", Welding Research Supplement, September 1986, pp. 244-250.
[57] Smith, I.F.C. and Smith, R.A.: "Defects and Crack Shape Development in Fillet Welded Joints", Fatigue of Engineering Materials and Structures, Vol. 5, No. 2, 1982, pp. 151-165.
[58] Scott, P.M. and Thorpe, T.W.: "A Critical Review of Crack Tip Stress Intensity Factors for Semi-Elliptic Cracks", Fatigue of Engineering Materials and Structures, Vol. 4, No 4, 1981, pp. 291-309.
[59] Maddox, S.J.: "An Analysis of Fatigue Cracks in Fillet Welded Joints", Welding Institute report E/49/72.
[60] El Haddad, M.H., Topper, T.H. and Topper, T.N.: "Fatigue Life Predictions of Smooth and Notched Specimens Based on Fracture Mechanics", Journal of Eng. Materials and Technology, Vol. 103, April 1981, pp. 91-96.
[61] Yee, R.D.: private communication.
[62] Connolly, M.P. and Dover, W.D.: "On the Fatigue Fracture Mechanics Analysis of Tubular Joints", Offshore Mechanics and Arctic Engineering - OMAE 1987, Houston.
[63] Bergez, D., Lebas, G. and Samier, P.: "Probabilistic Approach of Crack Growth and Instability", Ibid 5, paper TS 57.
[64] Lebas, G., Bergez, D. and Ferro, G: "A Probabilistic Approach to Crack Initiation", OMAE 1986, pp. 56.
[65] Amiot, P., Putot, C. and Radenkovic, D.: "Fatigue Life Prediction of Tubular Joints Under Constant Amplitude Loading," Ibid 1, paper 10.4.
[66] Snijder, H.H., Dijkstra, O.D. and ter Avest, F.J.: "Probabilistic Fracture Mechanics Approach of Fatigue and Brittle Fracture in Tubular Joints," Ibid 5, paper TS 56.
[67] Burdekin, F.M. and Thurlbeck, S.D.: "Defect Assessment of Offshore Tubular Connections," IIW Document X-1125-86.
[68] Denys, R.M.: "The Deviation of the Fatigue Crack Path in Fracture Toughness Testing," Ibid 5, paper TS 55.
[69] Besuner, P.M., Ortiz, K., Thomas, J.M. and Adams, S.D.: "Fracture Control for Fixed Offshore Structures", Ship Structures Committee report SSC-318, December 1984.

Table 1 Magnification Factors (M_k) Obtained by Dijkstra et al [15] For Edge Cracks at The Weld Toe

Geometry		0-01	0-1-1	0-2-1	0-1-3	0-2-3
ϕ		70°	70°	70°	70°	45°
ρ [mm]		0	0.5	0.5	5.0	0.5
T [mm]		70	70	40	70	70
ρ/T		0	0.0071	0.0125	0.0714	0.0071
a/T	load case					
0	B	-	4.2	3.4	1.91	3.8
	T	-	3.6	3.1	1.79	3.4
0.0071	B	2.555	2.438	2.329	1.747	2.250
	T	2.164	2.119	2.068	1.621	2.036
0 0250	B	1.664	1.645	1.630	1.508	1.599
	T	1.452	1.454	1.461	1.387	1.451
0.0625	B	1.289	1.282	1.275	1.265	1.299
	T	1.173	1.174	1.183	1.175	1.200
0.1375	B	1.104	1.101	1.101	1.102	1.113
	T	1.049	1.050	1.050	1.052	1.055
0.2750	B	1.025	1.024	1.024	1.024	1.026
	T	1.008	1.008	1.008	1.008	1.009
0.3875	B	1.007	1.007	1.007	1.007	1.007
	T	1.002	1.002	1.002	1.002	1.002
0.5000	B	1.001	1.001	1.001	1.001	1.001
	T	0.998	0.998	0.998	0.998	0.997

Table 2 Magnification Factors (M_k) Obtained by I.J Smith [18] For Edge Cracks at The Weld Toe

$\frac{a}{T}$	$\frac{t}{T}$=0.3	$\frac{t}{T}$=0.4	$\frac{t}{T}$=0.5	$\frac{t}{T}$=0.6
0.01	1.947	2.007	2.058	2.101
0.02	1.548	1.591	1.628	1.659
0.03	1.381	1.416	1.445	1.470
0.04	1.286	1.315	1.340	1.361
0.05	1.224	1.250	1.271	1.289
0.06	1.178	1.201	1.220	1.236
0.07	1.147	1.167	1.184	1.198
0.08	1.122	1.140	1.155	1.169
0.09	1.103	1.119	1.133	1.145
0.10	1.087	1.102	1.115	1.126
0.11	1.074	1.088	1.100	1.109
0.12	1.060	1.073	1.084	1.093
0.13	1.052	1.064	1.074	1.082
0.14	1.045	1.056	1.065	1.073
0.15	1.039	1.049	1.057	1.064
0.16	1.035	1.043	1.051	1.057
0.17	1.030	1.038	1.045	1.051
0.18	1.026	1.034	1.040	1.046
0.19	1.023	1.030	1.036	1.041
0.20	1.020	1.027	1.032	1.037

Table 3 Experimental and Corrected Values for Ratios of Initiation/Total and Propagation/Total Life for T-Plate Joints [61]

		INITIATION %				PROPAGATION %			
Plate Thickness (mm)	Stress Range (MPa)	$\frac{N_i}{N_T}$	$\frac{N_i}{N_{T1}}$	$\frac{N_i}{N_{T2}}$	$\frac{N_i}{N_{T3}}$	$\frac{N_p}{N_T}$	$\frac{N_{p1}}{N_{T1}}$	$\frac{N_{p2}}{N_{T2}}$	$\frac{N_{p3}}{N_{T3}}$
52	100	31.4	31.7	27.1	26.7	68.6	68.3	72.9	73.3
52	150	24.3	27.0	22.8	22.1	75.7	73.0	77.2	77.9
52	200	27.0	25.3	22.5	20.1	73.0	74.7	79.9	79.9
78	100	20.4	20.1	17.3	16.2	79.6	79.9	82.7	83.8
78	150	24.8	25.0	20.3	18.9	75.2	75.0	79.7	81.0
78	200	25.8	23.4	20.0	17.0	74.2	76.6	80.0	83.9

N_T = Experimental Life
N_i = Experimental Initiation Life (a_i=.5mm)
N_p = Experimental Propagation Life
N_{p1} = Propagation Life Based on Flat-Fronted Edge Crack Correction
N_{p2} = Propagation Life Based on Correction For Semi-Elliptic Crack (a^*/200)
N_{p3} = Propagation Life Based on Correction For Natural Growth of Semi-Elliptic Crack With Initial Aspect Ratio a^*/200
a^* = Depth of Crack Touching Plate Edges

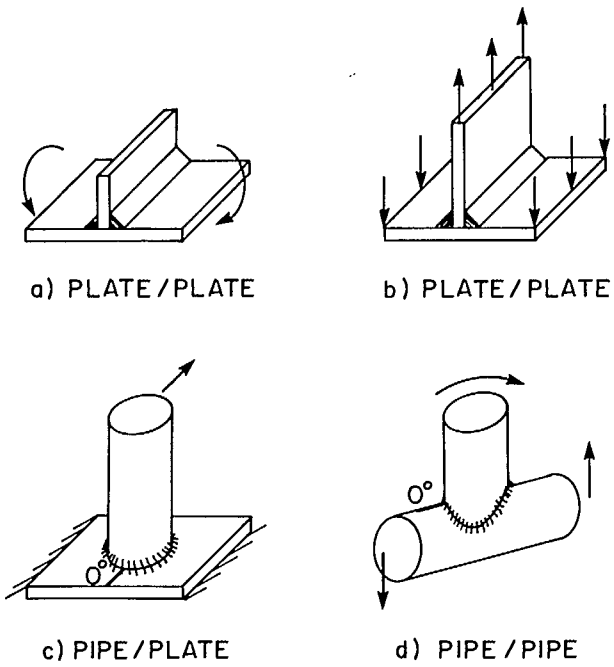

Figure 1: Full Penetration Welded Joints Subjected to Bending Loads.

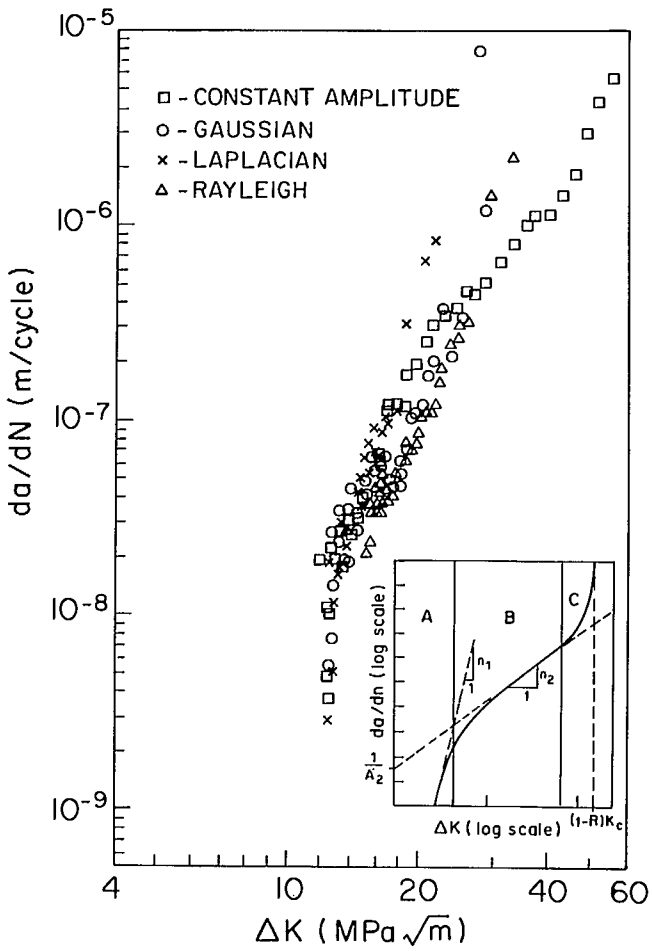

Figure 2: Variable Amplitude Fatigue Data From TS 50; Inset Schematic Shows Typical Relationship between da/dN and ΔK.

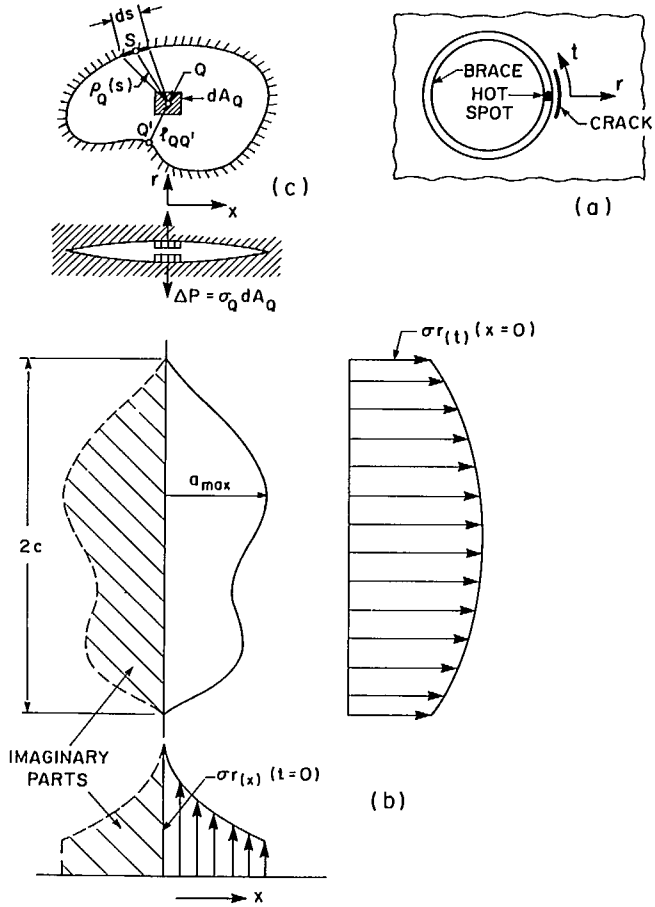

Figure 3(a): Fatigue Crack in Tubular Joint (b) "No Crack" Stress Field Normal to Fatigue Crack, (b) and (c) Equivalent Embedded Crack for 0 - Integral Formulation.

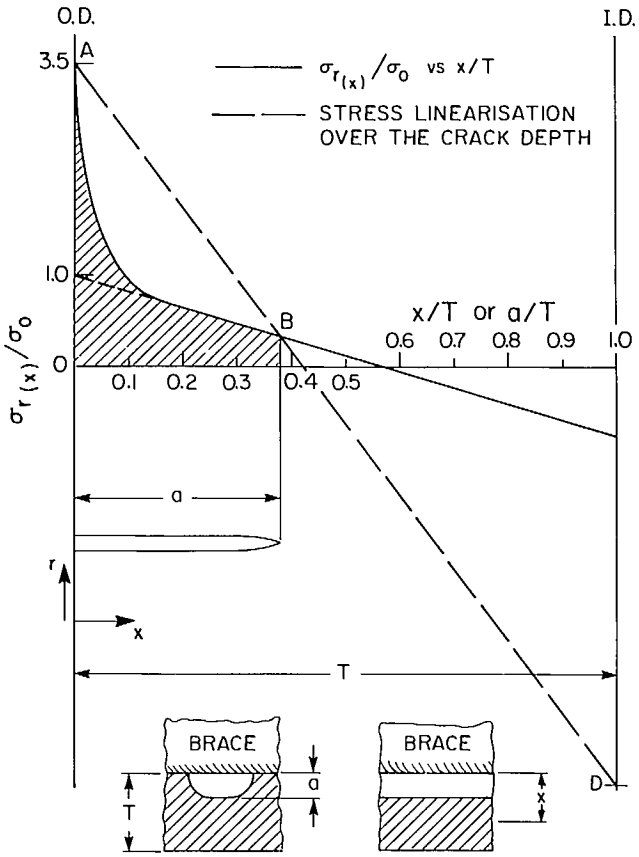

Figure 4: Typical Variation in 'No Crack' Stress Field Through the Chord Plate.

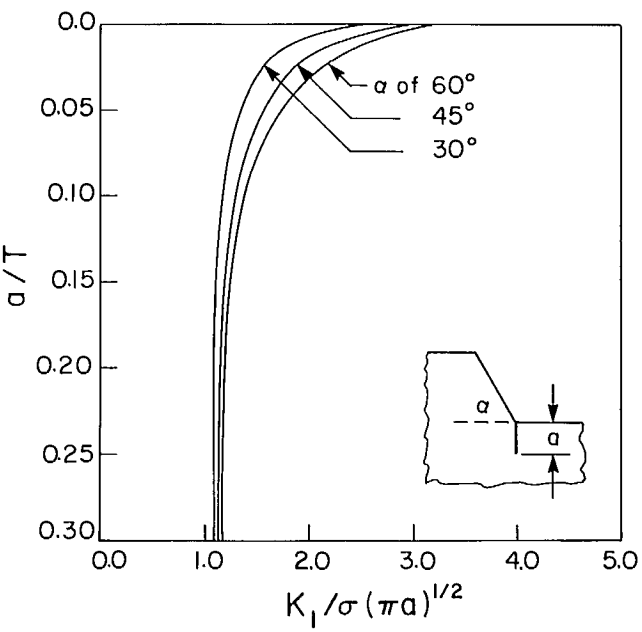

Figure 5: Effect of Weld Toe Angle on K_I.

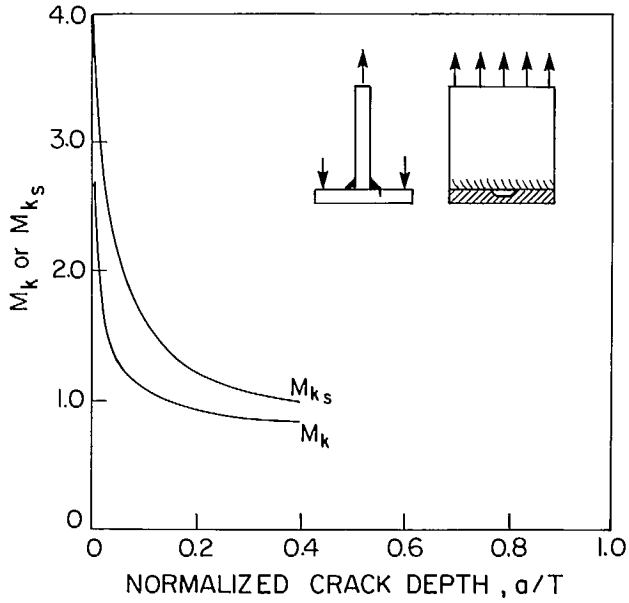

Figure 6: Magnification Factors for Deepest Point (M_k) and Surface (M_{ks}) of Semi-Elliptic Crack at Weld Toe.

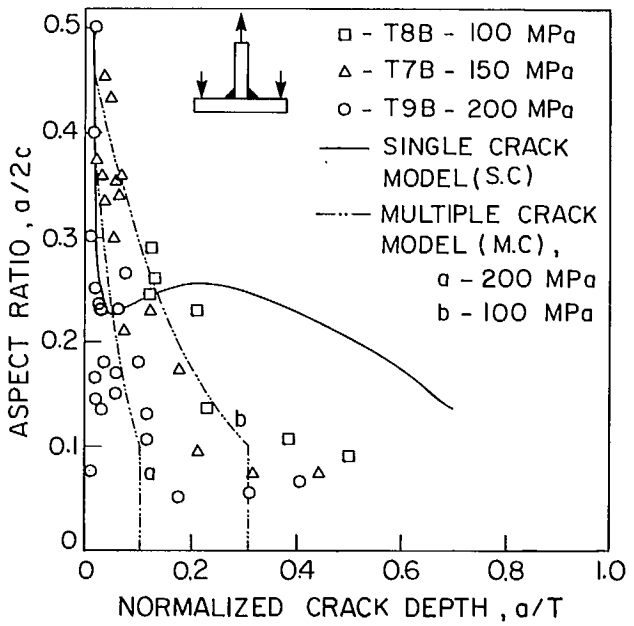

Figure 7: Crack Aspect Ratios, Measurements and Models, for Fatigue Cracks at Toe of Full Penetration Welds in T-Plates.

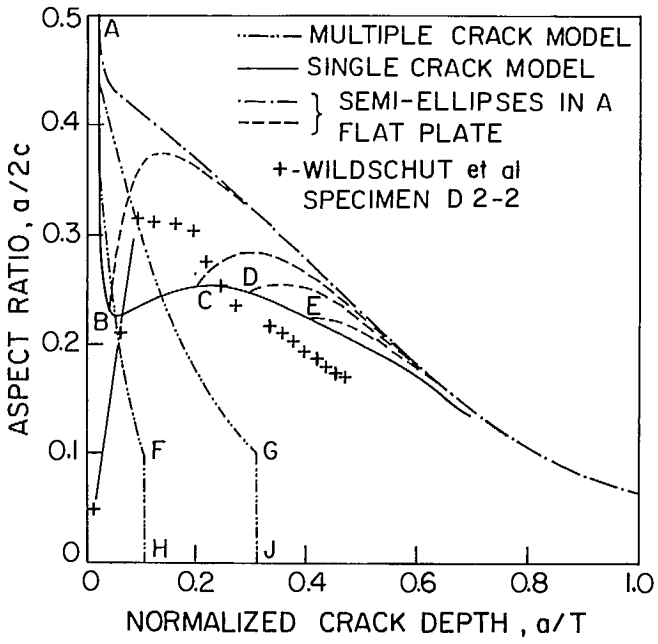

Figure 8: Various Models for Crack Aspect Ratio Development; Experimental Data from TS 51.

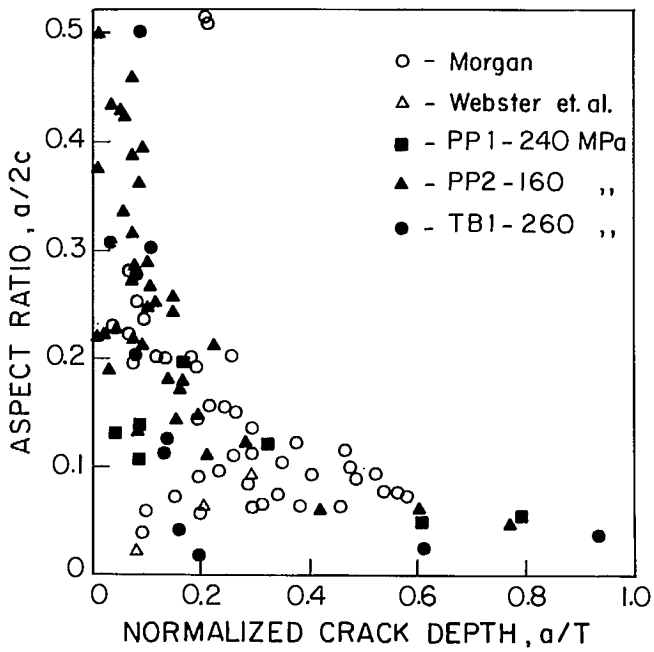

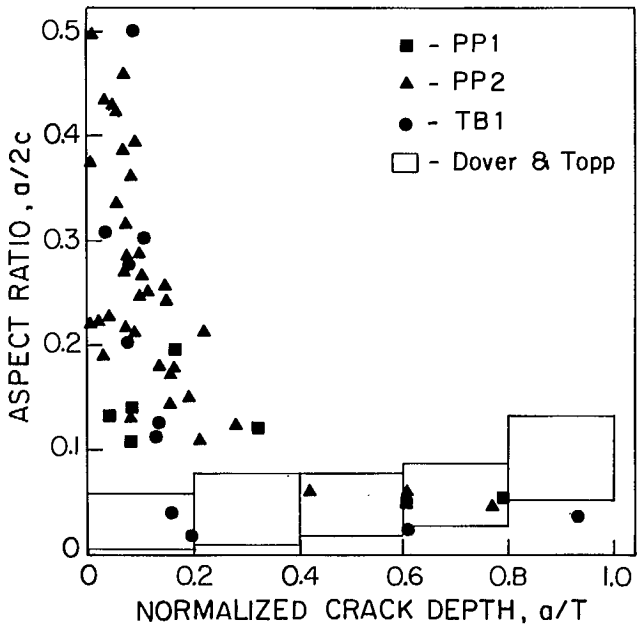

Figure 10: Comparison of Pipe-Plate (PP1 & PP2) and Tubular (TB1) Data with Scatter Bands for Aspect Ratio Reported by Topp and Dover

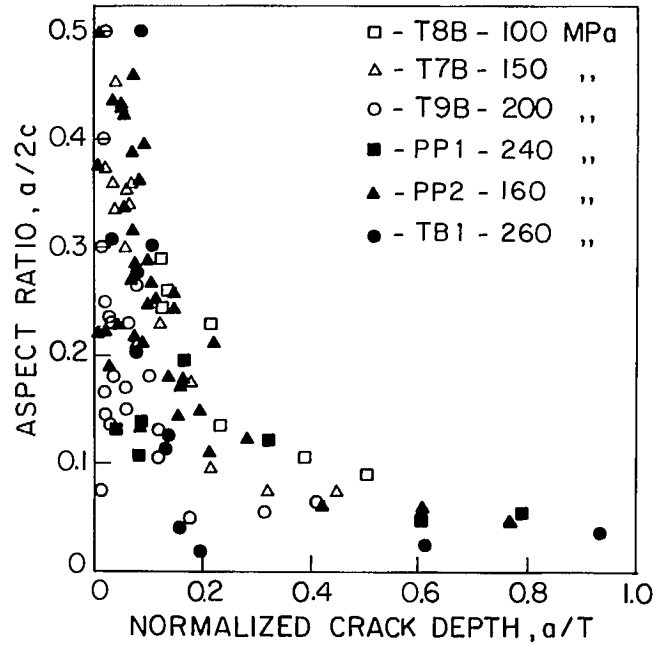

Figure 9(a) & (b): Measurements of Crack Aspect Ratios in Plate-Plate, Pipe-Plate and Tubular Full Penetration T Joints.

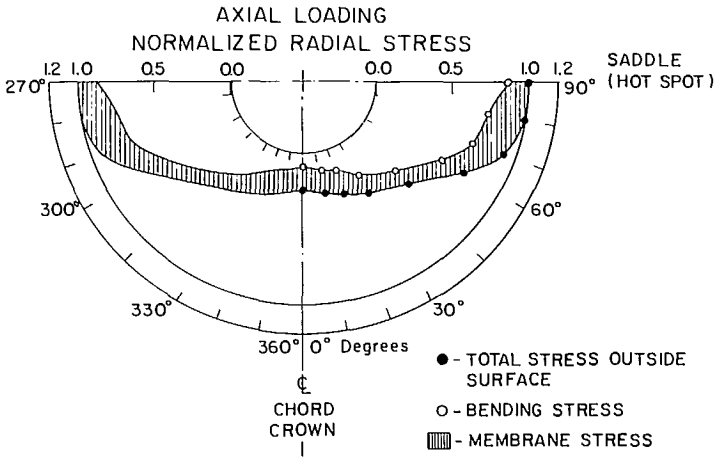

Figure 11: Axial Loading

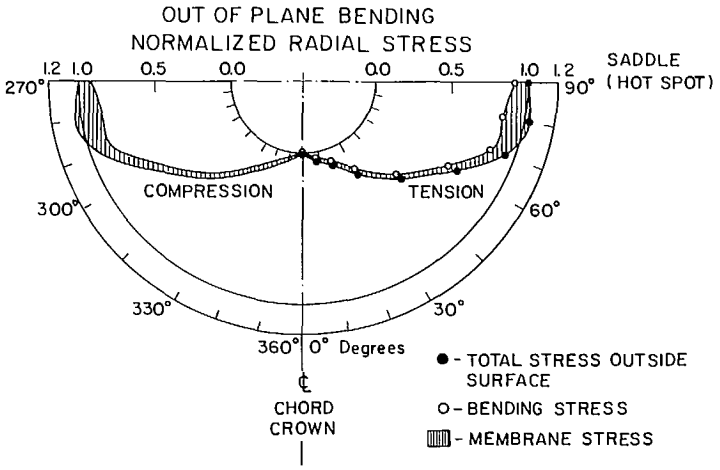

Figure 12: Out of Plane Bending

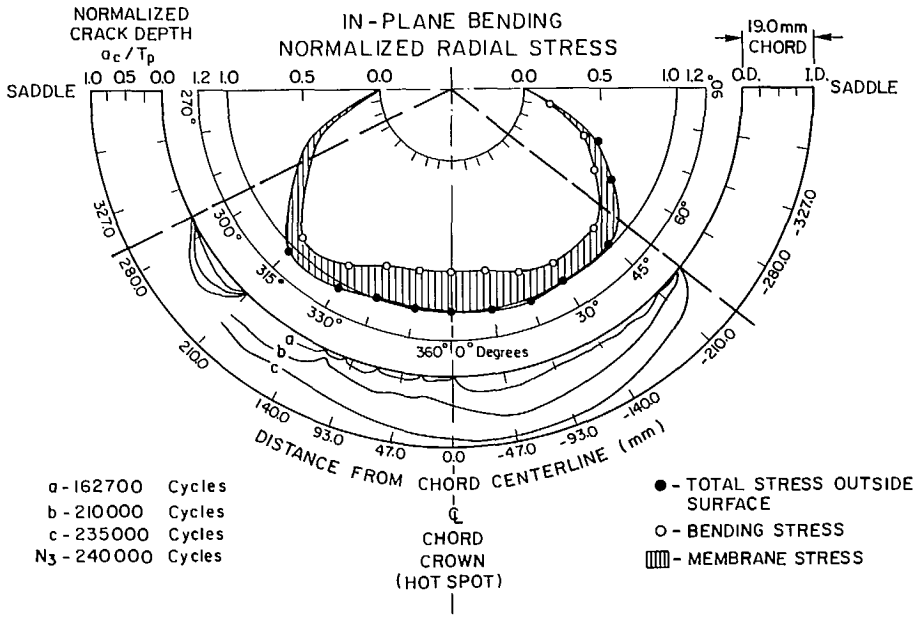

Figure 13: In Plane Bending Also Showing Fatigue Crack Development Monitored by DCPD.

Figure 11, 12 and 13: Nominal Radial Stresses at Weld Toe Normalised with Respect to Hot Spot Stress.

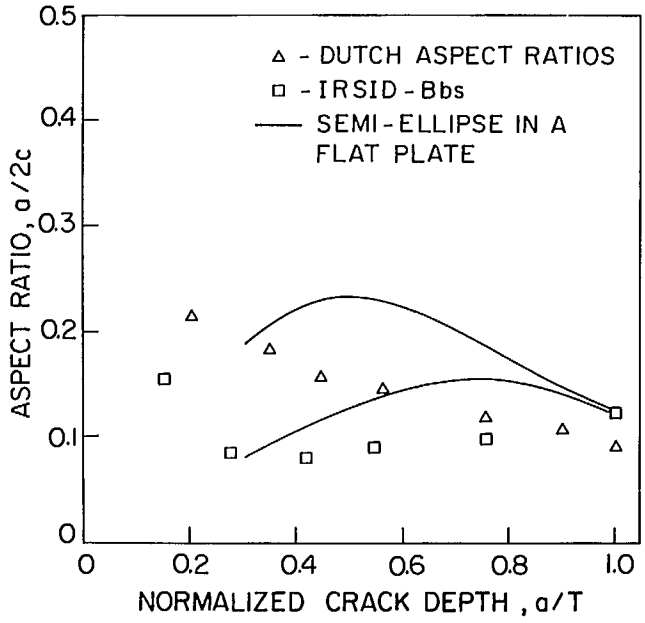

Figure 14: Aspect Ratios of Crack in Tubular Joints: Dutch Test (Axial Loading), IRSID (In-Plane Bending) and Flat Plate Predictions Commencing at a/t of 0.3.

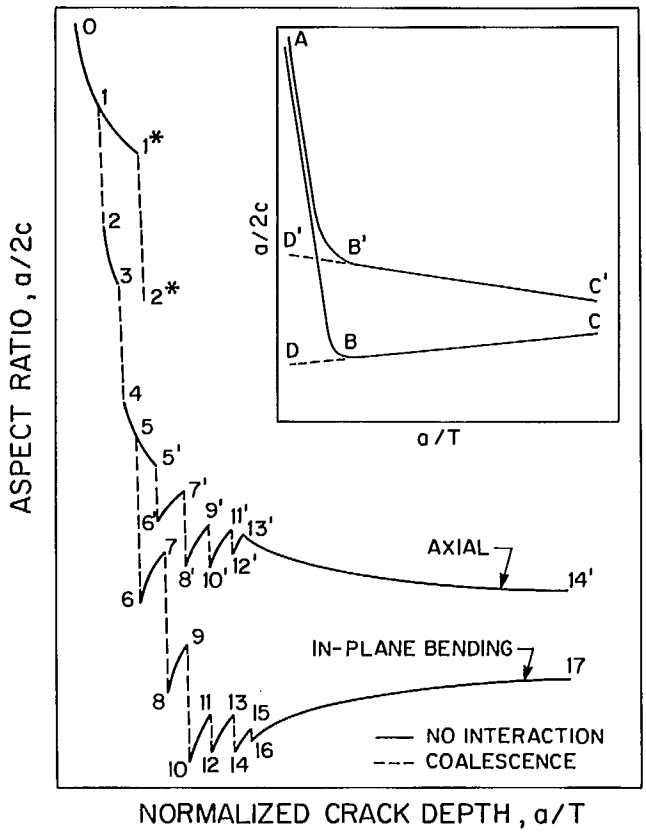

Figure 15: Schematic Showing Effect of Coalescence on Crack Shape Development; Inset Schmematic Showing Possible Forcing Functions

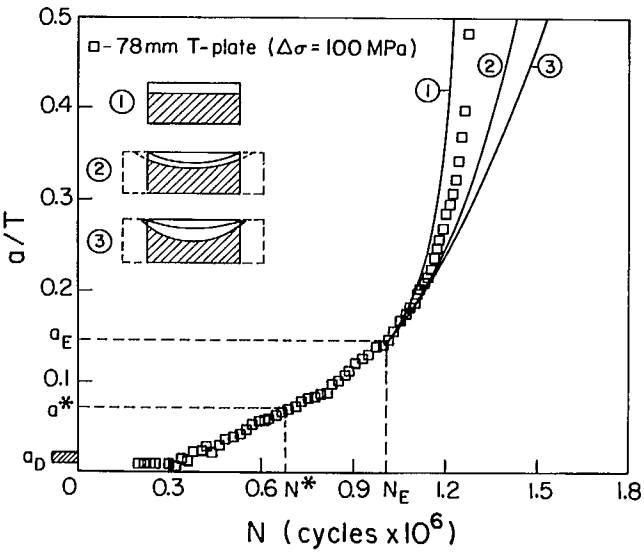

Figure 16: Assessment of Effect of Free Edges (Sides) on Propagation and Total Fatigue Life of Full Penetration Welded T-Plates.

A FRACTURE MECHANICS MODEL FOR LIFE PREDICTION OF WELDED PLATE JOINTS

DÉVELOPPEMENT D'UN MODÈLE BASÉ SUR LA MÉCANIQUE DE LA RUPTURE POUR PRÉDIRE LA DURÉE DE VIE EN FATIGUE DES JOINTS DE PLAQUES SOUDÉES

DÉVELOPPEMENT D'UN MODÈLE BASÉ SUR LA MÉCANIQUE DE LA RUPTURE POUR PRÉDIRE LA DURÉE DE VIE EN FATIGUE DES JOINTS DE PLAQUES SOUDÉES

R. Bell[1], O. Vosikovsky[2], D.J. Burns[3] et U.H. Mohaupt[3]

[1]Département de génie mécanique et aéronautique,
Université Carleton, Ottawa, Canada, K1S 5B6

[2]LRMP/CANMET, 568, rue Booth
Ottawa, Canada, K1A 0G1

[3]Département de génie mécanique, Université de Waterloo
Waterloo, Canada, N2L 3G1

RÉSUMÉ

Le présent document porte sur le développement et le contrôle d'un modèle mécanique de rupture pour prédire la durée de vie en fatigue des joints de plaques soudées.

Le rapport comprend l'analyse numérique bi-dimensionnelle et tri-dimensionnelle du facteur d'intensité des contraintes aux pieds des cordons de soudure de plaques sollicitées en flexion trois points ou quatre points. Les effets de la géométrie des fissures, de leur profondeur, de la forme du profil de la soudure et de la méthode utilisée pour le chargement présentent un intérêt particulier. Les analyses numériques ont été effectuées avec le programme général de recherche sur la méthode des éléments finis ASAS.

Les relations empiriques de K avec les variables ci-dessus ont été établies et sont inclues dans le programme réalisé pour prédire la durée de la vie en fatigue des joints soudés. Ce programme comprend également les rapports empiriques découlant des résultats des expériences effectuées en vue d'expliquer le développement, la croissance et la coalescence de fissures multiples.

Le programme de prédiction de la durée de vie en fatigue des soudures est validé par la comparaison des prédictions avec les résultats d'essais sur des joints en T dont l'épaisseur variait de 16 mm à 103 mm. Ces essais ont été réalisés par chargement à amplitude constante en flexion trois points. Les résultats des expériences seront présentés de façon détaillée dans un autre communiqué de cette conférence.

A FRACTURE MECHANICS MODEL FOR LIFE PREDICTION OF WELDED PLATE JOINTS

R. Bell,[1] O. Vosikovsky,[2] D.J. Burns[3] and U.H. Mohaupt[3]

[1]Dept. of Mechanical & Aeronautical Engineering, Carleton University, Ottawa, Canada. K1S 5B6
[2]CANMET/PMRL, 586 Booth Street, Ottawa, Canada. K1A OG1
[3]Dept. of Mechanical Engineering, University of Waterloo, Waterloo, Canada. N2L 3G1

ABSTRACT

This paper describes the development and testing of a fracture mechanics model for fatigue life prediction of welded plate joints.

Included are numerical investigations of 2-D and 3-D stress intensity factors at the weld toes of welded plates loaded in 3-point and 4-point bending. Of particular interest are the effects of crack geometry, crack depth, shape of weld profile and mode of loading. The numerical studies were performed using the general purpose finite element program ASAS.

Empirical relations for K as a function of the above variables have been established, and are included in a life prediction program for welded plate joints. Also included in this program are empirical relationships developed from experimental results to account for the development, growth and coalescence of multiple cracks.

The life prediction program is validated by comparison of predicted fatigue lives with test results for welded "T" joints with plate thicknesses ranging from 16 mm to 103 mm, loaded through the attachment in 3-point bending under constant amplitude loading. The experimental results are presented in detail in another paper at this conference.

1. INTRODUCTION

During the past number of years there has been an increasing and justified interest in the use of fracture mechanics procedures for estimating the life and the development and propagation of cracks in large offshore structures. Current design practice utilizes the S-N design curve approach and this will remain the primary method of design for some years to come. However, fracture mechanics procedures do present a method of dealing with a tubular structure which contains flaws and demonstrates the influence of a number of variables on the propagation fatigue cracks. Also the testing and analysis of full scale tubular joints is a costly and time consuming undertaking, therefore in many cases the crack propagation behaviour from the weld toe has been studied using welded "T" plate specimens loaded in 3-point and 4-point bending.

This paper describes a fracture mechanics model developed for the prediction of fatigue life and the investigation of fatigue crack propagation and coalescence at the weld toe of welded "T" plate joints as shown in figure 1.

From the Canadian experimental program described in detail in reference [1] and summarized in figure 2 it can be seen that the life of welded "T" plate joints is dominated by fatigue crack propagation and this accounts for about 70% of the life. This crack growth starts at small initial flaws at the weld toe which grow under the influence of cyclic loading into small cracks, which are initially of semi-elliptical shape. These cracks grow deeper and coalesce and finally grow as a single crack until failure of the specimen. Therefore, after making various assumptions on initial crack size and shape it is possible to describe the growth rate of a crack at the weld toe using a linear elastic fracture mechanics (LEFM) approach, in which the growth rate of the crack can be described by a single parameter, the stress intensity factor K. In this approach the crack growth rate da/dN is related to the stress intensity range ΔK by a law such as the Paris Law

$$da/dN = C\Delta K^m \quad \ldots\ldots\ldots\ldots\ldots\ldots \quad (1)$$

where C and m are material constants, and ΔK is given by

$$\Delta K = Y\Delta\sigma \sqrt{\pi a} \quad \ldots\ldots\ldots\ldots\ldots\ldots \quad (2)$$

and Y is a factor describing the geometry. The stress intensity factor, K describes the stress environment at the crack tip and for two different geometries of the same material the stress distribution will be identical if the stress intensities are equal. It follows that the fatigue crack propagation in two bodies will be identical if the cyclic variation in ΔK is the same. The value of K for complex geometries is best obtained using the finite element method and this procedure will be described in section 2.1.

It can be seen from figure 3 that the life of the welded joint can be described by considering three regions. These regions can be designated as (i) initiation, (ii) macro crack coalescence, and (iii) straight fronted crack growth.

Region (i) of the life which is commonly referred to as the initiation phase, includes the initiation of very small cracks on the micro scale, the micro coalescence of these small cracks and the commonly referred to short crack growth region. This region would include cracks up to approximately 0.5 mm. and will not be considered in this paper.

Region (ii) which will be referred to as the macro crack coalescence phase includes cracks of high aspect ratios, a/c, the coalescence of these cracks into fewer cracks of lower aspect ratio and eventually into one dominant semi-elliptical crack. Region (iii) of the life covers the growth of the dominant semi-elliptical crack into a crack of very low aspect ratio and the eventual growth of this crack as a straight fronted crack until final failure. These two regions which describe the propagation life of the joint will be considered in section 3 and will be included in the fracture mechanics model for life prediction of welded joints described herein.

2. FATIGUE CRACK GROWTH MODEL

The fatigue life prediction model developed herein is based on linear elastic fracture mechanics. The above equation (1) can be integrated to give:

$$N = \frac{1}{C} \int_{a_i}^{a_f} da/(\Delta K)^m \quad \ldots\ldots\ldots\ldots (3)$$

Thus the number of cycles N, to propagate a crack from an initial size a_i to a final size a_f, can be calculated. Therefore it is possible to estimate the fatigue life once a solution for K as a function of crack shape and depth is known.

2.1 S.I.F. Determination by FEM

The numerical calculations of SIF were performed using the general purpose finite element program ASAS. Both 2-D and 3-D analyses of the welded joints were carried out. The joints were modelled using quadratic isoparametric elements and the crack tip region by collapsed isoparametric elements which prescribe the $1/\sqrt{r}$ singularity at the crack tip, [2]. The stress intensity factors were evaluated using the classical Westergaard equations for displacements in the vicinity of the crack tip. In order to carry out the analyses at a reasonable cost the multi-level substructuring capabilities of the program were used extensively to perform the analysis for different loadcases and crack geometries.

2.1.1 2-D Solutions for K

A series of 2-D analyses were carried out for crack depth ratios, a/t, varying from 0.02 - 0.5, where a is the crack depth and t is the plate thickness. Three weld shapes were chosen arbitrarily for investigation of the effect of weld shape on the SIF at the weld toe. A 70° weld was chosen to be representative of a severe weld shape, a 45° shape as typical of an actual weld profile and a 30° weld shape as representative of a weld after profiling. The finite element models were loaded in tension, 3-point bending, (load-carrying weld), and also in 4-point bending, (non-load-carrying weld). A typical 2-D finite element mesh is shown in figure 4.

The results obtained from this series of analyses were normalized with respect to K for a plate without a weld and presented in terms of a SIF magnification factor M_k [3]. Curves were fitted to these results to describe the variation of K for the welded "T" plate joint with a straight fronted crack, (SFC). This 2-D solution for K was then included in the life prediction program described in section 4.

2.1.2 3-D Solution for K

Modelling semi-elliptical weld toe cracks in "T" plate joints is both time consuming and the data production is both tedious and error prone. Therefore a mesh generator was developed to produce the required meshes. Also the substructure analysis capability of the finite element program was used to make the series of analyses more cost effective. The calculations were performed for crack shapes in the range

$$1.0 > a/c > 0.25$$

and for crack depths

$$0.025 > a/t > 0.4$$

The loading conditions and the weld shapes

considered were those described in the previous section. A typical 3-D mesh and substructure analysis is shown in Figure 5 (a) and (b).

The SIF results obtained were presented in terms of a SIF magnification factor, M_k, which when multiplied by the SIF for a surface crack in a plate subjected to pure bending, gives the SIF for a weld toe crack as shown in equation (4).

$$K_{I,\ weld} = M_k \times K_{I,\ (pure\ bending)} \quad \ldots (4)$$

The solution for $K_{I,(pure\ bending)}$ was obtained from the empirical relationship of Newman and Raju [4] for a surface crack.

In order that these results could be included in a life prediction program it was necessary to fit curves to the data. However it was not possible to obtain a simple expression for the variation of SIF because the results vary with both a/c and a/t. Therefore, a method was developed in which bi-cubic spline functions were used to fit a surface to the results. In this procedure the entire surface was represented by bi-cubic spline co-efficients. To evaluate a SIF value one simply has to produce a fundamental B-spline for the particular co-ordinates of the independent variables and multiply it by the appropriate coefficients to obtain the curve fitted value of SIF. Using this procedure it was possible to reproduce the original FEM results to within several percentage points.

In order to compare the 2-D and 3-D SIF's for the "T" plate and to demonstrate the variation of SIF with crack shape, crack depth and weld angle the results were normalized with respect to an embedded circular crack and presented in figure 6. It can be seen from this figure the weld angle only effects the SIF results over the first 10% of the thickness of the plate.

3. CRACK SHAPE DEVELOPMENT

From examination of the ink stains and beach marks on the specimens tested in the experimental program reported in [1] it was found that there was a number of randomly distributed cracks initiated along the weld toe. The number, size and shape of these initial cracks depended on the stress range and thickness of the specimen as shown in figure 7 (a-c). These figures also show the development of the cracks as they grow through the thickness. The small cracks which are initially semi-elliptical coalesce as they grow deeper into a smaller number of cracks with lower aspect ratios, (a/c), until they eventually join into a single almost straight fronted crack (SCF). This crack grows until final failure occurs.

In order to characterize this behaviour in a life prediction program the number and aspect ratios of the cracks are plotted as a function of crack depth for all the specimens tested. It was found that if an assumption was made that the initial very small cracks were semi-circular, the crack shape development as a function of crack depth could be described by the exponential relationship

$$a/c = e^{-ka} \quad \ldots (5)$$

It was also shown that the parameter k, which describes the variation of mean aspect ratio of the crack with crack depth, could be described by an equation having the same form as Gurney's for fatigue strength [5]. Thus the equation relating the parameter k to the stress range and plate thickness could be stated as follows:

$$k = k_B \left(\frac{\Delta\sigma}{\Delta\sigma_B}\right)^2 \left(\frac{t}{t_B}\right)^{\frac{1}{2}} \quad \ldots (6)$$

where t_B is a reference thickness and $\Delta\sigma_B$ is the associated stress range, t is any thickness and $\Delta\sigma$ is its associated stress range.

In the present work a reference thickness of 26 mm and a stress range of $\Delta\sigma$ of 116 MPa were assumed, which corresponds to a value of $k = k_B = 0.2$. It should be noted that the above empirical equations (5) and (6) were developed for a specific welding procedure and therefore may only be valid for welds with similar weld toe geometries and in a strict sense for similar loading modes.

The above development of the empirical equation for crack shape variation is described in greater detail in [6].

As stated previously, and as shown in figure 3, the region of crack coalescence accounts for a significant portion of the propagation life. Therefore, in order to characterize the effects of crack coalescence on the life of the joint the above empirical equations were incorporated in the life prediction program described in the following section.

4. FATIGUE LIFE PREDICTION PROGRAM

The fatigue life prediction model described in this section is based on LEFM. Using equation (3), the number of cycles N, to propagate a crack from an initial size a_i to final size a_f can be calculated by a cycle by cycle integration of the growth law using a Runge Kutta numerical integration technique.

The relationships obtained for the SIF's, as described in section 2.1 were included in the computer program. Using the 2-dimensional SIF relationship it was possible to predict the growth of a straight fronted crack, hereafter referred to as the SFC case. The growth of a single semi-elliptical crack can be predicted using the expressions for 3-dimensional SIF's. In this case the growth law is integrated on a cycle by cycle basis in the depth direction to obtain the change in crack depth, a, and in the surface direction to obtain the change in crack length, c. Using these values a new elliptical crack shape is found and this procedure is designated the single crack (SC) solution.

However, as stated above it was noted that for crack propagation from a weld the case of multiple initiation and crack coalescence must be considered to accurately describe the propagation life. Therefore equations (5) and (6) were incorporated into the prediction program. To model the crack coalescence behaviour the following procedure was adopted. The initial crack size was chosen and the increase in crack depth a and crack surface length c were calculated as outlined above. To simulate crack coalescence the surface crack length c was updated at each increment of growth using the empirical relationships above. Also, when the crack aspect ratio reached a value of a/c = 0.2, the crack was assumed to be straight fronted and the 2-dimensional SIF solution was used for the remainder of the life. To accommodate the change from semi-elliptical to straight fronted crack growth some local smoothing in the ΔK values was performed. This procedure was designated the multiple crack, (MC) case.

An example of the predictions of the straight fronted, (SFC), the single crack, (SC), and the multiple crack, (MC), cases for a welded "T" plate specimen is shown in figure 8, compared with the experimental results of [1].

It can be seen that the SFC case is conservative, the SC case over predicts the life by a large amount and the MC case, which accounts for the multiple nucleation and coalescence of cracks, gives a good prediction.

5. COMPARISON OF PREDICTED AND EXPERIMENTAL RESULTS

This section of the paper describes the fatigue life prediction results for the welded "T" plate specimens using the computer program described in the previous section.

The specimen geometries considered are those described in [1] and [6] and shown in figure 1. In all cases the specimens were loaded in 3-point bending, the nominal weld angle was 45°, and the multiple crack case was simulated as described in section 3. After study of the results of the experimental program the initial crack size was chosen to be a_i = 0.5 mm, the initial crack shape, a/c was taken to be semi-circular and the life of the specimens was assumed to have expired when the crack reached a depth of a/t = 0.5. The value of initial crack depth was chosen to be 0.5 mm which was considered to be a valid initial condition for the application of LEFM. It should also be noted that this size of initial crack was considered to be the smallest crack that could be repeatably detected with confidence using the crack measuring systems employed in the Canadian experimental program [1].

A study of the literature, [7] - [9], describing extensive experimental work carried out in Europe on similar steels, was performed to obtain realistic values of material growth rate constants. The values of C and m, chosen for these studies were:

$$m = 3.0$$
$$C = 5.36 \times 10^{-12}$$

and the units in equation (1) were m/c for da/dN and MPa $m^{\frac{1}{2}}$ for ΔK.

An extensive series of computer calculations were carried out on five specimen thicknesses at five stress levels of 75, 100, 150, 200, and 300 MPa and a stress ratio of 0.05 for different initial crack depths to assess the behaviour of the prediction program. An example of the growth prediction behaviour of a/N for the three fracture mechanics models considered, compared with experimental results is shown in figure 8.

Figure 9 shows a S-N plot of the predicted propagation life, using an initial crack size of 0.5 mm, for the stress ranges and plate thicknesses investigated in the Canadian experimental program compared with experimental results. This figure clearly demonstrates the so called thickness effect, i.e., the reduction in fatigue life with increasing section thickness, and the good correlation between predicted and experimental results.

The predicted results produced in this work were also compared, on life - thickness plots, with experimental results from research centres involved in the European Coal and Steel, (ECSC), research program. These results were obtained from references [10] - [12] and are shown in figures 10, 11 and 12 for stress ranges of 100, 150 and 200 MPa. The points shown on these plots represent the total life of the plate joints, therefore the predicted results were modified to

include an initiation period. This initiation period was chosen to be 30% of the propagation life, a value arrived at after study of the Canadian experimental results shown in figure 2.

These plots further demonstrate the thickness effect and show the life predictions as a function of thickness for the three fracture mechanics models considered. It can also be seen from these plots that as the thickness of the specimen and the stress level increases the MC case tends towards the SFC case.

The predicted results for the present work are also presented on a log-log plot of relative fatigue strength at $1x10^6$ cycles versus thickness in the same manner as Gurney [5] and the latest edition of the Department of Energy Guidance Notes [13]. Shown on this plot, figure 13, is the Gurney line of slope -0.25 together with the predicted line with a slope of -0.3. Also plotted are the experimental results from the Canadian [1], the European [11], the British Steel Corporation [10] and UKOSRP [11] programs for an endurance life of $1x10^6$ cycles and normalised for a thickness of 32 mm.

The data shown in this plot includes results of specimens tested in the as welded condition, those subjected to PWHT, those welds tested in the load-carrying and non-load-carrying conditions and also those tested at various R ratios. It can be seen from this data and similar plots given elsewhere in the literature that the available results would seem to support the suggestion that the thickness effect shown would be better described by a line of slope greater than -0.25.

6. CONCLUSIONS

A fracture mechanics fatigue crack growth model for welded "T" plate joints has been reported. This model attempts to account for multiple initiation and crack coalescence in the predicted life of the joints for a wide range of thickness and stress range.

Stress intensity relationships were developed for straight-fronted and semi-elliptical weld toe cracks using the finite element method and the resulting predictions for SFC, SC and MC cases are reported.

The predicted results using the MC fracture mechanics model are in good agreement with and show similar trends to the observed experimental data.

7. ACKNOWLEDGEMENT

This research was funded by the Physical Metallurgy Research Laboratories of the Canada Centre for Minerals and Energy Technology.

8. REFERENCES

[1] Mohaupt, U.H., Burns, D.J., Vosikovsky, O., Bell, R., and Kalbfleisch, J.D.: "Fatigue Crack Development and Thickness Effects in Welded Plate to Plate Connections", Intl. Offshore Conf., Steel in Marine Structures, Paper TS3, Delft, June 1987.

[2] Barsoum, R.S.: "On the Use of Isoparametric Finite Elements in Linear Fracture Mechanics", Intl. J. of Num. Methods in Engineering, 10-1, 1976.

[3] Bell, R.: "Determination of Stress Intensity Factors for Weld Toe Defects" Carleton University Contract Report, DSS File No. 22ST.23440-2-9083/1, Oct. 1985.

[4] Newman, J.C. and Raju, I.S.: "An Empirical Stress Intensity Factor Equation For the Surface Crack", Engineering Fracture Mechanics, Vol. 15, No. 1-2, pp. 1985-192, 1981.

[5] Gurney, T.R.: "The Effect of Thickness on the Fatigue Strength of Welded Joints", Second Intl. Conf. on the Behaviour of Offshore Structures, London, 1979.

[6] Vosikovsky, O., Bell, R., Burns, D.J. and Mohaupt, U.H." "Fracture Mechanics Assessment of Fatigue Life of Welded Plate T-Joints, Including Thickness Effects", Proceeding of 4th Intl. Conf. on Behaviour of Offshore Structures (BOSS '85), pp. 453-464, Delft, 1985.

[7] Thorpe, T.W., Scott, P.M., Rance, A., and Silvester, D.: "Corrosion-fatigue of BS4360:50D Structural Steel in Seawater", Report AERE Harwell -R 10679, November 1982.

[8] Berge, S.: "Effect of Plate Thickness in Fatigue Design of Welded Structures" Offshore Technology Conference, Paper 4829, Houston, May 1984.

[9] Smith, T.J., and Hurworth, S.J.: "The Effect of Geometry Changes upon the Predicted Fatigue Strength of Welded Joints", Welding Institute Report No. 224/1984.

[10] Webster, S.E., Augsten, I.M. and Rudd, W.J.: "Fatigue, Corrosion Fatigue and

Stress Corrosion of Steels for Offshore Structures", British Steel Corp., Report FR103-6/832, April 1982.

[11] Long, D. and Webster, S.E.: "United Kingdom Offshore Steels Research Project", UKOSRP-II/PSC/P86-4, Feb. 1986.

[12] deBack, J. and Vaessen, G.H.G.: "Effect of Plate Thickness, Temperature and Weld Toe Profile on the Fatigue and Corrosion Fatigue Behaviour of Welded Offshore Structures", Report F7.4/81, Delft Institute of Technology, May 1984.

[13] UK Department of Energy,: "Offshore Installations: Guidance on Design and Construction", HMSO, 1984.

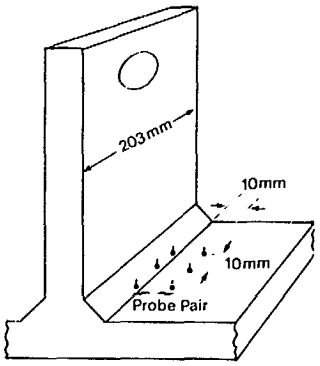

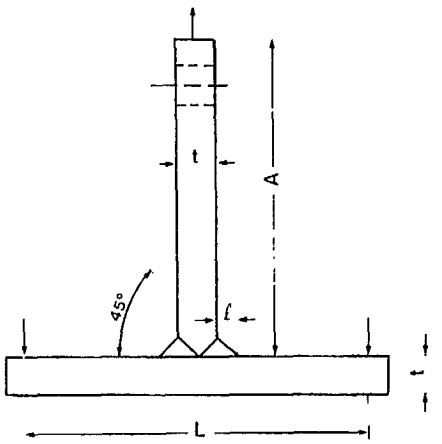

JOINT	t (mm)	ℓ (mm)	L (mm)	A (mm)
A	16	8-12	300	406
B	26	14-18	442	406
C	52	26-30	442	406
D	78	38-42	584	457
E	103	52-56	726	457

Figure 1

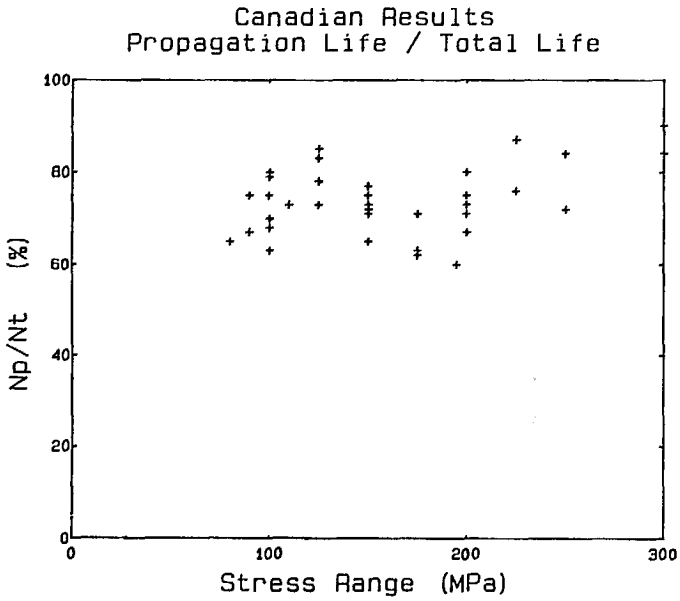

Figure 2

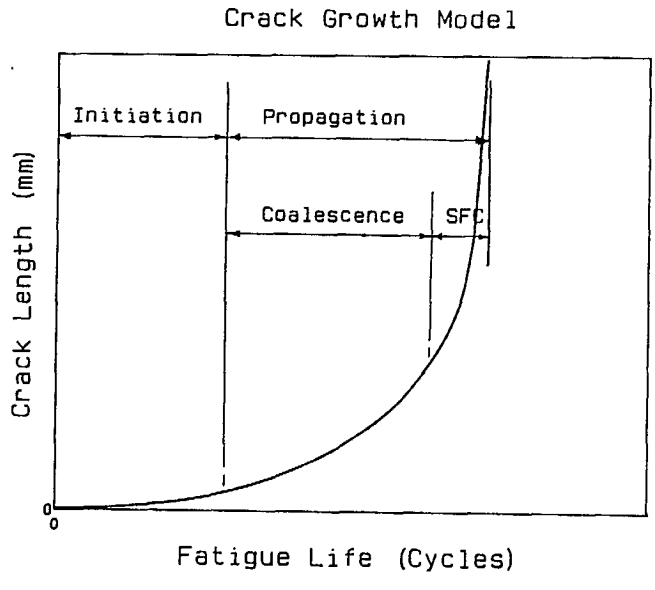

Figure 3

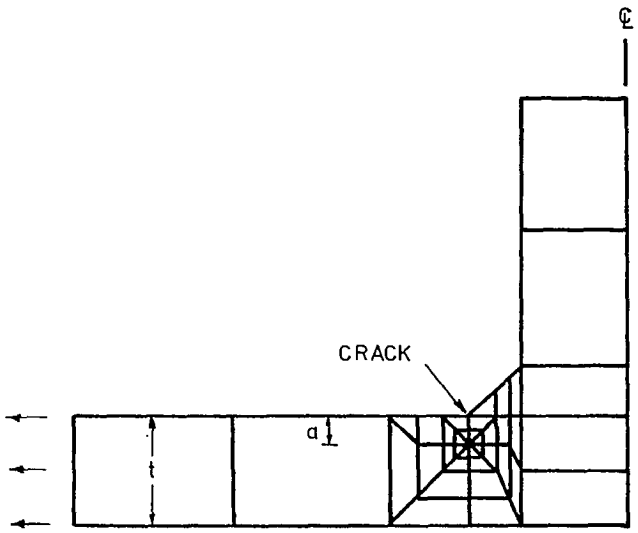

FE MODEL

Figure 4

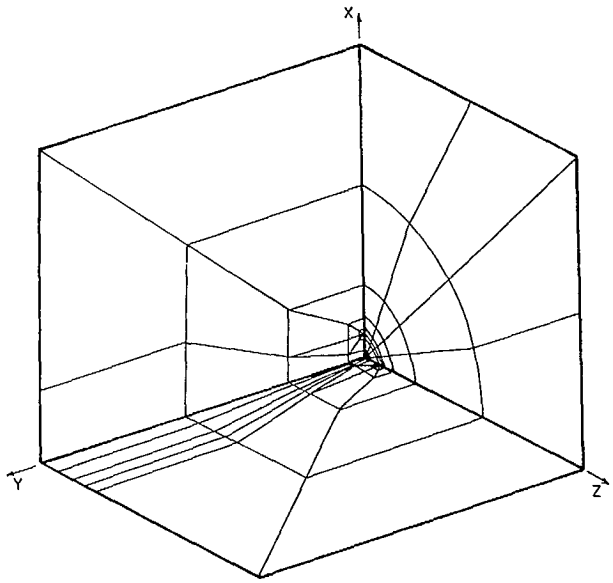

3-D FE MODEL

Figure 5(a)

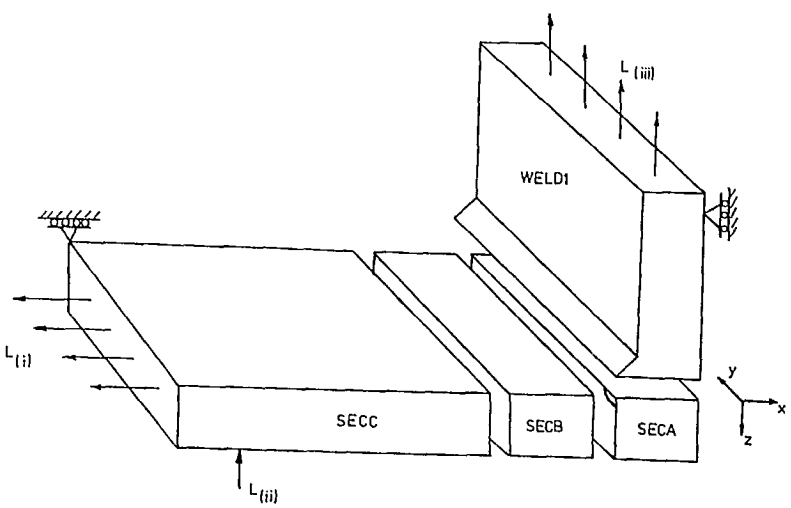

SUBSTRUCTURE MODEL

Figure 5(b)

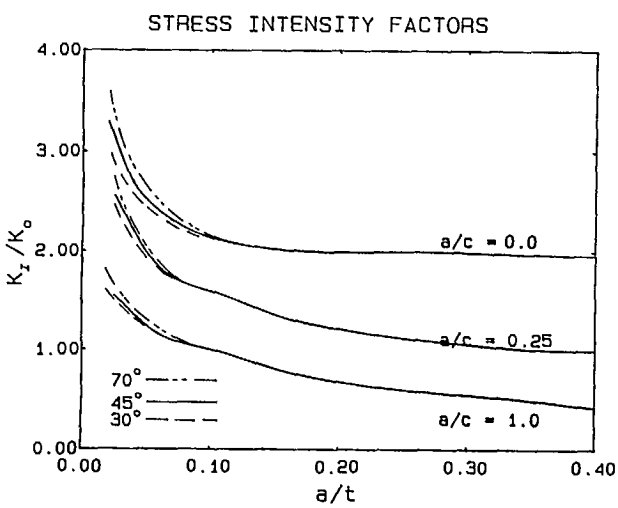

Figure 6

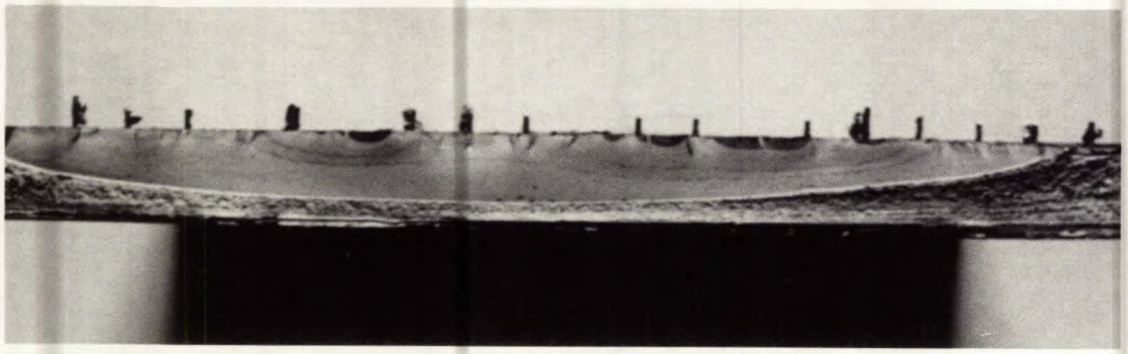

(a) t = 16 mm: $\Delta\sigma$ = 150 MPa

(b) t = 26 mm: $\Delta\sigma$ = 100 MPa

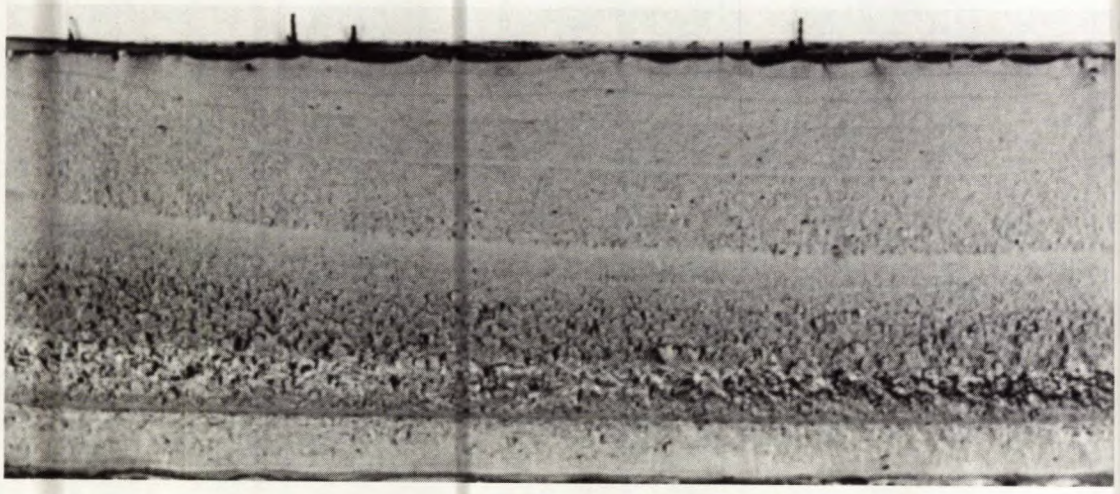

(c) t = 78 mm: $\Delta\sigma$ = 200 MPa

Figure 7

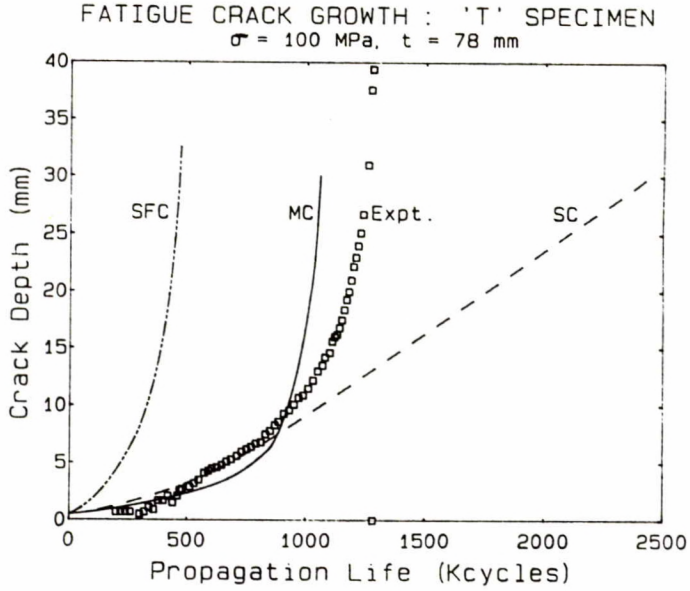

Figure 8

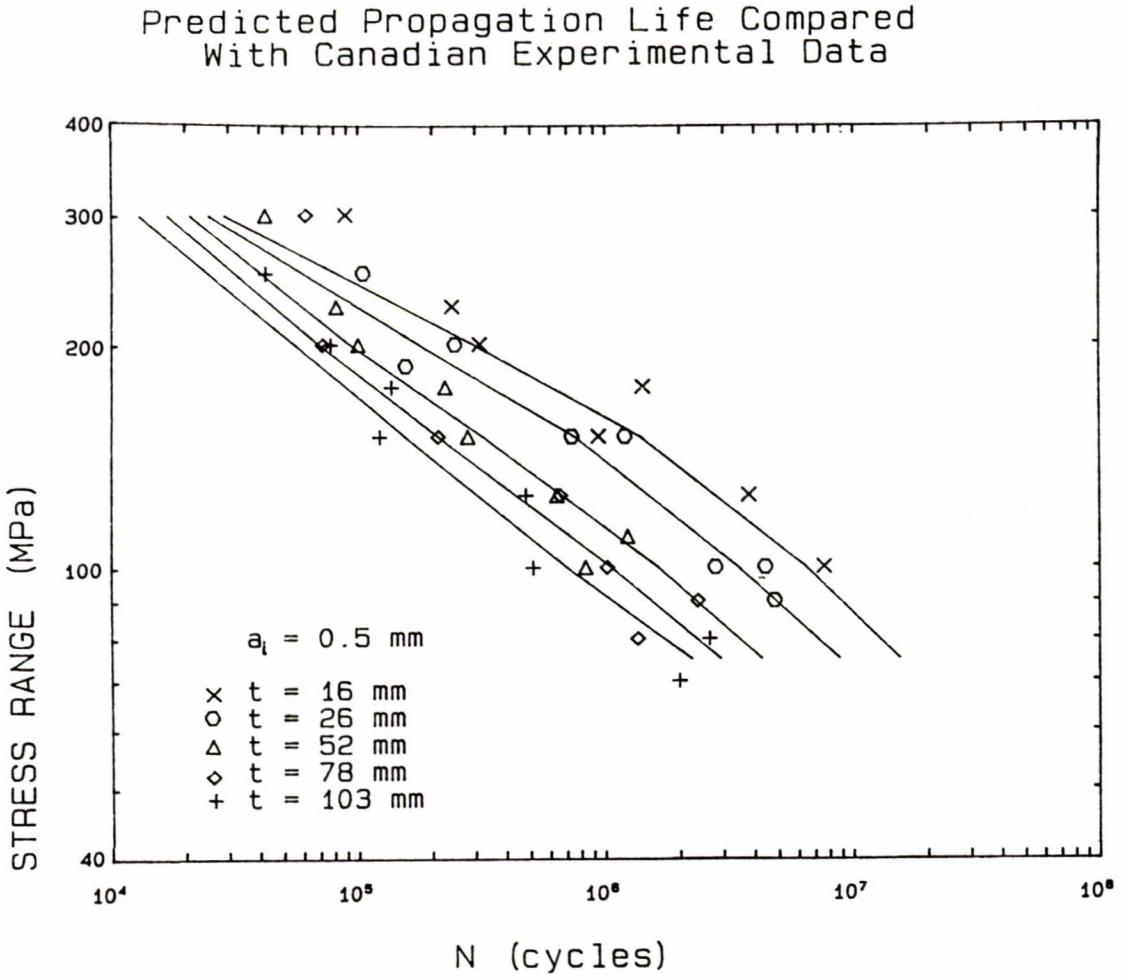

Figure 9

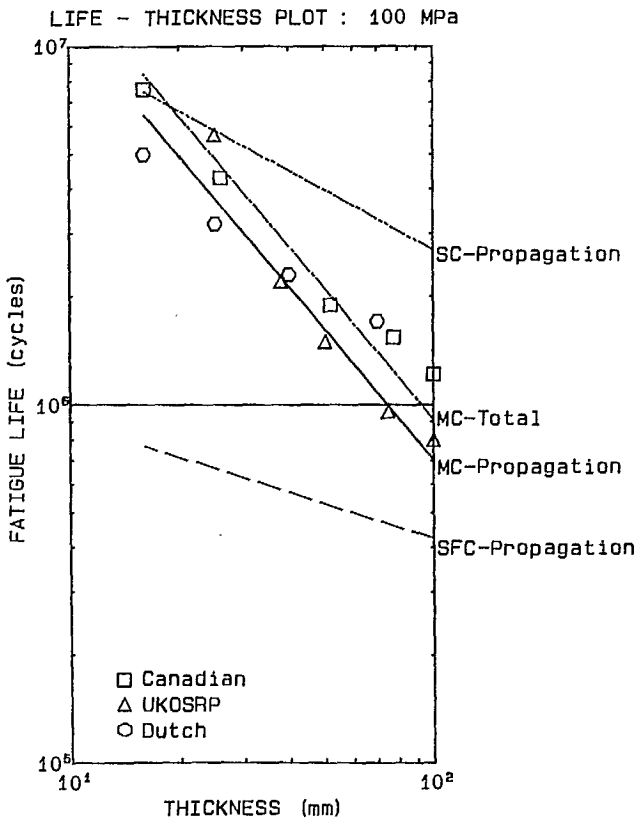

Figure 10

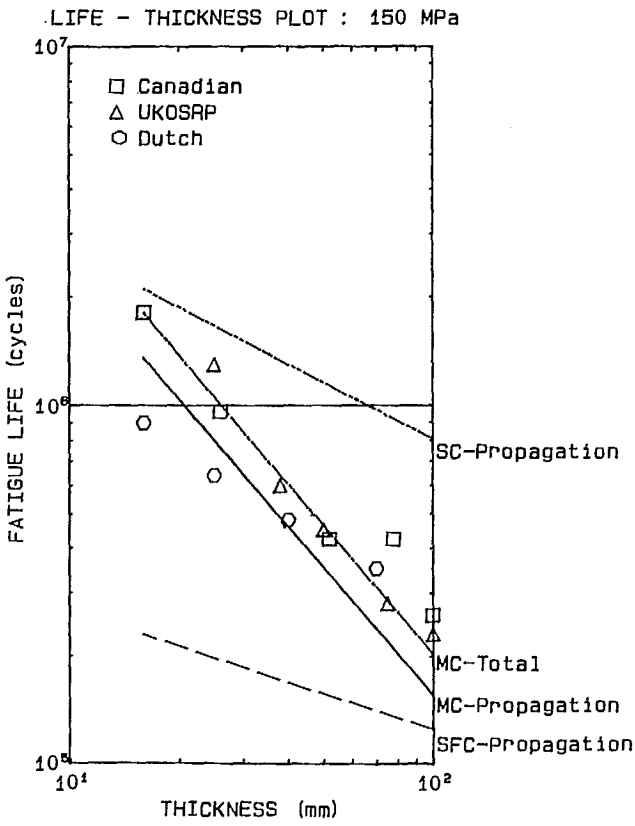

Figure II

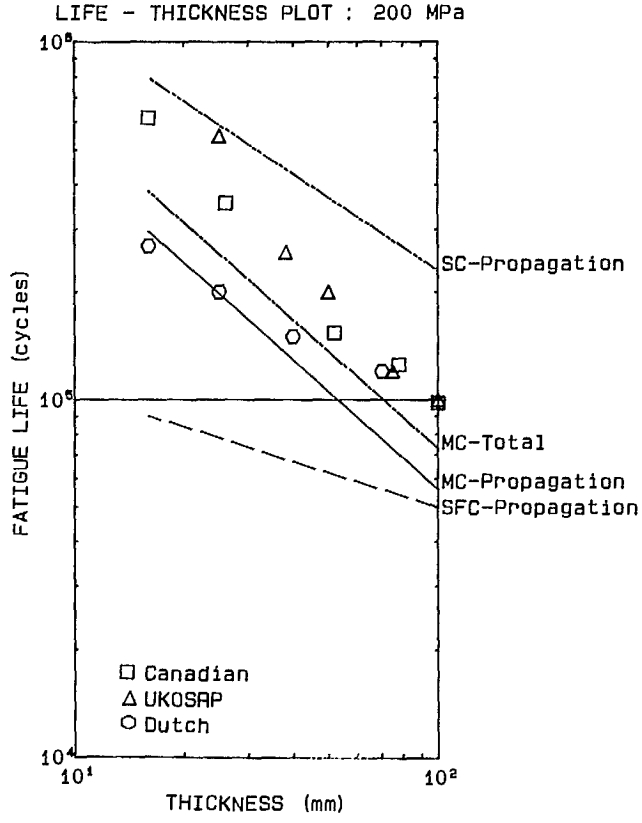

Figure 12

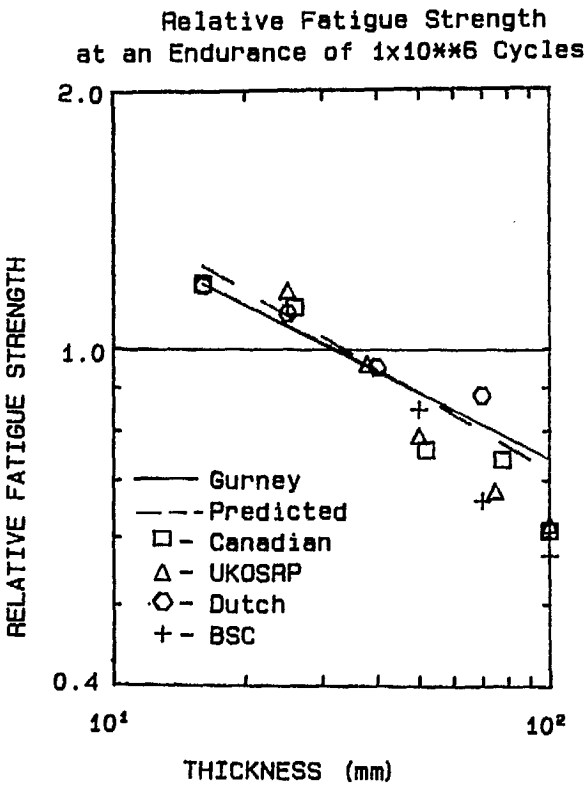

Figure 13

EFFECTS OF CATHODIC PROTECTION AND THICKNESS ON CORROSION FATIGUE LIFE OF WELDED PLATE T-JOINTS

LES EFFETS DE L'ÉPAISSEUR DE LA PLAQUE ET DE LA PROTECTION CATHODIQUE SUR L'ENDURANCE À LA FATIGUE PAR CORROSION DE JOINTS SOUDÉS EN T

LES EFFETS DE L'ÉPAISSEUR DE LA PLAQUE ET DE LA PROTECTION CATHODIQUE SUR L'ENDURANCE À LA FATIGUE PAR CORROSION DE JOINTS SOUDÉS EN T

O.Vosikovsky[1], R. Bell[2], D.J. Burns[3] et U.H. Mohaupt[3]

[1]LRMP/CANMET, 568, rue Booth
Ottawa, Canada, K1A 0G1

[2]Département de génie mécanique et aéronautique,
Université Carleton, Ottawa, Canada, K1S 5B6

[3]Département de génie mécanique, Université de Waterloo
Waterloo, Canada, N2L 3G1

RÉSUMÉ

Le présent article traite des essais à amplitude constante de joints soudés en T sur des plaques de 26 et 78 mm d'épaisseur, effectués dans l'eau de mer synthétique froide (5 °C), sous des conditions de corrosion libre, de protection cathodique optimale (−0,85 V vs Ag/AgCl) et de surproduction cathodique (−1,05 V). Ces essais ont été effectués à un rapport de tension de R = 0,05 et une fréquence cyclique de 0,2 Hz. La propagation des fissures de fatigue a été suivie à l'aide de la technique de mesure de différence de potentiel avec des sondes multiples.

Une comparaison effectuée sur des tests similaires, mais ceux-ci dans l'air, montre que l'eau de mer réduit l'endurance totale à la fatigue par un facteur de deux à trois pour les trois types d'environnement étudiés et pour les deux épaisseurs. Ce n'est qu'à longue échéance que la protection cathodique fournit une amélioration sur le comportement de la fatigue sous corrosion par rapport à la corrosion libre.

Les effets de la protection cathodique sur l'initiation des fissures et l'endurance à la propagation sont évalués et discutés. Les endurances à la fatigue mesurées ont été comparées avec des données tirées d'autres programmes de recherche et des conclusions d'ordre général sont fournies sur l'influence de la protection cathodique.

L'influence de l'épaisseur en eau de mer sous les trois conditions étudiées est équivalente à celle mesurée dans l'air.

EFFECTS OF CATHODIC PROTECTION AND THICKNESS ON CORROSION FATIGUE LIFE OF WELDED PLATE T-JOINTS

O. VOSIKOVSKY[1], R. BELL[2], D.J. BURNS[3], and U.H. MOHAUPT[3]

[1]CANMET/PMRL, 568 Booth Street, Ottawa, Ontario, Canada
[2]Dept. of Mech. & Aero Eng., Carleton University, Ottawa, Ontario, Canada
[3]Dept. of Mech. Eng., University of Waterloo, Waterloo, Ontario, Canada

ABSTRACT

Results of constant amplitude tests of welded plate T joints, 26 and 78 mm thick, in cold (5°C) synthetic sea water under free corrosion, optimum cathodic protection (-0.85V vs Ag/AgCl), and cathodic overprotection (-1.05V) conditions are reported. Tests are conducted at a stress ratio R = 0.05 and cyclic frequency of 0.2 Hz. Fatigue crack growth was monitored using a multi-probe potential drop technique.

Comparison with corresponding tests conducted in air shows that sea water reduces the total fatigue life by a factor of two to three for all three environmental conditions and both thicknesses. Only at long lives, does cathodic protection provide an improvement in corrosion fatigue behaviour over free corrosion.

The effects of cathodic protection on crack initiation and propagation lives are evaluated and discussed. The measured fatigue lives are compared with data from related research programs and some general conclusions on the influence of cathodic protection are made.

The effect of thickness in sea water under the three conditions tested is equivalent to thickness effect measured in air.

1. INTRODUCTION

In the first part of the Canadian program on fatigue of steel for offshore structures, the effect of section thickness, from 16 to 100 mm, on the life of welded plate T-joints was investigated in air. The results are reported at this conference in Ref. [1]. Associated fracture mechanics predictions of fatigue life, accounting for multiple initiation and coalescence of fatigue cracks, are compared with the experimental results in Ref. [2].

In the second part of the program, reported in this paper, the effect of section thickness, T = 26 and 78 mm, is examined in a seawater environment. Test joints identical to those used in air were tested in 5°C synthetic seawater under three environmental conditions: free corrosion, optimum cathodic protection (-0.85V), and cathodic overprotection (-1.05V vs Ag/AgCl). The majority of tests were performed at the Physical Metallurgy Research Laboratories/CANMET, the remainder at the University of Waterloo.

The experimental study has two main objectives:

1) To ascertain whether the effect of section thickness on fatigue life of welded joints measured in air is equally applicable to corrosion fatigue conditions. A previous systematic study of thickness effect in seawater at free corrosion potential was reported in Ref. [3] for plate thicknesses of 16 and 40mm. The seawater results indicated a larger thickness effect than observed for tests in air. No systematic data on thickness effect from one laboratory are available for cathodically protected joints.
2) To ascertain whether adequate cathodic protection restores corrosion fatigue behaviour in seawater to that expected in air, as assumed in design codes [4], and concluded by several reviews [5-9]. The beneficial effect of cathodic protection should be reflected in increased crack initiation, and short crack propagation, lives [10-12]. The crack propagation lives for long cracks, with associated stress intensity factors well above threshold, should be shorter since cathodic protection increases fatigue crack growth rate [13-16]. In order to separate the initiation and propagation lives, fatigue crack growth was monitored in all test joints using multiprobe AC (PMRL/CANMET) or DC (University of Waterloo) potential drop techniques.

A recent review [17] of cathodic protection effects on total life of welded joints showed that, for plate joints, cathodic protection tends to restore corrosion fatigue lives to values found in air for long lives, $>10^6$ cycles. For short lives, life reductions close to a factor of two are found for both unprotected and cathodically protected joints. For tubular joints, all lives are reduced equally, by a factor close to two.

2. EXPERIMENTAL TECHNIQUES

2.1 Test joints and material

The plate T-joints, 203 mm wide with equal attachment and base plate thicknesses t = T = 26 and 78 mm, were, welded from plates manufactured to Lloyd's LT60 specification. The minimum specified yield strength was 350 MPa; actual yield strength (average of two tests) was 405 and 370 MPa for T = 26 and 78mm respectively.

The T-joints were manually welded with full-penetration welds using a balanced welding technique. Nominally 45° degree welds were deposited in the 3G position with no restraint. The weld-toe pass, controlled by the "dime" test, was deposited before the capping passes. More details on joint geometry, material, welding, and weld toe geometry are given in Ref. [1, 18, 19]. All joints were tested in the as-welded condition.

2.2 Testing procedures

The T-joints were tested in three-point bending with constant amplitude loads applied through the attachment plate. The load ratio R = 0.05, and cyclic frequency f = 0.2 Hz, were used in all seawater tests. The calculated weld-toe stress range, and the alignment of the specimens, were checked using strain gauges near the weld toes on each side of the attachment. The loads were selected to produce stress ranges of 80, 100, 110, 150 and 200 MPa.

Synthetic seawater, prepared to ASTM D1141 standard, was cooled in a 250 L main tank and circulated at a flow rate of 1L/min through the environmental chamber attached over one weld (instrumented for PD measurements) of the test joint. The resulting temperature in the weld area was 5 $\pm$ 2°C. The seawater was continuously aerated by bubbling air through the main tank; pH varied from 7.9 to 8.2. A new batch of seawater was prepared every two months.

Cathodic potentials in optimum cathodic protection tests (-850 $\pm$ 10 mV), and in overprotection tests at the University of Waterloo (-1050 $\pm$ 10 mV), were controlled using a potentiostat in conjunction with an Ag/AgCl electrode. In cathodic overprotection tests at PMRL sacrificial zinc anodes were used. In these tests the initial potential was close to -1050 mV (vs Ag/AgCl), and during the test it slowly drifted close to -1V. The duration of the longest tests was over half a year.

2.3 Crack growth monitoring

In each test joint at PMRL, the weld toe exposed to seawater was instrumented with eighteen active spot-welded probe pairs spaced at 10 mm. Only two reference probes, located one quarter distance from joint edges, were used. The weld toe on the opposite side of the attachment was ground to ensure that fatigue cracks first started from the instrumented weld toe exposed to the corrosive environment.

The AC potential drop (ACPD) was measured with a Unit Inspection Crack Microgauge, Model U7G [20]. The potential signal was fed into the Microgauge through a 20 channel low voltage switching unit. The amplified DC signal from the Microgauge was monitored using a computer. A potential scan was done periodically throughout the test. During the scan, the load was held at a mean level.

To convert the potential into a crack depth equation (1), in combination with empirically derived crack-shape correction factors, were used [20, 21]

$$a = A\left[\left(\frac{V}{V_o}\right)_a - \left(\frac{V}{V_o}\right)_{a=o}\right] \qquad (1)$$

V is the potential measured across the crack

V_o is the reference potential measured next to the crack

A is the calibration constant. For straight-fronted cracks, A equals half the distance between probe contacts.

In the previous test series in air, where extensive beach-marking was used for ACPD measurement calibration, it was shown that a number of cracks, with an initial shape close to being semi-circular, initiate from the weld toe [18]. These cracks coalesce forming fewer semi-elliptical cracks with lower aspect ratios. After breaking through the plate edges, the semi elliptical cracks turn into an almost straight-fronted crack. Equation (1), with A = 5 mm, strongly underestimates the depth of semi-elliptical cracks, particularly in the initial growth stages, where several small cracks are usually indicated as one long crack. In order to determine the actual maximum depth of a crack, shape correction factors were derived from beach marks and potential distribution measurements conducted in the air test series. These corrections, which are given as a function of surface crack length indicated by potential distribution, and expressed in terms of the number of probes within a particular crack, are incorporated

into calibration constant A in equation (1). A detailed description of this computerized calibration procedure is given in Ref. [21]. The estimated accuracy of crack depth determination is ± 20% for cracks deeper than 3 mm, and ± 0.5 mm for shallower cracks.

The DC potential-drop technique used to monitor crack growth in tests conducted at the University of Waterloo, is described in Ref. [1].

3. TEST RESULTS

Corrosion fatigue lives of all T-joints tested are summarized in Table 1. The endurance, N_t, is defined by a maximum crack depth equal to half of the plate thickness, a_f = T/2. The life to the first detected crack is the number of cycles observed before the beginning of a steady increase in potential, measured by the probe nearest to the first initiating crack. The crack initiation life, N_i, is defined by a_i = 0.5 mm. This criterion for crack initiation has been selected since it appeared to be the smallest crack size which could be measured with reasonable confidence using our potential-drop techniques [1]. Secondly, the 0.5 mm deep crack is near the lower bound for "long cracks", treatable by simple linear fracture mechanics methods [2, 8, 10, 11]. The crack propagation life, $N_p = N_t - N_i$.

The detection, initiation and total lives were determined from plots of maximum crack depth, a, vs N, shown for 26 mm thick joints and 100, 150, 200 MPa stress ranges in Figs 1a, b, c, and for 78 mm thick joints and 80, 100, 150 and 200 MPa stress ranges in Figs 2a, b, c, d. As can be seen from Table 1 cracks are detected by the ACPD technique before they reach the specified depth of 0.5 mm for initiation.

The data from Table 1 are plotted on standard S-N diagrams; crack initiation lives in Fig. 3a, b, propagation lives in Fig. 4a, b, and total lives (endurances) in Fig. 5a, b (Fig. 3a - 5a show data for T = 26 mm, Fig. 3b - 5b for T = 78 mm). The reference lives, measured in air [1], are included for comparison. In Fig. 5a, b, the class F mean design curves for the corresponding thicknesses [4] are drawn. Regression curves, defined by equation (2), are fitted to the data for each environmental condition.

$$\log N = \log K - m \log \Delta\sigma \quad (2)$$

The values for negative inverse slope m, and intercept, K, for each regression curve are given in Table 2. Also included are environmental life reduction factors, defined by ratio of life in air to the life in seawater, N_A/N_E, at low and high stress ranges of 100 and 200 MPa.

4. DISCUSSION OF TEST RESULTS

4.1 Effects of seawater

The mean life reduction factors for total lives of 26 and 78 mm thick joints tested in this program, listed in Table 2, show that seawater reduces the endurances by 1.5 to 3.5 compared with air. Little distinction in the life reduction factors for different environmental conditions is observed. However, when the fatigue crack initiation and propagation lives, and crack shape development are examined, distinct differences in behaviour between unprotected and cathodically protected joints emerge.

4.1.1 Free corrosion potential

The fatigue lives of unprotected joints, Figs. 3-5, show very little scatter compared with cathodically protected joints, or even with joints tested in air. The crack initiation life reduction factors (Table 2) at $\Delta\sigma$ = 100 MPa are almost twice as high as those at $\Delta\sigma$ = 200 MPa, reflecting the length of exposure to the corrosive environment.

Examination of the AC potential distribution along the weld toe showed that a high number of cracks initiated, forming an almost straight-fronted crack across the whole width of the joint, in the early stage of crack development ($a_{max} \leq$ 5 mm). Almost all free corrosion crack growth curves in Figs 1, 2 exhibit an abrupt increase in slope at a_{max} ~5 mm. This distinguishes the free corrosion fatigue crack developments from those found in joints tested in air, or with cathodic protection. For the latter environmental condtions, particularly at low stress ranges, and with thin plates [18, 19], few cracks initiate, and these persist as semielliptical cracks through most of the life; up to a_{max} ~15 mm.

The early formation of straight-fronted crack in unprotected joints undoubtably contributed to shorter crack propagation lives, indicated by higher life reduction factors in Table 2, compared with cathodically-protected joints. The higher stress intensity factors associated with straight-fronted cracks in unprotected joints accelerate crack growth. This is reflected in shorter lives, particularly at low $\Delta\sigma$, even though crack growth rates at cathodic potentials can be faster than with free corrosion [13-16].

4.1.2 Cathodic protection

Fatigue lives of cathodically protected joints, in particular of those 26 mm thick are widely scattered. The crack initiation lives, and to a lesser degree, the total lives, exhibit much wider scatter than tests in air, Fig. 3a, 5a. For fatigue crack propagation lives, the scatter is consistent with the scatter obtained in air, Fig. 4a, b.

For the majority of the tests, the lives of cathodically protected joints at both potentials were comparable with those obtained under free-corrosion conditions. However, in several tests, three for 26 mm thick joints (tested at 200, 150, and a run-out test at 100 MPa), and two for 78 mm joints (tested at $\Delta\sigma$ = 100 and 80 MPa), the initiation lives exceeded the mean N_i for air, Fig. 3a, b. For these tests the initiation life varied between 40 to 70% of endurance, Table 1, whereas for tests in air [2], and the remaining tests with cathodic protection, N_i varied between 15 to 45% of endurance. As seen from a vs N plots in Figs. 1b, c and 2a, b, delayed crack initiation and slow growth of small cracks are responsible for the excessively long total lives.

In contrast to the free corrosion conditions only few crack initiation sites were detected along the length of the weld toe; one to three in 26 mm thick joints, and two to five in 78 mm joints. In 26 mm joints with extremely long N_i only one initiation site was indicated, much less than the number of sites expected from tests at corresponding $\Delta\sigma$ in air [18]. The initiation site can contain one, or several closely spaced, semi-elliptical cracks.

Locations with high stress concentration along the weld toe (small weld toe radius, steep weld toe angle, undercut, or slag inclusions) serve as crack initiation sites. Such sites are randomly distributed along the weld toe and their severity, or the probability that a crack initiates from that site, will increase when more than one of the above listed factors combine at one location. It has been shown for tests in air [18], that the number of active sites (i.e. sites which initiate a fatigue crack) increases with increasing stress range and plate thickness. A high density of active sites leads to an early coalescence of growing cracks, i.e. early transition from semi-elliptical cracks to a single straight-fronted crack.

A relatively low number of initiated cracks in cathodically protected joints means that less severe initiation sites either do not activate a crack, or, if only one nearly semi-circular crack initiates, its growth could be slowed down or even arrested by a build-up of calcareous deposits [10, 11, 14, 22]. Such an arrested crack would resume growth only after it coalesces with a neighbouring crack creating a longer crack with lower aspect ratio. The crack mouth opening of a semi-elliptical crack will be smaller than that of a straight-fronted crack of the same depth. As a result, the effective stress intensity factor range for a semi-elliptical crack will be relatively more reduced by a calcareous deposit of a given thickness than for a straight-fronted crack.

If we accept the build-up of calcareous deposits within small semi-elliptical cracks as a primary cause of delayed crack initiation and slower growth of small cracks, it means that cathodic protection should become more effective for lower stress ranges, and thinner plates, because of the smaller number of active initiation sites, and for more negative potentials, because of faster build-up of the deposits. The results from regression analysis of N_i in Table 2, considering the scatter and barely sufficient number of tests, confirm this trend, at least for 78 mm thick joints. The inverse negative slope m is highest, and the life reduction factor N_A/N_E at $\Delta\sigma$ = 100 MPa is lowest, with cathodic overprotection. For 26 mm thick joints the regression analysis results are misleading because of wide scatter in N_i, (Fig 3a) and because the run out test at 100 MPa and -1.05 V was excluded from the regression analysis. If this test was completed, and included in analysis, the same trend would have been observed as for 78 mm joints. Similar trends on the effects of cathodic protection on crack initiation are reported by Maahn [22].

The fatigue crack propagation lives (with the exception of one anomalous test of a 26 mm joint at 200 MPa and -0.85 V) do not appear to be affected by calcareous deposits. The life reduction factors of over two at -0.85 V and over three at -1.05 V are in broad agreement with corresponding increases in fatigue crack growth rates [13-15].

4.1.3 Comparison with results from related research programs

Corrosion fatigue tests of welded joints in seawater from ECSC, UK, Canadian and Japanese offshore projects were recently reviewed [17]. Endurances from constant amplitude tests of cruciform and T-welded plate joints, adjusted to a common thickness of 38 mm, are reproduced in Figs 6 to 9. Results from air reference tests are presented in Fig 6, from free corrosion tests in Fig. 7, and from tests at optimum cathodic protection and cathodic overprotection in Figs. 8 and 9 respectively. The class F design and mean curves for air [4] are also shown in the N_t diagrams for comparison. The parameters for fitted regression curves are given, together with environmental life reduction factors at the end of Table 2.

Similar to Canadian data presented earlier, the endurances for air and free corrosion, Figs 6, and 7, are dispersed within relatively narrow scatterbands. The scatter of endurances for cathodically protected joints, Figs 8, 9, is markedly wider. Standard deviations for the fitted curves are almost twice as high for cathodically protected joints as those for tests in air or under free corrosion [17]. The in-air

endurances from single programs are uniformly dispersed through the scatterband. The corrosion fatigue endurances, particularly those from optimum cathodic protection tests, Fig. 8 show, a certain program or laboratory bias. Most of the data from the UKOSRP program are located close to the upper limit of the scatterbands.

The life reduction factors for free corrosion potential measured here compare well with those from the reviewed data, Fig. 7. Slightly higher life reduction factors are measured at a low stress range; 2.4-3.2 compared with 1.8-2.8 for a high stress range (Table 2).

For cathodically-protected joints the life reduction factors derived from the reviewed data, Figs 8,9, are significantly smaller than those from the present data, Table 2. The increase in m, resulting in the strongest environmental effects at high stress ranges (as opposed to free corrosion conditions), is more marked in the reviewed data, particularly for optimum cathodic protection, Table 2, Fig. 8.

The endurances of cathodically protected joints, measured in UKOSRP are comparable with excessively long lives measured on several joints in this program. These joints exhibited only one crack initiation site, and the long endurance resulted from an extremely long initiation life. As discussed earlier, lack of sufficiently severe initiation sites leads to initiation of only a few widely-spaced semi-elliptical cracks with high aspect ratios. Such cracks are easily slowed down or arrested by calcareous deposits. For densely spaced initial cracks, blocking by deposits can be overcome by coalescence. Thus the quality of the weld toe can have an overriding effect on the fatigue life of cathodically protected joints. The longer life measured in UKOSRP may simply reflect a uniformly better technique used for deposition of the weld toe pass.

Comparison of air reference data with class F mean and design curves in Fig. 6 shows F-curves to be highly conservative the - F mean curve could serve as a design curve for the air data. As a result, the F - design curve appears to be adequate for cathodically protected joints, Fig. 8, 9. For joints tested under free corrosion, Fig. 7, the design curve should be shifted to a shorter life by a factor of two [4]. This would result in a degree of conservatism comparable with that for air.

4.2 Effect of thickness

Comparison of the life reduction factors, of N_A/N_E in Table 2, for 26 and 78 mm thick joints tested under free corrosion potential conditions shows generally lower N_A/N_E for thicker joints. This implies a smaller thickness effect than in air.

For cathodically protected joints, due to fewer active initiation sites in thinner joints, an increased effect of thickness may be expected However, the life reduction factors in Table 2 do not support these trends, mainly because of a wide scatter in the data.

The effect of thickness in seawater tests is illustrated in life vs thickness plots at $\Delta\sigma$ = 100 and 200 MPa in Figs 10a, b,. Here the endurances in the three environments are compared with experimental data and fracture mechanics predictions for air. Additional data for free corrosion, and thicknesses of 16 to 40 mm at $\Delta\sigma$ = 100 MPa from the ECSC Dutch program [3] are included in Fig. 10a.

The thickness effect from seawater tests for both unprotected and cathodically protected joints is, within the limits of usual scatter, equivalent to size effect measured in air, and can be predicted using a fracture mechanics model which takes into account multiple crack initiation and coalescence [2]. The reduction in life for all environmental conditions and both stress ranges is almost exactly linearly proportional to increase in thickness.

The linear proportionality was used to adjust data for different thicknesses in Figs 6-9. The adjustment brought the data from air and free corrosion tests with actual thicknesses varying from 26 to 78 mm, within narrow scatterbands of about equivalent width for both environmental conditions.

5. CONCLUSIONS

Fatigue life of plate-welded joints tested at low cyclic frequencies in seawater is significantly reduced compared with air, whether cathodic protection is applied or not.

For unprotected joints both crack initiation and propagation lives are reduced. The reduction in N_i is greater at long life, ~2.5 compared to ~1.5 for short life, reflecting the effect of longer exposure to corrosive environment. The reduction in propagation life by a factor of 2-4 is equivalent to the increase in fatigue crack growth rate measured on standard laboratory specimens. The total life is reduced by about a factor of 2 at high stress ranges and 2.5 at low stress ranges.

For cathodically-protected joints the initiation life varies widely (15 to 70% of endurance, compared with 8 to 40% for air) and largely depends on the severity and density of crack initiating sites along the weld toe. The growth of single, close to semi-circular cracks, particularly in tests at low stress ranges, is believed to be slowed down or even arrested by calcareous deposits, unless they

can coalesce with neighbouring cracks. The reduction in propagation life, by a factor of 1.6 to 2.6 for optimum cathodic protection, and 2.4-3.6 for cathodic overprotection is, as for free corrosion, equivalent to the increase in fatigue crack growth rates measured on standard laboratory specimens. The total lives, due to wide fluctuations in N_i vary widely. Mean lives at high stress ranges are close to those for unprotected joints, at low stress ranges close to lives measured in air. Due to shorter propagation lives, the total lives with cathodic overprotection tend to be shorter than those at optimum cathodic protection.

The effect of increasing plate thickness on fatigue life reduction measured in seawater at the three environmental conditions is equivalent to the effect determined from tests in air. The fatigue life drops linearly with increasing thickness.

6. ACKNOWLEDGEMENTS

The authors wish to thank M.J. Pates formerly of AMCA Int., presently of ARCTEC Canada Ltd., for his contribution to the program.

REFERENCES

[1] Mohaupt, U.H., Burns, D.J., Vosikovsky, O., Bell, R., and Kalbfleisch, J.: "Fatigue Crack Development and Thickness Effects in Welded Plate to Plate Connections" Paper TS3, Int. Offshore Conference, Steel in Marine Structures 1987, Deft, June 15-18, 1987.

[2] Bell, R., Vosikovsky, O., Burns, D.J., and Mohaupt, U.H.: "A Fracture Mechanics Model for Life Prediction of Welded Plate Joints", Paper TS 53, ibid.

[3] DeBack, J., Vaessen, G.H.B.: "Effect of plate thickness, temperature, and weld toe profile on the fatigue and corrosion fatigue behaviour of welded offshore structures"; ESCS Convention Report 7210-KG/601, Delft, Apeldoorn, May 1984.

[4] Offshore Installations: Guidance on Design and Construction, U.K. Department of Energy, HMSO London 1984.

[5] Jaske, C.E., Broek, D., Slater, J.E. and Anderson, W.E. "Corrosion fatigue of structural steels in seawater and for offshore applications; Corrosion Fatigue Technology ASTM STP642, 1978.

[6] Tompkins, B.: "Corrosion fatigue of welded joints", Rapporteur's notes European Offshore Steels Research Seminar, The Welding Institute, Cambridge, 1978.

[7] Walker, E.F.: Rapporteur's Report on the "Effect of Marine Environment", International Conference on Steels in Marine Structures, Paris, Oct. 1981.

[8] Burnside, O.H., Hudak, S.J. Jr., Oelkers, E., Chan, K. and Dexter, R.J.: "Long-term corrosion fatigue of welded marine steels", Ship Structure Committee Report, SSC-326, Washington, D.C., 1984.

[9] Bardal, E.: "Effects of marine environment and cathodic protection in fatigue of structural steels". Fatigue Handbook, Offshore Steel Structures, Tapir, Trondheim, 1985.

[10] Bignonnet, A.: "Corrosion Fatigue of Steel in Marine Structures", Proceedings of CANMET Workshop on "Cathodic Protection: a + or in Corrosion Fatigue, Halifax, Canada Sept. 30, 1986.

[11] Dickson, J.I., Blanchette, Y., and Bailon, J.P.: "The Effect of Cathodic Protection on the Propagation of Long and Short Fatigue Cracks", ibid.

[12] Maahn, E.: "Crack Tip Chemistry under Cathodic Protection and it's Influence on Fatigue Crack Growth", ibid.

[13] Scott, P.M. and Silvester, P.R.V.: "The influence of seawater on fatigue crack propagation rates in structural steel". UKOSRP 3/03, Report, Dec. 1975.

[14] Thorpe, T.W., Rance, A., Silvester, D.R.V. and Scott, P.M.: "The effect of North Sea service conditions on fatigue crack growth in structural steel". Proceedings of Conference on Fatigue in Offshore Structural Steels, London, Feb. 1981.

[15] Vosikovsky, O., Neill, W.R., Carlyle, D.A. and Rivard, A.: "The effect of seawater temperature on corrosion fatigue crack growth in structural steels". CANMET Report ERP/PMRL 83-27(OP-J), April 1983.

[16] Booth G.S., and Dobbs S.J.: "Corrosion Fatigue Crack Growth in BS4360 Grade 50D Steel an Analysis", The WI Research Bulletin, Vol. 27, No. 9, p. 293-297, Sept. 1986.

[17] Vosikovsky, O., and Tyson, W.: "Review of Data from Laboratory Tests of Welded Plate and Tubular Joints", Proceedings of CANMET Workshop on "Cathodic Protection: a + or in Corrosion Fatigue", Halifax, Canada, Sept. 30, 1986.

[18] Vosikovsky, O., Bell, R., Burns, D.J. and Mohaupt, U.H.: "Fracture mechanics assessment of fatigue life of welded plate T-joints including thickness effect"; BOSS '85 Conference Proceedings, Delft, The Netherlands, July 1985.

[19] Vosikovsky, O., and Rivard, A.: "Effect of Thickness on Fatigue Life of Welded Plate T-joints; PMRL Report 85-65(TR), Nov. 1985.

[20] Collins, R., Dover, W.D., and Michael, D.H.: "The Use of A.C. Field Measurements for Nondestructive Testing", Nondestructive Testing Vo. 8. pp. 211-267, Academic Press, London 1985.

[21] Vosikovsky, O., Charr, M., and Bouchard, R.: "Calibration of AC Potential Drop Technique for Sizing of Fatigue Cracks in Welded Joints", PMRL Report 87-1(TR), Jan. 1987.

[22] E., Maahn. "Environmental Effects in Fatigue Crack Initiation" Paper TS 36, Int. Conference, Steel in Marine Structures 1987, Delft., June 15-18, 1987.

Table 1. Results of corrosion fatigue tests of all T-joints.

Spec. No/ Thickness (mm)	Potential (V)	Stress Range (MPa)	N_t Endurance kc	N_d First detected crack kc	N_d First detected crack % End.	Initiation life N_i for ai = 0.5 mm kc	Initiation life N_i for ai = 0.5 mm % End.	Crack Prop. Life Np kc
T15B/26	f.c.	100	1660	580	34.9	760	45.8	900
6/26*		110	932	-	-	325	34.9	607
T10B/26		150	318	80	25.2	130	40.9	188
T12B/26		150	312	85	27.2	146	46.8	166
T16B/26		200	106	22	20.8	39	36.8	67
T20B/26	-0.85	100	2950	480	16.2	750	25.4	2200
7/26*		110	1006	-	-	370	36.8	636
T13B/26		150	355	60	16.9	155	43.7	200
T14B/26		200	404	155	38.4	175	43.3	229
T18B/26		200	131	20	15.3	26	19.8	105
T21B/26	-1.05	100	-	>2110	-	-	-	-
8/26*		110	837	-	-	220	26.3	617
T11B/26		150	910	520	57.1	630	69.2	280
T23B/26		150	420	200	47.6	232	55.2	168
T17B/26		200	90	20	22.2	27	30.0	63
T15D/78	f.c.	80	1033	70	6.8	150	14.5	883
T11D/78		100	490	120	24.5	150	30.6	340
4/78*		110	398	-	-	97	24.4	301
T4D/78		150	167	20	12.0	44	26.3	123
T9D/78		200	66	12	18.2	17	25.8	49
T14D/78	-0.85	80	962	140	14.6	200	20.8	762
T17D/78		100	924	325	35.2	385	41.2	539
5/78*		110	340	-	-	67	19.7	273
T6D/78		150	165	26	15.8	30	19.4	135
T7D/78		200	81	12	14.8	18	22.2	63
T12D/78	-1.05	80	1975	610	30.9	800	40.5	1175
T10D/78		100	692	172	24.9	220	31.8	472
6/78*		110	420	-	-	151	36.0	269
T5D/78		150	123	23	18.4	33	26.9	90
T8D/78		200	54	6	11.2	8	15.0	46

* Specimens tested at University of Waterloo.

Table 2. Values of m and K for regression S-N curves, and enviromental life reduction factors N_A/N_E.

Thickness mm	Environment	m	K	N_A/N_E at $\Delta\sigma$ = 100 MPa	N_A/N_E at $\Delta\sigma$ = 200 MPa
		Crack initiation life N_i			
26	Air	4.32	6.76×10^{14}	-	-
	Seawater f.c.	3.94	4.90×10^{13}	2.4	1.8
	Seawater -0.85v	3.24	1.81×10^{12}	2.5	1.2
	Seawater -1.05v	3.41	4.35×10^{12}	2.3*	1.2
78	Air	3.65	5.99×10^{12}	-	-
	Seawater f.c.	2.53	1.29×10^{10}	2.6	1.2
	Seawater -0.85V	3.15	2.81×10^{11}	2.1	1.5
	Seawater -1.05V	4.96	2.04×10^{15}	1.2	2.6
		Crack propagation life N_p			
26	Air	3.97	2.97×10^{14}	-	-
	Seawater f.c.	3.78	3.16×10^{13}	3.9	3.3
	Seawater -0.85V	3.30	5.02×10^{12}	2.6	1.6
	Seawater -1.05V	3.81	3.92×10^{15}	1.2	2.6
78	Air	2.97	8.77×10^{11}	-	-
	Seawater f.c.	3.04	4.88×10^{11}	2.6	2.7
	Seawater -0.85V	2.80	1.68×10^{11}	2.3	2.1
	Seawater -1.05V	3.57	6.15×10^{12}	3.6	3.1
		Total life N_t			
26	Air	4.04	5.96×10^{14}	-	-
	Seawater f.c.	3.85	7.63×10^{13}	3.2	2.8
	Seawater -0.85	3.24	5.69×10^{12}	2.6	1.5
	Seawater -1.05V	3.68	4.04×10^{13}	2.7*	2.1
78	Air	3.06	1.76×10^{12}	-	-
	Seawater f.c	2.95	4.09×10^{11}	2.5	2.3
	Seawater -0.85V	2.90	3.76×10^{11}	2.3	2.4
	Seawater -1.05V	3.93	5.15×10^{13}	1.9	3.5
		Total life from reviewed tests with T adjusted to 38 mm			
38	Air	3.15	4.8×10^{12}	-	-
	Seawater f.c.	2.78	3.4×10^{11}	2.4	1.9
	Seawater -0.85V	3.70	7.4×10^{13}	0.7	1.3
	Seawater -1.05V	3.50	1.6×10^{13}	1.5	1.9

* The values would be significantly smaller if a run out test at $\Delta\sigma$ = 100MPa was completed

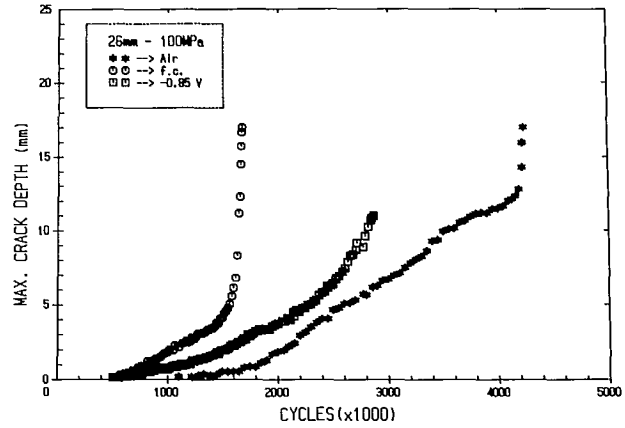

a) $\Delta\sigma$ = 100 MPa

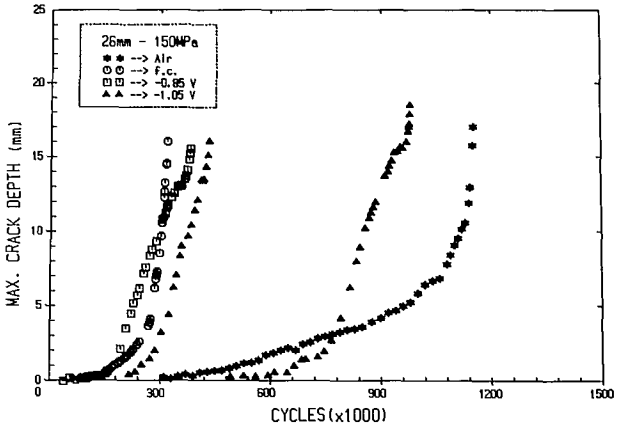

b) $\Delta\sigma$ = 150 MPa

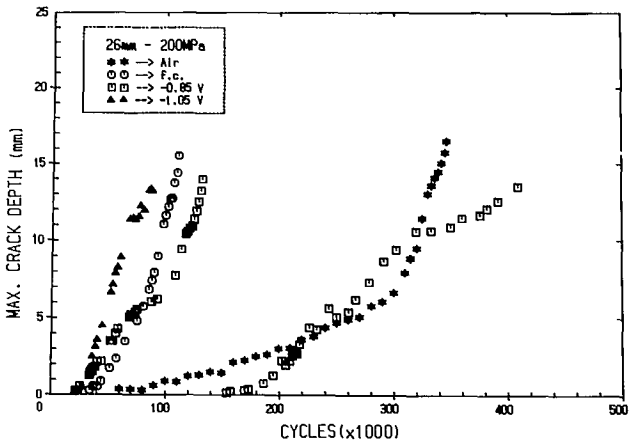

c) $\Delta\sigma$ = 200 MPa

Figure 1. Growth of the first initiating fatigue cracks in 26 mm thick joints tested in seawater at free corrosion, optimum cathodic protection, cathodic over-protection, and in air.

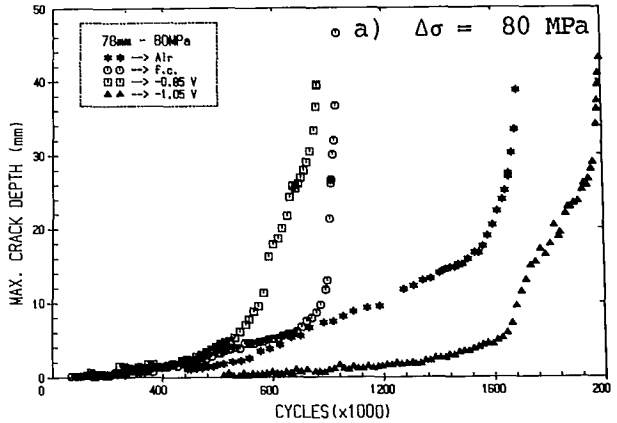

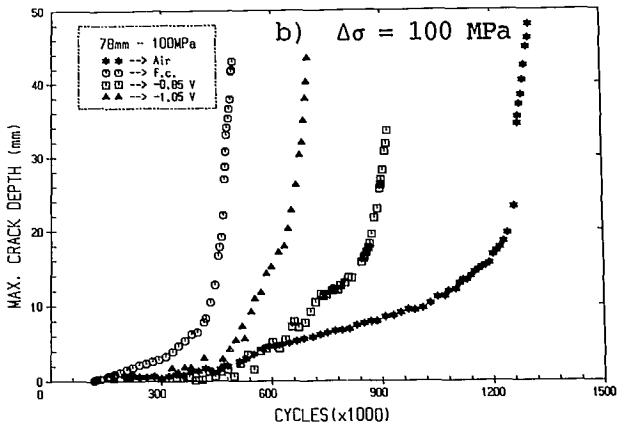

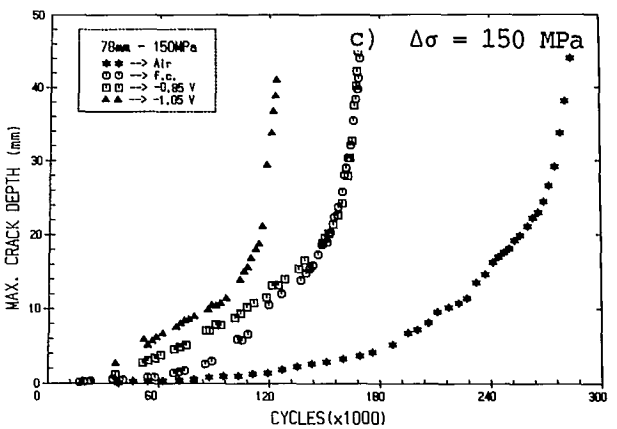

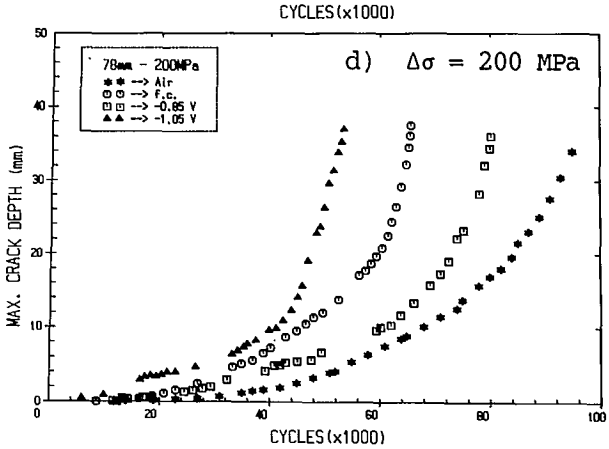

Figure 2. Growth of the first initiating fatigue cracks in 78 mm thick joints tested in seawater at free corrosion, optimum cathodic protection, cathodic over-protection, and in air.

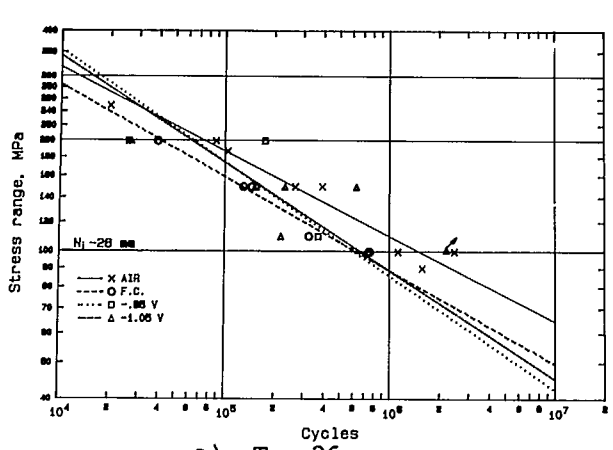

a) T = 26 mm b) T = 78 mm

Figure 3. Fatigue crack initiation lives (a_i = 0.5 mm) of joints tested in seawater at free corrosion, optimum cathodic protection, cathodic overprotection, and in air.

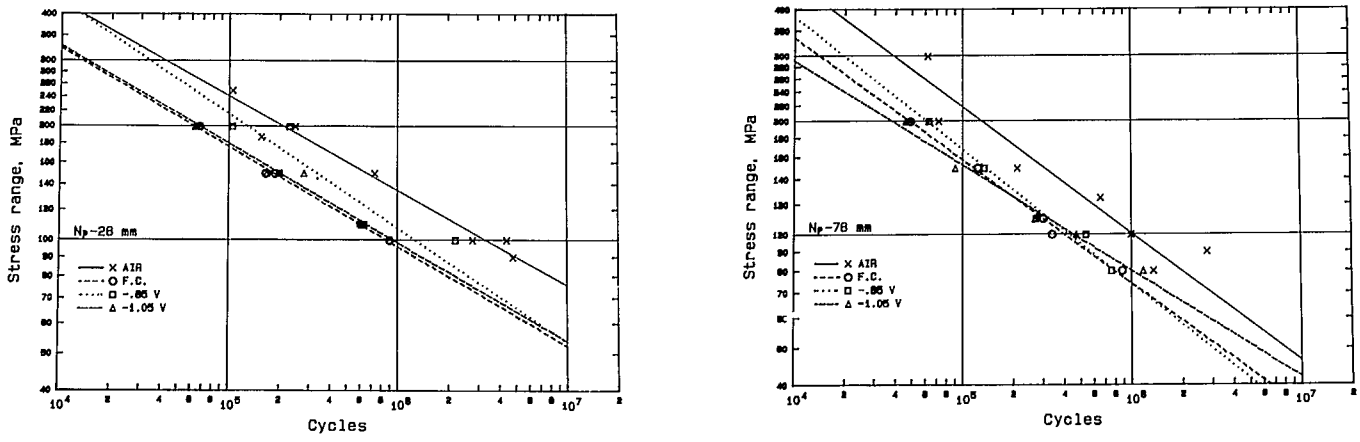

a) T = 26 mm b) T = 78 mm

Figure 4. Fatigue crack propagation lives of joints tested in seawater at free corrosion, optimum cathodic protection, cathodic overprotection, and in air.

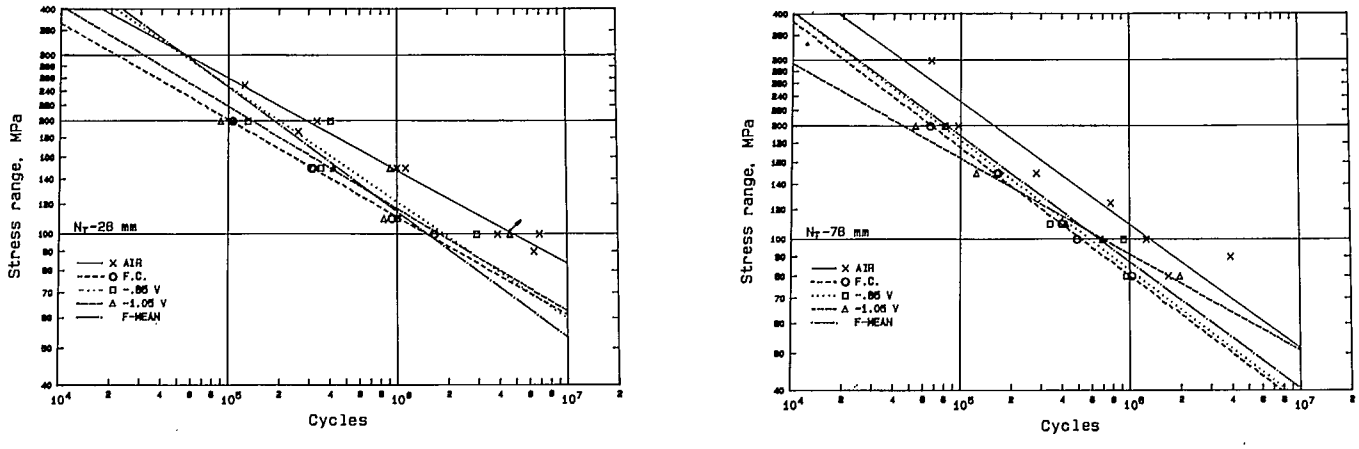

a) T = 26 mm b) T = 78 mm

Figure 5. Total fatigue lives of joints tested in seawater at free corrosion, optimum cathodic protection, cathodic overprotection, and in air.

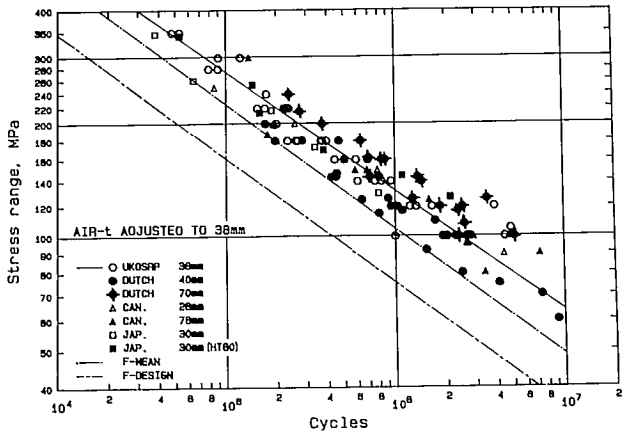

Figure 6. Total fatigue lives adjusted to T = 38 mm of welded plate joints tested in air from UKOSRP, ECSC, Canadian and Japanese programs [17].

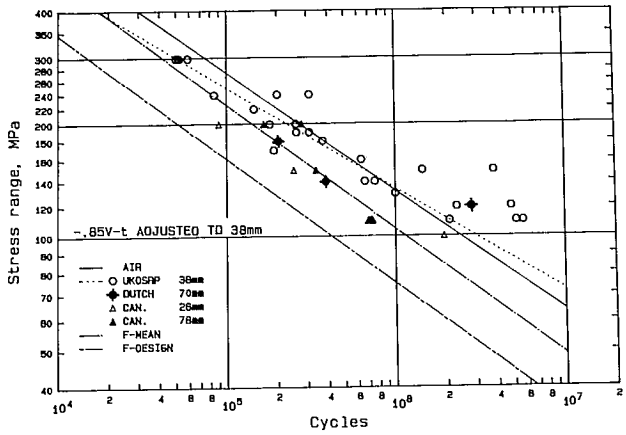

Figure 8. Total fatigue lives adjusted to T=38 mm of welded plate joints tested in seawater at optimum cathodic protection from UKOSRP, ECSC, and Canadian programs [17].

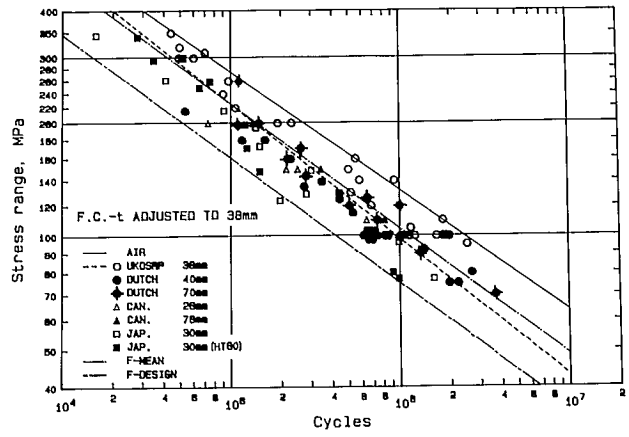

Figure 7. Total fatigue lives adjusted to T=38 mm of welded plate joints tested in seawater at free corrosion from UKOSRP, ECSC, Canadian and Japanese programs [17].

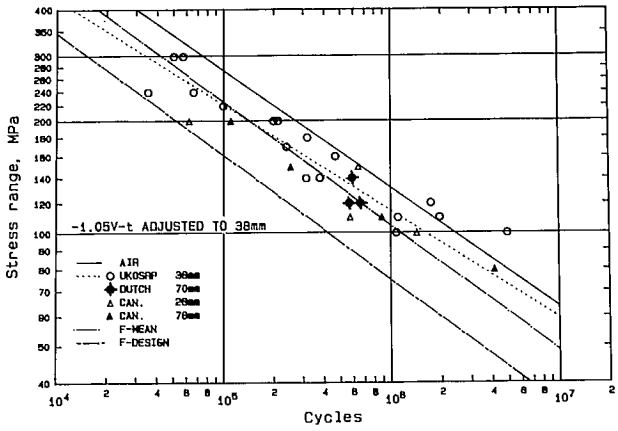

Figure 9. Total fatigue lives adjusted to T=38 mm of welded plate joints tested in seawater at cathodic overprotection from UKOSRP, ECSC, and Canadian programs [17].

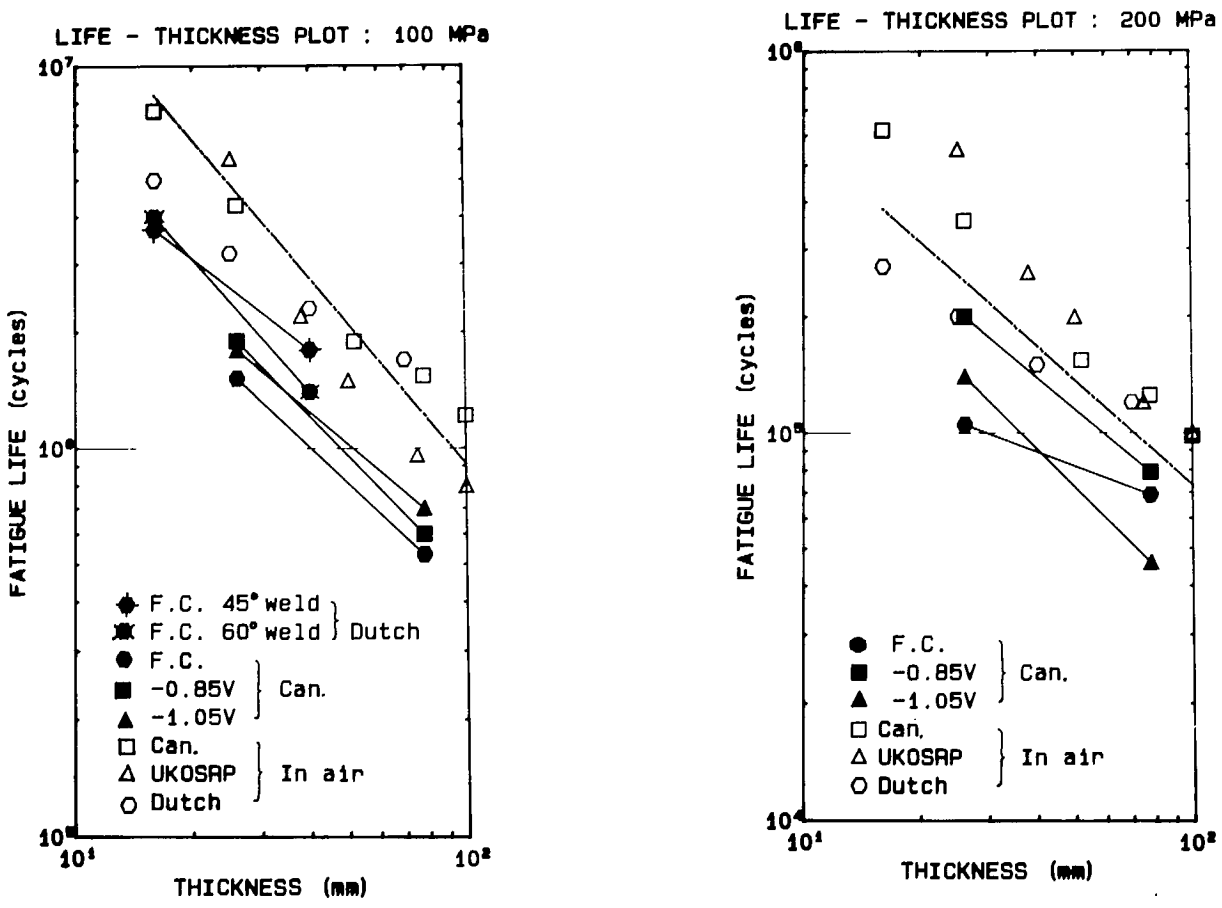

a) $\Delta\sigma$ = 100 MPa

b) $\Delta\sigma$ = 200 MPa

Figure 10. Effect of plate thickness on total fatigue life in air, and in seawater at free corrosion, optimum cathodic protection, and cathodic overprotection from present, UKOSRP, and ECSC programs. The curve for air is predicted by fracture mechanics [2].

FATIGUE CRACK DEVELOPMENT, THICKNESS AND CORROSION EFFECTS IN WELDED PLATE-TO-PLATE JOINTS

DÉVELOPPEMENT DES FISSURES EN FATIGUE: EFFETS DE L'ÉPAISSEUR ET DE LA CORROSION SUR DES JOINTS DE PLAQUES SOUDÉES

DÉVELOPPEMENT DES FISSURES EN FATIGUE: EFFETS DE L'ÉPAISSEUR ET DE LA CORROSION SUR DES JOINTS DE PLAQUES SOUDÉES

U.H. Mohaupt[1], D.J. Burns[2], J.G. Kalbfleisch[1]
O. Vosikovsky[2] et R. Bell[3]

[1]Université de Waterloo, Waterloo (Ontario) Canada

[2]LRMP/CANMET, Ottawa (Ontario)

[3]Université Carleton, Ottawa (Ontario)

RÉSUMÉ

Les techniques de mesure de différence de potentiel AC et CC ont été utilisées pour déceler l'initiation de fissures en fatigue et pour dimensionner ces fissures dans des plaques soudées en T. Les données recueillies ont été utilisées pour évaluer les effets de l'amplitude de la contrainte, de l'épaisseur des plaques et de l'environnement sur l'initiation et la propagation des fissures en fatigue. Des techniques d'analyse statistiques ont été employées pour interpréter les données. Les essais de fatigue à l'air indiquent qu'une augmentation de l'épaisseur des plaques réduit le temps d'initiation et la durée de vie du spécimen. Les essais effectués dans de l'eau de mer artificielle, avec ou sans protection cathodique, montrent que la durée de vie est réduite dans une proportion de 2,5 à 3 et que les avantages de la protection cathodique, s'il y en a, sont peu importants.

FATIGUE CRACK DEVELOPMENT, THICKNESS AND CORROSION EFFECTS IN WELDED PLATE TO PLATE JOINTS

U.H. MOHAUPT[1], D.J. BURNS[1], J.G. KALBFLEISCH[1], O. VOSIKOVSKY[2] and R. BELL[3]

1 University of Waterloo, Waterloo, Ontario. Canada
2 CANMET/PMRL, Ottawa, Ontario
3 Carleton University, Ottawa, Ontario

ABSTRACT

AC and DC potential drop techniques have been used to detect the early stages of crack development and to size fatigue cracks in plate to plate welded T-joints. This data has been used to assess the influence that stress amplitude, plate thickness and environment have on fatigue crack initiation and propagation. Statistical techniques have been used to interpret the data. Fatigue tests in air indicate that increasing plate thickness decreases initiation and propagation life. Tests in artificial seawater, with or without cathodic protection indicate that fatigue life is reduced by a factor of 2.5 to 3 and that the beneficial effects, if any, of cathodic protection are small.

1. INTRODUCTION

The deleterious effect of increasing section thickness on the fatigue life of welded joints has received much attention in recent years, particularly for steels used in offshore platforms. Most of the test programs have been for cruciform or T-plate joints with non-load carrying welds loaded either in tension or in three or four point bending, with thickness up to 100 mm.

A previous paper by the authors [1] presented the preliminary results of a Canadian program on this effect of section thickness. The constant amplitude fatigue data presented was for welded T-plate joints fatigued in air. These specimens had plate thicknesses from 16 to 103 mm, see Table 1, and load-carrying welds with the loads applied through the attachment as shown in Figure 1. In these tests at CANMET, Ottawa, an effort was made to monitor the early stages of crack development, i.e. multiple initiation and coalescence, and to provide some characterisation of crack shape variation with increasing crack depth. This information was used to develop a linear elastic fracture mechanics (LEFM) model, which explained, in part, the thickness effect seen in these tests.

In the interim the CANMET test program in air has been completed and followed by a program of tests in seawater. In addition, similar specimens have been tested in air and seawater at the University of Waterloo. This paper presents all of the S-N data obtained in these studies at CANMET and Waterloo. Data obtained using AC and DC potential drop techniques is used to define the number of cycles required to initiate a small crack, about 0.5 mm. Statistical techniques are used to assess the influence that section thickness has on "initiation" life (N_i), "propagation" life (N_p) and total life (N_T) for specimens tested in air or seawater.

Another paper in this conference [2] compares these experimental estimates of N_p for in-air tests with estimates obtained using LEFM techniques. Another paper in this conference [3] examines in detail the results of the tests in seawater and the effects of cathodic protection.

2. EXPERIMENTAL TECHNIQUE

2.1 Test Joints and Material

The T-plate joints had attachment and base plates of equal thickness, see Figure 1. The plates were manufactured to Lloyd's specification, LT60. The minimum specified yield was 350 MPa; the average of two tests was 421, 405, 390, 370, and 350 MPa for

thicknesses of 16, 26, 52, 78 and 103 mm respectively. Chemical compositions and details of the full penetration welds are given in reference [1].

The width, W, of the T-plates, see Figure 1, was always 203 mm. The loading spans, L, used in the CANMET tests are listed in Table 1; these were determined by the frame dimensions and actuator capacities of the machines. The loading span, L, used in the Waterloo tests was always nine times the thickness of the plate. This ratio of L/T was chosen because it ensured that the nominal tensile stress in the attachment plate of the specimens was similar to that in the brace of T-tubular joints subjected to axial brace loading. At the time it was argued that the magnitude of the nominal brace (attachment) stress might influence the initiation or direction or rate of growth of fatigue cracks.

The ratio L/T = 9 was obtained as follows. The nominal stress range, σ, in an attachment plate, thickness t, is given by $\sigma=F/Wt$ where W is plate width and F is actuator force. If the reaction supports on the base plate, thickness T, and width W are set at a span, L, see Figure 1, the nominal bending stress range, S, at the weld toe, ignoring weld thickness, is given by

$$S = \frac{(F/2)(L-t)T/2}{1/12\ WT^3} \quad \ldots\ldots\ldots\ldots\ldots\ldots(1)$$

Therefore the ratio of this stress range, S, to the nominal stress range, σ, in the attachment plate is

$$S/\sigma = \frac{1.5\ (L-t)t}{T^2} \quad \ldots\ldots\ldots\ldots\ldots\ldots(2)$$

If the stress ratio in the T plate is to be similar to that in a T tubular joint subjected to axial loading then published stress concentration factors (SCF) for tubular joints [4,5] can be substituted for S/σ in equation (2) remembering that in the present tests t = T.

2.2 Fatigue Test Procedure

All joints were tested in the as-welded condition with a load ratio, R, of 0.05 and constant amplitude cycling. As mentioned earlier the loads were applied through the attachment plate. The weld toe (hot spot) stress ranges and the alignment of the specimens were checked by strain gauges, near the weld toes on each side of the attachment. The weld toe on one side of the attachment was ground to ensure that cracking initiated on the other side, thereby reducing by half the number of potential drop probes required to monitor crack development. In only one case did cracks also initiate at the ground toe.

The constant amplitude loads were servo controlled to produce hot spot stress ranges of 80 to 300 MPa. For the in-air tests the loading frequency was in the range 2.5 to 8.0 Hz. For the tests in ASTM standard D1141, synthetic seawater the frequency was 0.2 Hz and the temperature was 5 ± 2°C. Details on cathodic protection tests are given in reference [3].

2.3 Fatigue Crack Detection and Sizing

2.3.1 ACPD Measurements at CANMET

A combination of beach marking and AC potential drop measurements was used to determine the shape and the maximum depth of growing fatigue cracks. Four to six beach marks were produced on each specimen. The first beach mark was made by ink staining to indicate the number and shape of initiated cracks. The first beach mark was applied when the deepest crack reached 2-4 mm depth. The remaining beach marks were made by a 50% reduction of the load range and doubling the frequency for an appropriate number of cycles to produce a small crack extension. These beach marks were produced after 3-8 mm crack depth increments. After completion of each test the specimens were broken, and the lengths and maximum depths of each crack indicated by beach marks were measured to determine their shape, defined by aspect ratio a/2c = max depth/surface length. The maximum depths were also used for calibration of ACPD measurements.

A Unit Inspection Crack Micro-Gauge was used for ACPD measurements. Eighteen probe pairs were spot welded at 10 mm spacing along one weld toe and monitored throughout the test. The depth of the crack when it was first detected depended on its relative location to the ACPD probes. It is estimated that a 0.1 mm deep crack might be detected if a probe pair happened to be located at the middle of the surface length (2c) of the first crack. If the nearest probe pair happened to be not over the crack or not over the crack centre, the sensitivity was lower. An examination of ink stains and P.D. data indicates that this probe layout and equipment was likely to detect surface cracks with a depth, a, of about 0.5 mm. By chance this also happens to be the detection level estimated for the probe layout and DCPD equipment used in the tests at Waterloo.

2.3.2 D.C.P.D. Measurements at Waterloo

A schematic of the pulsed DCPD system designed by M. Van Reenen for this and other

crack measurement studies is shown in Figure 2. Two copper bars, screwed to the ends of the base plate, were connected to a 50 Amp power supply. The current was pulsed approximately twice a second. Each active probe pair consisted of two 0.9 mm wires spot welded to the surface, equidistant from the weld toe. The span, s, of the probe pair was 6.35 mm and the pitch, b, of the probe pairs was 12.7 mm. A total of thirteen active pairs plus one reference probe was used. The span for the reference pair was 6.35 mm.

Another paper will discuss in detail the various analytical and experimental techniques that have been used to calibrate this pulsed DCPD system [6,7]. After extensive studies it has been shown that calibrations based on aluminum foil replicas of cracked T plates can be used to size cracks once coalescence has occurred. When coalescence occurs the crack tends to be a semi-ellipse of low aspect ratio. Prior to coalescence, the DCPD system will detect but not size the small cracks that form at points along the weld toe.

To illustrate this detection capability, Figure 3 shows the cracks detected by ink staining two of the T plate joints tested at Waterloo. This ink staining was done sometime after the PD probes had first detected cracking. It will be noticed that the cracks tend to be semi-elliptic with aspect ratios (a/2c) of 0.25 to 0.33. The data on crack depth,a, and potential drop measurements obtained from probes located somewhere along the crack surface lengths, 2c, have been used to prepare Figure 4. This plot of normalized voltage against crack depth differentiates between voltage measurements obtained from probe pairs at or near the center of a surface crack and measurements from probe pairs well to one side of the crack centre. Figure 4 also shows theoretical estimates, prepared by R. Yee [7], of the relationship between normalized voltage and crack depth. These estimates were obtained using a solution [8,9] for semi-elliptic cracks in a semi-infinite space. Estimates are shown for two aspect ratios, and for two probe positions, see inset diagrams on Figure 4.

The agreement between experimental data and the theoretical solutions is reasonable considering the difference between real and theoretical geometry. Also, the theoretical solutions indicate that crack depths of 0.5 to 1.0 mm should be detectable if electrical noise does not mask the crack signals.

3. TEST RESULTS

3.1 Crack Development and Life Definitions

Figure 5 is a schematic plot of crack depth vs cycles, which illustrates the process of crack development in these T plate joints and relates this process to the problem of detecting fatigue cracks and defining endurance (life).

Two crack growth curves, G and H, are shown. In both cases micro cracks exist or form along the weld toe, some then coalesce to form small semi-elliptic cracks of low aspect ratio. As these micro cracks grow, their aspect ratios tend to increase. During the next phase of growth, analysis is complicated by crack closure effects (short crack region) and interaction effects. Eventually crack closure effects are minimal and interaction effects dominate (macro-crack region). The end of the coalescence phase occurs when a group of macro cracks have coalesced to form a dominant semi-elliptic crack, usually of low aspect ratio.

As shown on Figure 5, the detection band for the ACPD and DCPD systems, 0.2 to 0.5 mm depending on probe position, lies in the short crack/macro crack regions. Detection of a crack of about 0.5 mm depth is used herein to define the end of crack initiation i.e. a crack initiation life, N_i.

The difference between cases G and H is that the next transition is from semi-elliptic to edge crack and this occurs at a much smaller crack depth, (a_E compared to $a_{E'}$) in case G. As a result of this earlier transition, the test life of specimen G is shorter than that of specimen H. This occurs because of the significant differences between crack tip stress intensity factors for semi-elliptic and edge cracks.

In this paper the endurance or total life, N_T, of a specimen is that when the crack depth is one half of the plate thickness. In some cases, e.g. case G, this crack depth, a_T, is reached after an edge crack has formed and in other cases, H, before edge cracking.

Crack propagation life, N_p, is $N_T - N_i$. This clearly includes some coalescence, growth of a dominant semi-elliptical crack and in some cases growth of an edge crack. As mentioned earlier, another paper in this conference [2] explains how LEFM techniques have been used to predict N_p.

3.2 Fatigue Tests in Air

Figures 6, 7 and 8 are S-N curves for total life (N_T), initiation life (N_i) and propagation life (N_p) respectively. Visual examination of these three figures clearly

indicates that fatigue life (N_i, N_p or N_T) reduces with increase in section thickness and that a statistical analysis is desirable if the thickness effect is to be quantified.

Figures 9 and 10 are plots of N_i/N_T and N_p/N_T against hot spot stress range (S). Figure 9 shows that usually between 20 and 40% of the life had gone before the PD systems detected small cracks about 0.5 mm deep. Visual examination of these curves indicates that there may be a tendency for the initiation ratio (N_i/N_T) to reduce with increase in stress range. However it must be remembered that the total life, N_T, will be reduced if an edge crack forms before the crack depth has reached the defined limit of 50% of plate thickness. A measure of this free edge effect is available because all of the CANMET specimens were beach marked and given a detailed post mortem examination.

Table 2 presents the results of this post mortem examination. It shows the maximum crack depth along the crack front when the crack first reached one (a.s.) or both (s) free edges. It also shows the number of cycles (N_E or $N_{E'}$ on Figure 5) when this occurred and the ratio of N_E/N_T or $N_{E'}/N_{T'}$. For the thinner plates, 16 mm and 26 mm, this cycle ratio exceeds unity so the edge effect is not an issue. For the thicker plates, 52, 78 and 103 mm, this cycle ratio is less than unity and the ratio decreases with increase in stress range. For the 103 mm specimens there was an additional complication; fast fractures initiated in some tests [10].

Table 2 shows that this free edge effect was an issue in our tests on thicker plates, thereby tending to reduce total life as shown schematically in Figure 5. Thus the thickness effect seen during the propagation phase of our tests was increased by this free edge effect but the magnitude of this increase cannot be directly assessed without further testing. However a comparison of total lives obtained in our tests with those obtained in other studies [11 - 13] does not indicate that our tests are showing a more severe effect of thickness, see figures in reference [2] and [3] for some detailed comparisons. In two of these other studies [11, 12] on plate-plate joints, the specimen width was increased as the specimen thickness was increased. This has two implications. The chance of a dominant semi-elliptic crack developing near a free edge will be reduced as the specimen width is increased. However the applied stress field does not vary across the specimen width in plate-plate tests so increasing the specimen width will also tend to increase the number of initiation sites and this may tend to reduce the initiation life, N_i.

In a tubular joint, there are no free edges and the aspect ratio and surface length of the toe crack appear to depend on the variation in stress field along the weld [14]. This stress variation depends in turn on mode of loading and tubular geometry. Together these differences and load redistribution may tend to give a thickness effect in tubulars that is less severe than that seen in plate-plate joints.

3.3 Fatigue Test in Seawater

Table 3 summarizes the test conditions and lives, N_i and N_T, obtained in corrosion fatigue tests on 26 and 78 mm thick T-plate joints. The tests were in synthetic seawater with free corrosion, optimum cathodic protection (-0.85v vs Ag/AgCl) or cathodic overprotection (-1.05v).

An examination of the PD data obtained during tests with free corrosion indicated that there were far more initiation sites than in the in-air tests and that an almost straight fronted crack formed when the maximum crack depth was 5 mm. The effect of cathodic protection was to reduce the number of initiation sites to a value comparable to that observed in the in-air tests. A more detailed analysis, including discussion of the effect of calcareous deposits, is given in reference [3]. In this paper, this data will only be used for statistical comparisons with the S-N data obtained in air.

4. STATISTICAL ANALYSIS OF S-N DATA

Since there were differences in loading spans, test machines and crack monitoring techniques used at CANMET and Waterloo it was decided to first analyse the two sets of data separately. For convenience the following symbols are used: Y is log life, x is log stress range, ϕ is the reciprocal of thickness T, Δ^2 is the variance and df are the degrees of freedom. Natural logarithms are used throughout.

4.1 Tests at Waterloo-Initiation Life (N_i)

A series of five parallel lines in x, with a different intercept for each specimen size, was found to give a good fit to the in-air data ($\Delta^2 = 0.2249$, 16 df). A simplification of this model, is that the intercepts are approximately linear in ϕ, the reciprocal of specimen size. The fitted model is then

$$E(Y) = 31.819 + 36.250\phi - 4.150x \quad \ldots\ldots (3)$$

with $\Delta^2 = 0.2042$, 19 df. Residual plots are acceptable except for one very large

residual corresponding to specimen #2 of size 16 mm. Investigation revealed that due to human error there were far fewer than usual P.D. measurements available for estimating the initiation time for this specimen.

The data were reanalysed with the outlying point (16 mm #2) removed. The fitted model was then

$$E(Y) = 32.240 + 30.807\phi - 4.214x \quad \ldots\ldots(4)$$

with $\Delta^2 = 0.1446$, 18 df.
Using this model, equation (4), one can predict "in-air" initiation times for those data points excluded from the analysis i.e #2,16 mm and the corrosion fatigue tests, see Table 4.

As expected specimen #2, 16 mm, had a much larger initiation life than predicted; another in air 16 mm specimen, #4, shows a similar trend but there is no obvious explanation for this except scatter. Table 4 shows that initiation occured much earlier in specimens tested with free corrosion, optimum cathodic protection or cathodic over protection. The actual initiation lives being less than half the predicted in-air lives.

4.2 Tests at Waterloo-Propagation Life (N_p)

Again, a series of five parallel lines in x gives a reasonable fit to the in-air data, ($\Delta^2 = 0.0969$, 16 df), and the intercepts are approximately linear in ϕ. The fitted model is

$$E(Y) = 30.295 + 32.846\phi - 3.601x \quad \ldots\ldots(5)$$

with $\Delta^2 = 0.1116$, 19 df. In this case specimen 78 mm #3 has a large positive residual and specimen 16 mm #4 has a large negative residual. However, no explanation has been found which would justify removing them from the analysis.

Table 5 shows predicted propagation times, based on model equation (5), for data points excluded from the analysis. For 16 mm specimen #2, the propagation time is much smaller than model (5) would predict, which is consistent with the earlier conclusion that its initiation time was overestimated. For specimens tested under free corrosion, optimum cathodic protection or cathodic over protection, propagation times are all about 28% of the values predicted by model (5) for in-air tests.

4.3 Tests at Waterloo - Total Life (N_T)

The initiation and propagation models, equations (4) and (5), together can be used to predict total lifetime. Very similar results are obtained by analysing the total lifetime data directly. A series of five parallel lines in x gives a reasonable fit to the data ($\Delta^2 = 0.0942$, 17 df), and the intercepts are approximately linear in ϕ. The fitted model is

$$E(Y) = 31.132 + 333.360\phi - 3.7106x \quad \ldots\ldots(6)$$

with $\Delta^2 = 0.0956$, 20 d.f. Two points, 16 mm #4 and 78 mm #3, give large positive residuals.

Table 6 compares "in-air" predictions from model, equation (6), with observed total lifetimes for specimens tested in seawater, with or without cathodic protection. For comparison, the predicted in-air lifetimes from models equation (4) and (5) are 3,087,743 cycles for the 26 mm specimens, and 1,349,044 cycles for the 78 mm specimens.

4.4 Comparison of CANMET and Waterloo Data

An analysis similar to that used for the Waterloo data was attempted for the CANMET data. A series of five parallel lines in x appeared to give a reasonable fit to the CANMET, in-air data for initiation life, for propagation life, and for total life. However, because there was less data, it was not possible to check the parallel line models as thoroughly as with the Waterloo data. The following are the variance estimates for parallel line models for the in-air, CANMET data.

Initiation	$\Delta^2 = 0.0297$,	8 df
Propagation	$\Delta^2 = 0.0139$,	8 df
Total	$\Delta^2 = 0.0089$,	8 df

Note that the variance estimates are smaller by an order of magnitude than those for the Waterloo data. The CANMET data show an almost perfect linear relationship between log life and log stress; there is much more scatter in the Waterloo data.

As mentioned earlier, the Waterloo results show a linear dependence of log life on ϕ, the reciprocal of specimen thickness, as assumed in the models, equations (4), (5) and (6). Models assuming this linear dependence do not adequately fit the CANMET data because of the small differences in lifetimes observed there in tests on 16 mm and 26 mm specimens. Recognizing this difference, it was decided to re-analyse the two sets of data, separately and together, using a parallel straight line model

$$E(Y) = \alpha + \beta x + e \quad \ldots\ldots(7)$$

where e is an error term and the slope, β, is assumed to be the same for all specimen

sizes. Therefore the intercept, α, reflects the thickness effect plus any effect of the environment. This means that the effect of a particular environment, e.g. free corrosion, is assumed to be the same for all specimen thicknesses. This model, equation (7), was fitted to each data set by least squares. Various statistical tests and graphs were used to check the assumptions of linearity, equality of slopes and additivity on the log scale.

Table 7 summaries the predictions of this model for specimens tested in air at a stress range, S, of 150 MPa. The analyses for initiation (N_i) and propagation life (N_p) did not include specimen #2, 16 mm because of the known error in defining the initiation/propagation boundary for this specimen. As well as showing the effect of thickness on life, this table brings out another difference between the Waterloo and CANMET data sets. N_i, N_p and N_T for Waterloo tests were generally larger than for the CANMET tests. This difference may be caused by differences in restraint in the loading fixtures used at Waterloo and CANMET; the latter having less degrees of freedom. This difference and the much smaller variance of the CANMET data set indicates that it is not strictly correct from a statistical viewpoint to combine these in-air data sets. Nevertheless, both data sets give a clear indication of trends. In particular both data sets indicate that increasing plate thickness decreases propagation life, N_p; the propagation life for a 103 mm specimen being about one seventh that for a 16 mm specimen. Except for a difference for 103 mm specimens, both data sets indicate that increasing plate thickness also decreases initiation life, N_i.

This model, equation 7, was also fitted to each of the data sets obtained in seawater. To illustrate the effects of free corrosion, optimum cathodic protection and cathodic overprotection, Table 8 lists correction factors, ψ_1, ψ_2 and ψ_3 respectively, that must be applied to air lives predicted by equation 7 for each thickness, see Table 7. In addition, Table 8 lists the slopes, β, and the error variances for the parallel straight line model. Note that in these environments, the variances for the Waterloo and CANMET sets are of the same order.

As mentioned earlier, N_i, N_p and N_T for air tests were generally larger for the Waterloo data. This may partly explain why the correction factors, ψ_1, ψ_2 and ψ_3 are smaller for the Waterloo data. The correction factors for the Waterloo data show that cathodic protection, optimum or overprotection, had very little if any beneficial effect from a fatigue viewpoint. The correction factors for the CANMET data show that cathodic protection, particularly optimum protection, had a small beneficial effect.

Ignoring the statistical differences between the in-air data obtained at Waterloo and CANMET, an overall analysis of the Canadian data shows that the seawater environment reduces the fatigue life by a factor of about 2.5 to 3.0 and that the beneficial effects, if any, of cathodic protection are too small to be recognized in fatigue design guidelines or codes.

5. CONCLUSIONS

1) In these T-plate tests, usually between 20 and 40% of the fatigue life had gone before small cracks, about 0.5 mm deep, were detected.
2) Using this detection level as the boundary between initiation life (N_i) and propagation life, N_p, it was possible to statistically assess the influence of plate thickness on N_i and N_p. All of the in-air data indicates that increasing plate thickness reduces N_p. Except for a difference between Waterloo and CANMET data for 103 mm specimens, the in-air data indicates that increasing plate thickness also decreases initiation life, N_i.
3) A comparison of data obtained in air with that obtained in artificial seawater, with or without cathodic protection, indicates that fatigue life is reduced by a factor of about 2.5 to 3.0 and the beneficial effects, if any, of cathodic protection are too small to be recognized in fatigue design guidelines or codes.

6. ACKNOWLEDGEMENTS

This research was funded by the Physical Metallurgy Research Laboratories of the Canada Centre for Minerals and Energy Technology. The authors wish to particularly thank M.J. Pates, formerly of AMCA International presently of ARCTEC Canada Ltd. for his contribution. Also, earlier or ancillary studies at Waterloo by M. Rayman, R. Yee and S. Lambert highlighted or solved the problems of using D.C.P.D. crack monitoring systems. Grants or Scholarships from the Natural Sciences and Engineering Research Council of Canada have supported these students.

7. REFERENCES

1) Vosikovsky, O., Bell, R., Burns, D.J. and Mohaupt, U.H. "Fracture Mechanics Assessment of Fatigue Life of Welded Plate T-Joints including thickness effect". Proc. of 4th Intnl. Conference on Behaviour of Offshore Structures, J.A. Battjes (editor) Elsevier Science Publishers B.V. Amsterdam 1985, 453-464.

2) Bell,R., Vosikovsky, O. Burns, D.J. and Mohaupt, U.H., "A Fracture Mechanics Model for life prediction of welded plate joints". Proc. of this Intnl Offshore Conf. "Steel in Marine Structures, Delft, 1987.

3) Vosikovsky, O., Bell, R., Burns, D.J. and Mohaupt, U.H., "Effects of Cathodic Protection and Thickness on Corrosion Fatigue Life of Welded Plate T Joints 1987 Ibid (2).

4) Clayton, A.M., "Stress in Tubular Joints" Interim Technical Report UKOSRP2/04, May 1978.

5) de Back, J. and Vaessen, G.H.G. "Fatigue and Corrosion Fatigue Behaviour of Offshore Steel Structures". Final Report ECSC Convention 7210-KB/6/602 (J.7.1 f/76). Delft, April 1981, p. 3-39.

6) Rayman, M.I., "Detection and Prediction of Fatigue Crack Growth in Plate to Plate Welds", University of Waterloo, MASc. Thesis, 1985.

7) Yee, R., Lambert, S., Mohaupt, U.H. and Burns, D.J. "Detection and Sizing of Fatigue Cracks at Weld Toes using a DCPD technique", to be published 1987/88.

8) Gangloff, R.P. "Electral Potential Monitoring of Crack Formation and Sub-critical Growth from small defects", Jnl. of Fatigue of Engineering Materials and Structures, Vol. 4, No. 1 (1981), 15-33.

9) Van Stone, R.H., Krueger, D.D. and Duvelius, L.T. "Use of a d.c. Potential drop crack monitoring technique in the development of defect tolerant disk alloys". Fracture Mechanics 14th Symposium, Vol. II, Testing and Applications, ASTM, STP 791, 1983, II,553 - II 567.

10) Tyson, W.R., Vosikovsky, O., Faucher, B. and Burns, D.J., "Brittle Fracture in Heavy Section Welded T Joints: Correlation Between Stress Intensity at Fracture and Small Specimens Toughness Tests. CANMET, PMRL 86/75 (OP/J).

11) Berge, S. "Effect of Plate Thickness in Fatigue of Cruciform Welded Joints". The Norwegian Institute of Technology. Department of Marine Technology, Report MK/R/67, March 1983.

12) Booth, G.S. Testing in Air of Welded Specimens for UKOSRP (Phase II) - The Influence of Thickness on the fatigue strength of welded plate specimens. Report of the Welding Institute. 3733/10/84 September 1984.

13) de Back, J. and Vaessen, G.H.G. Effects of plate thickness, temperature and weld toe profile on the fatigue and corrosion fatigue behaviour of welded offshore structure, Part 1. Report ECSC Convention 7210-KG601 (F7.4/81) Delft , May 1984.

14) Burns, D.J. and Mohaupt, U.H. Crack Growth Behaviour and fracture mechanics approach. Plenary Session 6, Ibid (2), 1987.

JOINT	T (mm)	ℓ (mm)	L (mm)	A (mm)
A	16	8-12	300	406
B	26	14-18	442	406
C	52	26-30	442	406
D	78	38-42	584	457
E	103	52-56	726	457

Table 1 : Specimen Dimensions

T mm	S MPa	a_E or a_E^1 mm	N_E or N_E^1 k cycles	N_E/N_T or N_E^1/N_T^1 %
16	200	10(s)	475	103
16	150	10(a.s)	1320	104
26	200	12(a.s)	330	98
26	150	15(a.s)	1140	101
26	100	15(s)	4140	106
52	200	5(a.s)	96	70
52	150	12(a.s)	300	81
52	100	14(s)	1120	93
78	200	6(a.s)	56	58
78	150	12(a.s)	224	79
78	100	11(a.s)	1080	86
78	80	17(s)	1510	89
103	100	16(a.s)	590	89
103	70	20(a.s)	1860	78

(s) both edges i.e. symetric

(a.s) one edge i.e. asymetric

Table 2 : Incidence of Edge Cracking

THICKNESS (mm)	POTENTIAL (volts)	STRESS RANGE (MPa)	N_T (kilocycles)	N_i (kilocycles)
26	f.c.	100	1660	760
		110	932	325
		150	318	130
		150	312	146
		200	106	39
26	-0.85	100	2950	750
		110	1006	370
		150	355	255
		200	404	175
		200	131	26
26	-1.05	110	837	220
		150	910	630
		150	420	232
		200	90	27
78	f.c.	80	1033	150
		100	490	150
		110	398	97
		150	167	44
		200	66	17
78	-0.85	80	962	200
		100	924	385
		110	340	67
		150	165	30
		200	81	18
78	-1.05	80	1975	800
		100	692	220
		110	420	151
		150	123	33
		200	54	8

fc free corrosion

Table 3 : Corrosion Fatigue Data

Specimen		Air Life+ Predicted	Actual Life+	Actual Life/ Predicted Air Life
16mm - (in air)-	#2****	25	80	3.19
	#4	243	860	3.54
26mm - seawater-	#6*	820	325	0.396
	#7**	820	370	0.451
	#8***	820	220	0.269
78mm - seawater-	#4*	373	97	0.260
	#5**	372	67	0.179
	#6***	372	151	0.404

Table 4 : Predicted initiation life based on model, equation (4).

Specimen		Air Life+ Predicted	Actual Life+	Actual Life/ Predicted Air Life
16mm -	#2****	135	89	0.659
26mm - seawater-	#6*	2,267	607	0.268
	#7**	2,267	636	0.280
	#8***	2,267	617	0.272
78mm - seawater-	#4*	977	300	0.308
	#5**	977	273	0.280
	#6***	977	269	0.276

Table 5 : Predicted propagation times based on model, equation (5).

Specimen		Predicted	Actual	Actual/ Predicted
26mm - seawater-	#6*	3,183	932	0.293
	#7**		1,006	0.316
	#8***		837	0.263
78mm - seawater-	#4*	1,353	397	0.294
	#5**		340	0.251
	#6***		420	0.310

Table 6 : Predicted total lifetimes based on model, equation (6).

* - Free Corrosion
** - Optimum Cathodic Protection
*** - Cathodic Oveprotection
**** - Experimental Problems
\+ - all lives in kilocycles

		Specimen size (mm) 16	26	52	78	103
Initiation - Life	W*	607	254	107	87	103
	0*	364	298	94	66	35
	W & 0*	515	283	97	72	68
Propagation- Life	W*	1732	715	393	408	248
	0*	894	588	249	257	130
	W & 0*	1388	676	326	318	195
Total - Life	W	2330	997	505	510	355
	0	1265	905	344	311	164
	W & 0	1905	992	427	386	266

* - Initiation & Propagation - omit 16 mm #2
W - Waterloo
0 - CANMET

Table 7 : Predicted lifetime (kilo cycles) for tests in air at stress level 150 MPa

Life	Slope	Correction Factors			Error Variance
	β	γ_1	γ_2	γ_3	Δ^2 (df)
Initiation					
- W	-4.124	.333	.295	.342	0.2132(19)
- 0	-3.598	.481	.608	.685	0.2704(28)
- W & 0	-3.652	.456	.537	.598	0.2900(56)
Propagation					
- W	-3.595	.259	.253	.248	0.0895(19)
- 0	-3.436	.368	.561	.405	0.0766(28)
- W & 0	-3.395	.312	.434	.331	0.1145(56)
Total					
- W	-3.705	.270	.260	.263	0.0877(20)
- 0	-3.501	.407	.586	.511	0.1006(28)
- W & 0	-3.445	.348	.462	.409	0.1332(57)

γ_1 - free corrosion W - Waterloo
γ_2 - optimum protection 0 - CANMET
γ_3 - cathodic overprotection

Table 8 : Estimates of correction factors for seawater tests.

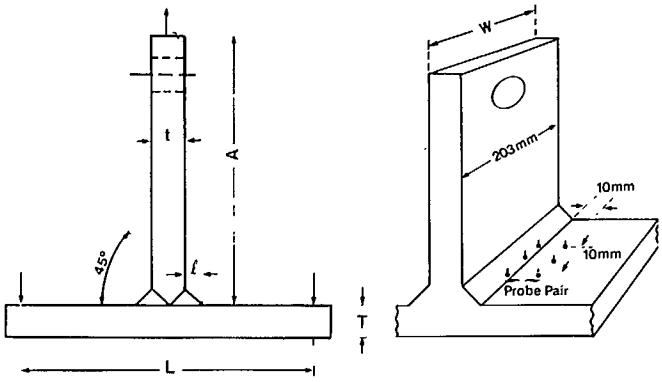

Figure 1 : T plate geometry

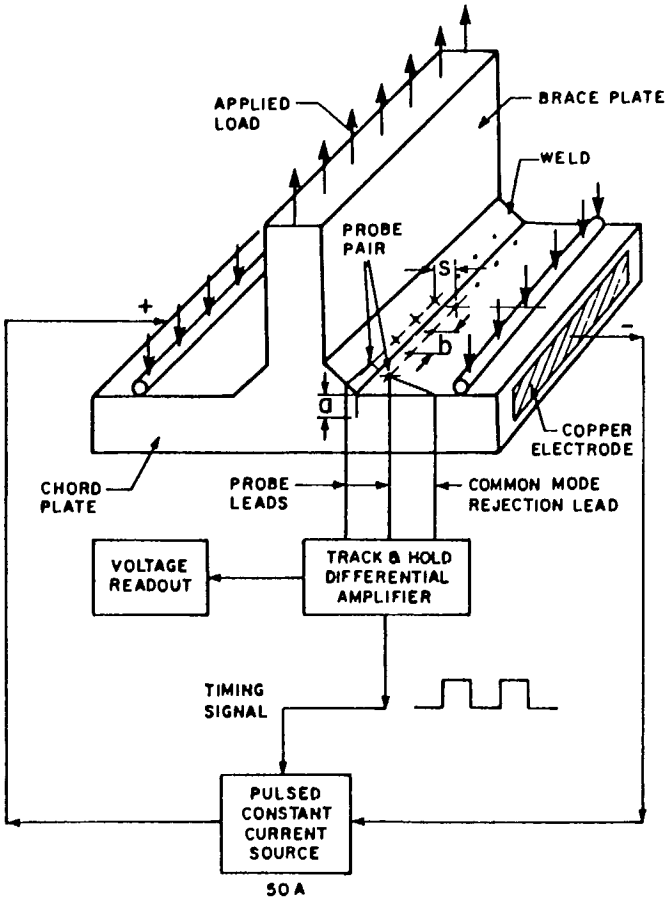

Figure 2 : Pulsed D.C. Potential Drop System

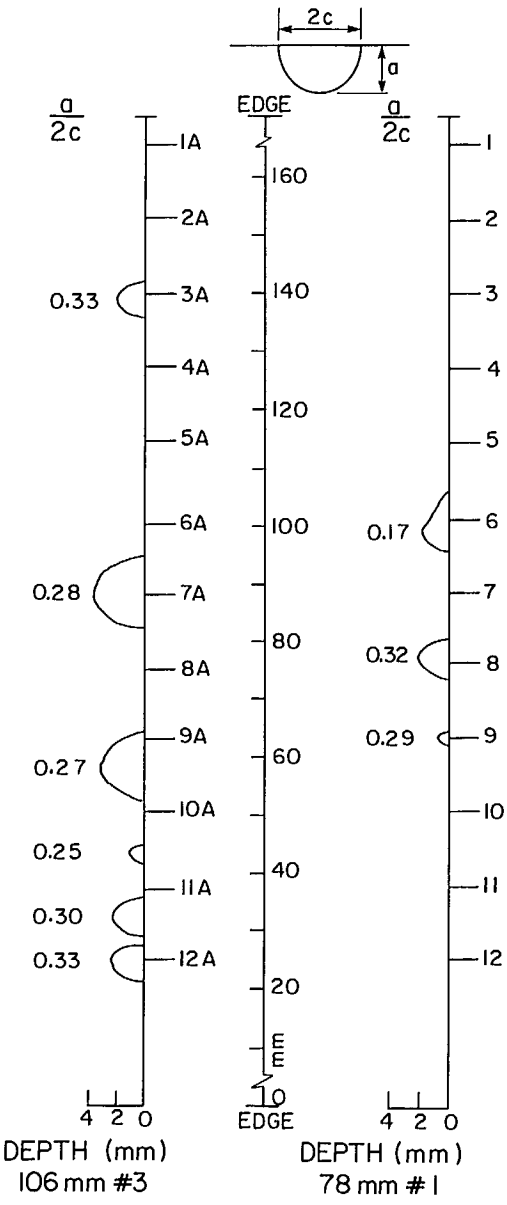

Figure 3 : Cracks detected by ink staining two specimens

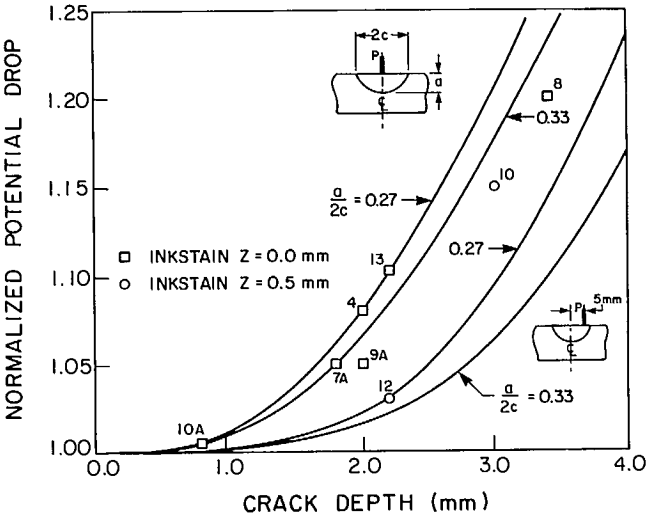

Figure 4: Experimental and theoretical relationship between normalized voltage and maximum crack depth.

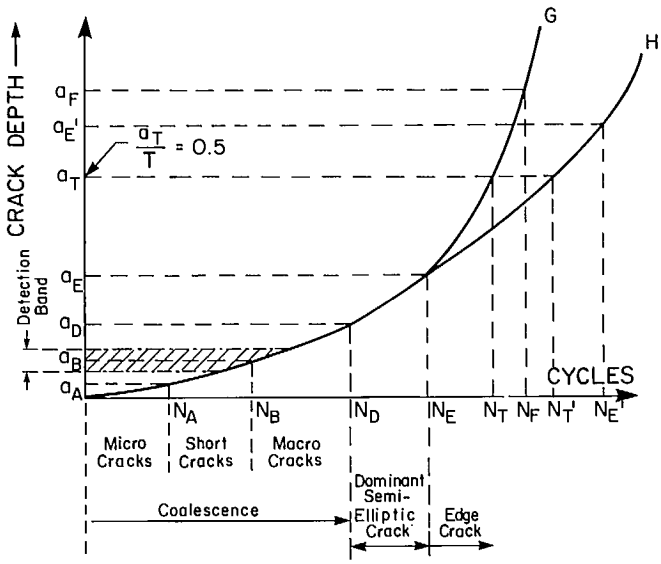

Figure 5 : Crack development in T plate joints

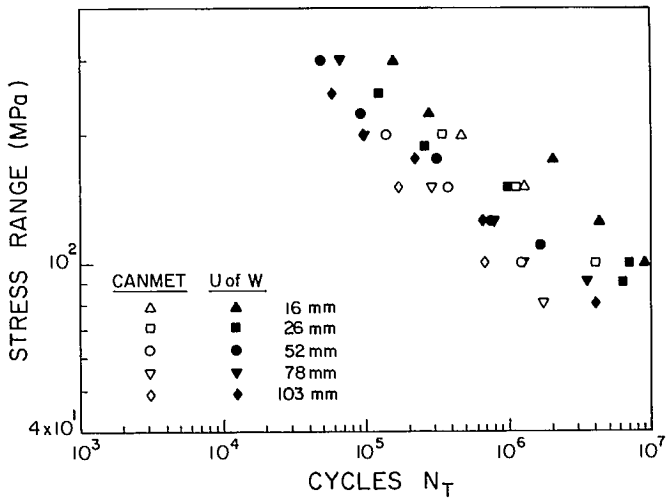

Figure 6 : Hot spot stress range (S) vs Total Life N_T

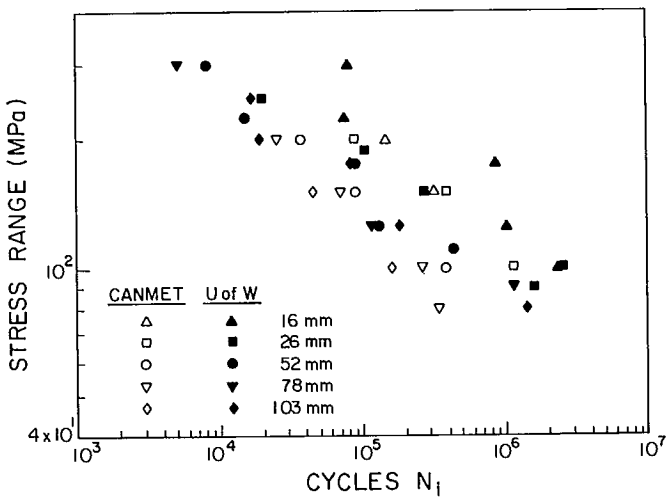

Figure 7 : Hot spot stress range (S) vs. Initiation Life (N_i)

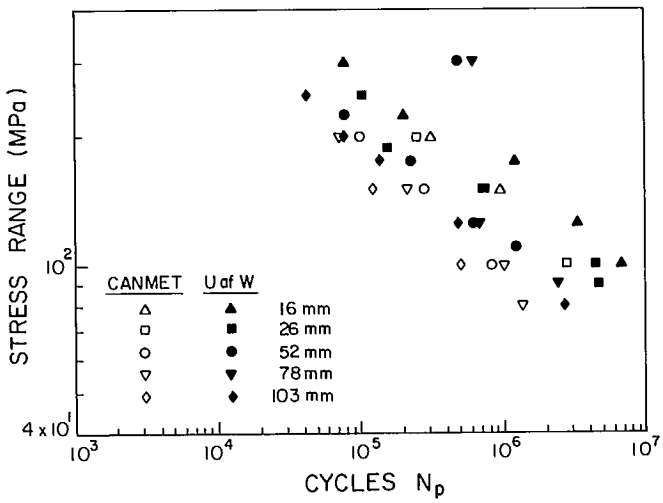

Figure 8 : Hot spot stress range (S) vs. Propagation Life (N_p)

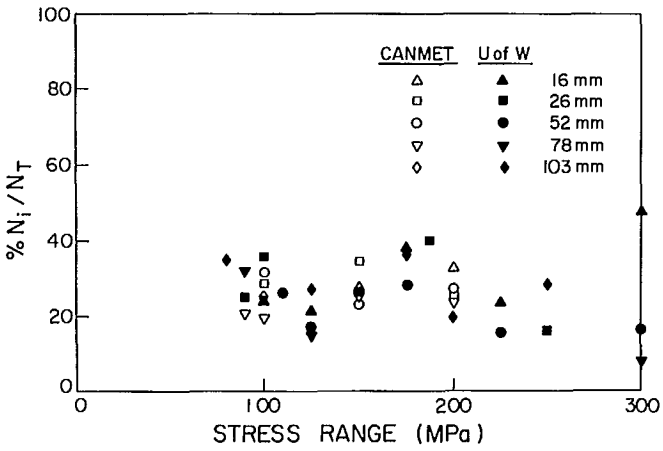

Figure 9 : Effect of Hot Spot Stress Range on ratio of N_i/N_T

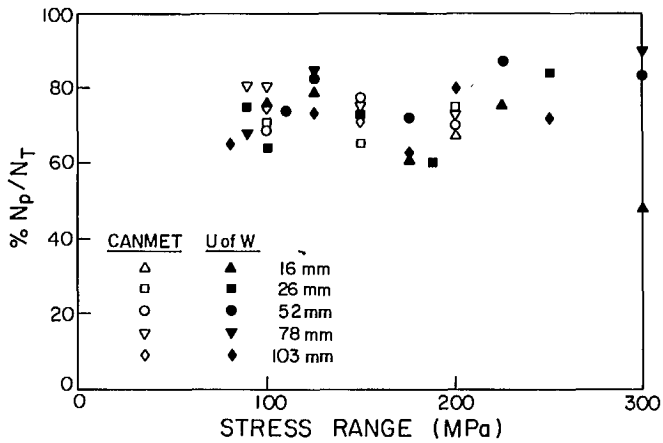

Figure 10 : Effect of Hot Spot Stress Range on ratio of N_p/N_T

SIMULATION OF FATIGUE BEHAVIOUR OF TUBULAR JOINTS USING A PIPE-TO-PLATE SPECIMEN

SIMULATION DE LA RÉSISTANCE EN FATIGUE DE JOINTS TUBULAIRES EN UTILISANT COMME ÉCHANTILLON UN TUYAU SOUDÉ À UNE PLAQUE

SIMULATION DE LA RÉSISTANCE EN FATIGUE DE JOINTS TUBULAIRES EN UTILISANT COMME ÉCHANTILLON UN TUYAU SOUDÉ À UNE PLAQUE

S.B. Lambert[1], U.H. Mohaupt[1], D.J. Burns[1], et O. Vosikovsky[2]

[1]Génie mécanique, Université de Waterloo,
Waterloo (Ontario) Canada

[2]CANMET/LRMP, Ottawa (Ontario) Canada

RÉSUMÉ

Un tuyau soudé à une plaque a servi d'échantillon pour modéliser le comportement en fatigue de joints tubulaires soudés en T. La technique de mesure de différence de potentiel en courant continu a été utilisée pour évaluer le développement de la fissure dans deux échantillons d'un tuyau soudé à une plaque. Ces données sont comparées à d'autres semblables obtenues à partir d'essais menés sur des joints tubulaires et de plaques soudées en T. Le taux de croissance de fissure a été utilisé pour dériver un facteur d'intensité de contraintes empirique qui a été comparé à d'autres valeurs publiées provenant de diverses configurations de joints tubulaires. Ces comparaisons démontrent que les spécimens employés modélisent bien les joints tubulaires et conviennent d'avantage que les plaques soudées en T pour l'étude de la propagation de fissure en fatigue dans l'eau de mer.

SIMULATION OF FATIGUE BEHAVIOR OF TUBULAR JOINTS USING A PIPE-TO-PLATE SPECIMEN

S.B. LAMBERT[1] , U.H. MOHAUPT[1] , D.J. BURNS[1] , and O. VOSIKOVSKY[2]

[1]Mechanical Engineering, University of Waterloo, Waterloo, Ontario, Canada
[2]CANMET/PMRL, Ottawa, Ontario, Canada

ABSTRACT

A pipe-to-plate specimen has been developed to model the fatigue behavior of welded T-tubular joints. DC potential drop techniques have been used to monitor crack development in two pipe/plate specimens in air. This data is compared with similar data for a T-tubular and T-plate joints. Crack growth rates were used to derive empirical stress intensity factors for comparison with like data published for various tubular configurations. These comparisons indicate that the pipe/plate specimen is a reasonable model of a tubular joint. It is much more suitable than the usual T-plate specimens for studies of the influence of seawater on fatigue crack propagation.

1. INTRODUCTION

Fatigue tests on welded tubular joints for offshore structures [1,2] have shown that multiple cracks initiate at the weld toe early in the fatigue life. These grow and coalesce until ultimately, a single large semi-elliptic crack forms. This then grows through the chord wall. Failure of the joint is usually defined as crack breakthrough.

Of the tubular joints tested in Europe, a very small percentage have been tested in a seawater environment at realistic cycling frequencies. Instead, simpler plate-to-plate welded specimens have been used extensively to study the influence of a corrosive environment on fatigue life. These plate specimens do not have the same crack shape development as tubular joints. As cracks coalesce, they may reach the edges of the specimen at which time crack growth rate increases markedly. Thus, although plate joints may provide a useful model of initiation and early crack growth, they do not model the entire life of a tubular joint. It therefore may be inappropriate to use welded plate fatigue life results to make recommendations on the effects of corrosion on the life of tubular welded joints [3].

As part of an overall Canadian program to investigate the fatigue behavior of welded joints for offshore structures, a pipe-to-plate specimen has been developed. This specimen offers advantages of cost and ease of analysis compared with tube-to-tube joints. At the same time, it more accurately models crack shape development and large crack growth behavior than plate-to-plate joints. Initial testing of two joints in air has been performed to demonstrate the feasibility of this specimen, to verify the accuracy of our crack monitoring technique, and to develop stress intensity factor calibrations. Tests are now being performed in a synthetic seawater environment at a temperature of 5 °C under constant amplitude loading at 0.2 Hz. The test matrix for the seawater tests consists of six specimens; two each with free corrosion, optimum cathodic protection (-0.85 volts with respect to Ag/AgCl electrode), and over-protection (-1.05 volts). For each environment, tests will be conducted at 240 and 160 MPa hot-spot stress levels at an R-ratio of 0.05.

In this paper, the pipe/plate specimen will be described. The results in air will be presented and compared with T-plates and a T-tubular joint tested in the Canadian program. The seawater results will be reported when all tests have been completed.

In the T-plate program, load carrying fillet welds with plate thicknesses from 16 to 103 mm were tested in air and seawater environments. These joints were tested in three-point bending with the constant amplitude load applied through the attachment

plate. Tests were performed at CANMET in Ottawa, and at the University of Waterloo. During this testing, careful monitoring of crack initiation and subsequent growth was performed. Thus it was possible to distinguish the effects of environment on initiation and early crack shape development. Preliminary results from the T-plate program were presented earlier [4]. The remaining results are discussed in papers presented at this conference [5,6,7]. Herein, only the results for two 26 mm T-plate joints tested in air will be discussed.

The T-tubular joint results are part of a program to investigate the effect of chord ring-stiffening on fatigue behavior. Twelve specimens will be tested with constant amplitude loading; six at the University of Waterloo and six at Memorial University in Newfoundland. The specimens consist of a 457 mm diameter brace welded at right angles to a 914 mm chord. Both brace and chord use 19 mm wall thickness. The first specimen in each test series is unstiffened. The testing fixture at the University of Waterloo has been designed to allow In-Plane Bending (IPB), axial, and Out-of-Plane Bending (OPB) loading modes. As a result, uncracked stress distributions are available for the unstiffened specimen for each of these loading modes. The fatigue test discussed herein was conducted using in-plane bending at a hot-spot stress range of 260 MPa. The static and fatigue testing of this unstiffened tubular joint had three purposes; to provide stress distributions for comparison with those in the pipe/plate, to confirm the accuracy of the DC potential drop system for tubular joints, and to provide a benchmark for comparison with the subsequent tests by J. Forbes [8] on stiffened joints. The results from the stiffened tubular program will be discussed in forthcoming papers.

1.1 Pipe/Plate Description

The pipe/plate specimen is shown in place on the test fixture in Figure 1. The specimen itself consists of a 26 mm thick flat plate, approximately 1020 mm wide by 1520 mm long. The plate is hot-rolled from structural steel conforming to Lloyds LT60. The chemical composition and mechanical properties are given in [4]. A 457 mm diameter, 30 mm wall thickness pipe is welded to the centre of this plate. The pipe material is structural steel with a minimum 350 MPa yield strength. A typical cross-section, illustrating the weld geometry, is included in Figure 2.

Under test, the plate is bolted along its longitudinal edges to the base of the loading fixture as shown in Figure 1. The load is applied horizontally through a pin and yoke arrangement, approximately 1220 mm above the plate surface. This produces a general cantilevered bending in the pipe or brace, and a local bending through the thickness of the plate at the weld toe. A girder is positioned over one side of the plate as shown, but contacts the plate surface only at two bearing points as illustrated in Figure 2. These bearing points were selected by experiment to achieve the desired stress distribution (see next section).

Instrumentation for each specimen consisted of strain gauges to monitor initial stress distribution and stress redistribution after cracking. In addition, a Direct Current Potential Drop (DCPD) system was used to detect initiation and to monitor subsequent fatigue crack shape development.

2. STRESS ANALYSIS

Strain gauges were mounted on the tension side of the first pipe/plate specimen as shown in Figure 2. A similar pattern was used on the bottom of the plate to permit identification of membrane/bending components of stress. Gauges were positioned to monitor the stress field approaching the weld toe at the hot-spot location. In addition, gauges were used at stations 10, 20, 30 and 45 degrees from the hot-spot to define the stress distribution along the weld. At least two gauges were used at each station to allow an extrapolation to the weld toe.

The initial stress distribution along the zero degree line (i.e. at the hot-spot) is shown in Figure 3 for the pipe/plate along with the in-plane bending results for the unstiffened T-tubular joint. These results have been normalized with respect to the hot-spot stress. This is a ficticious weld toe stress obtained by linearly extrapolating the top surface stresses from the two gauges mounted closest to the weld toe. For the tubular joint, the gauges have been positioned following UKOSRP recommendations [9]. For the pipe/plate, these same recommendations have been applied in conjunction with a ficticious chord (or plate) diameter of 914 mm. It can be seen from Figure 3 that the radial stress in the pipe/plate is essentially linear within three plate thicknesses from the weld toe. Therefore, the calculated hot-spot stress is relatively insensitive to the chosen gauge positions.

The stress distribution along the weld toe, obtained by extrapolation, is shown in Figure 4 for the pipe/plate and for three types of loading for the T-tubular joint. Note that the zero degree line for the tubu-

lar joint may refer to the crown or saddle position, depending on the mode of loading. For the pipe/plate joint, the stress is maximum at the hot-spot (zero degree) position and has decreased by 25 per cent when 45 degrees from the hot-spot. Thereafter, the stress decays rapidly to zero at 90 degrees from the hot-spot. This corresponds to the neutral axis for brace bending. The maximum stress at the weld toe can be increased by moving the bearing points for the girder (Figure 2) inward, toward the weld toe. Conversly, a more even stress profile may be obtained by moving these points away. A compromise was selected which lies between the tubular results for various loading modes. A very flat profile was avoided to encourage crack initiation near the centre of the specimen. Due to the nature of the specimen, and its constraint, results may be suspect if the crack growth is very asymmetric.

An important characteristic of the stress field is the ratio of membrane to bending stress in the chord. In the pipe/plate specimen, the stresses are predominantly bending with no membrane component. This is consistent with results reported by Clayton [10] for tubular joints. His finite element results indicated that, for the in-plane bending case, as the brace/chord diameter ratio (β) is reduced, the membrane component became less significant, tending toward 10% at a β-ratio of 0.25. Thus the pipe/plate can be considered a simulation of very low β-ratio tubular joints. In comparison, for in-plane bending of our unstiffened tubular joint, which has a β-ratio of 0.5, the membrane component is 27% of the total.

3. CRACK SHAPE MONITORING

The initiation, and subsequent growth of fatigue cracks from the toe of the weld through the plate has been carefully monitored using a Direct Current Potential Drop (DCPD) technique. The complete DCPD system, designed in-house by M. Van Reenen, is shown schematically in Figure 5. An axi-symmetric initial current field is set up in the specimen between two large copper bars bolted to the top and bottom of the specimen, concentric with the plate centre. This current is supplied by a DC power supply (50 amp capacity) and the polarity is switched, approximately twice every second, under the control of a timing circuit housed in the amplifier box. This reversing is performed to counteract thermocouple effects and to eliminate the effect of amplifier zero offset errors.

An active probe pair consists of two 0.9 mm wire leads spot-welded to the surface along a radial line, straddling the weld toe. These probes have a span of 6.35 mm centred at the weld toe. Such probe pairs are distributed along the weld at 6.35 mm increments within 120 mm of the hot-spot location. Beyond this, 12.7 and 25.4 mm pitch is used to obtain coverage to +/- 200 mm from the hot-spot. This corresponds to an angle of 45 degrees from the hot-spot. In addition, reference probes are mounted near to the weld toe with a span of 25.4 mm; these probes share a common probe with an active probe pair. Reference probes are distributed at 25.4 mm increments around the weld toe. They are used to compensate for global changes in input current level that may occur during a test. For example, toward the latter stages of life the input current must be decreased, as the voltages across the active probes increase, to avoid saturation of the amplifier.

In total, 50 active probes and 14 reference probes are monitored for each test. These are input into a series of four sixteen-channel multiplexers. These pass the signal from a particular probe to the amplifier depending on the channel selected. The selected signal is amplified and directed to track-and-hold circuitry which operates on the same timing as the power supply. The result is a DC level voltage which is passed on to the computer interface.

One of the most difficult problems associated with the DCPD technique is calibrating the measured voltage changes to the actual crack depth. The philosophy is to apply a two-dimensional aluminum foil calibration [11] at each station cross-section. It is accepted that very small cracks cannot be sized, only detected, with this method. It is conservatively estimated [5] that 0.5 mm deep semi-circular surface cracks will not escape detection within the zone of intense coverage (+/- 120 mm from hot-spot). Initiation is said to have occured when a crack is first detected. As these cracks grow and coalesce, the system can be used to determine the maximum depth and shape of the crack. Obviously, the accuracy of the two-dimensional, i.e. flat-fronted, calibration technique will improve as the aspect ratio decreases. A more detailed discussion of this DCPD system and the calibration procedures used will be discussed in a forthcoming paper by Yee et al [12].

During the fatigue testing of the two pipe/plate specimens in air, the weld toe was wet with ink to mark the crack surface after the DCPD system had indicated one or more distinct cracks. Subsequently, at several stages in the specimen life, beachmarks were left on the fracture surface.

These inkstains and beachmarks were measured after fracture with a travelling microscope and are shown in Figure 6 for both specimens along with the corresponding DCPD predictions. These DCPD predictions are based strictly on two-dimensional foil calibrations. Note that the depth direction has been expanded for clarity. As a result, the cracks appear to have a high aspect ratio (a/2c).

An examination of these figures shows that the DCPD predictions are very good in general, and particularly good for deeper, more flat-fronted cracks. For small irregular cracks some averaging of the crack depth occurs due to three-dimensional current flow. This is particularly evident in the results for the second specimen, tested at 160 MPa. Here, multi-initiation along the weld toe led to irregular crack shape development for a/T less then 0.4. For the specimen tested at 240 MPa, crack growth was dominated by a single crack which initiated near to the hot-spot location. The resulting crack grew more regularly, and hence the accuracy of the DCPD predictions was better throughout the life.

4. RESULTS

The fatigue behavior of the first two pipe/plate specimens, cycled in air, will be discussed in terms of crack shape development, crack growth behavior, and crack growth rate behavior. The crack growth rate behavior is presented as an empirically derived stress intensity correction factor. Throughout this discussion, comparisons will be drawn between the pipe/plate (with a 26 mm plate), the 26 mm thick T-plate and the unstiffened T-tubular joint (19 mm wall thickness).

4.1 Crack Shape Development

Crack shape development during fatigue is governed by the geometry of the specimen, the stress distribution, and the density, distribution and severity of initial defects. The incidence of these defects causes variability in crack shape development; this is particularly evident in initiation and early crack growth behavior.

Figure 6 shows the crack shape development for the two in-air pipe/plate specimens. The first specimen, tested at a hot-spot stress level of 240 MPa, showed only two distinct cracks when inkstained at 126k cycles. Of these cracks, the one closest to the hot-spot dominated subsequent crack growth. In the second test, a large number of initiation sites were indicated at 360k cycles , when the weld toe was stained with ink. These grew and coalesced into a single dominant semi-elliptic crack.

Crack shape development is summarized in Figure 7. Here the aspect ratio (a/2c), as determined from measured inkstains and beachmarks, is plotted versus the normalized crack depth. A solid line has been drawn to indicate the presence of a single dominant semi-elliptic crack at deeper crack depths. Dashed lines serve to present trends during the final stages of coalescence. The results for the unstiffened tubular joint are included for comparison.

For both pipe/plate specimens a single semi-elliptic crack was present beyond 0.4T. Below this, the crack growth was very dissimilar. The resulting semi-elliptic crack, however, followed the same aspect ratio development after coalescence. The coalesced crack grew both in the length and depth directions such that the aspect ratio stayed approximately constant at 0.05.

For the tubular joint, multiple initiation sites were evident when the weld toe was stained with ink. These sites were distributed along the weld toe in the region of essentially constant stress and quickly coalesced into a single semi-elliptic crack. Then the depth of this crack increased with no significant increase in length. As a result, the aspect ratio increased after coalescence to a maximum value approaching 0.05 at through-thickness cracking. This is shown clearly in Figure 7.

In the T-plate specimens the stress distribution is constant across the width of the specimen (200 mm). However, due to the welding operation, there are higher tensile residual stresses in the plate centre than at the edges. There is a tendency, therefore, for the cracks to initiate away from the free edges of the specimen. In addition, as the cracks grow and coalesce, the growth at the edges seems to be slowed, perhaps because of the plane stress conditions. Therefore, the ensuing crack has a relatively high aspect ratio. Results from CANMET [5] for 26 mm T-plates show that the crack may not reach the edges of the specimen, and hence become flat-fronted, before the centreline cracked depth is 50 per cent or more of the thickness. This is evident in the aspect ratio development plot presented in [4] which showed the aspect ratio (a/2c) tending toward 0.1 at 0.5T. As the crack reaches the edges of the specimen the aspect ratio moves quickly toward zero. The life thereafter is very short, due to an increase in the stress intensity factor.

4.2 Crack Growth Behavior

Crack growth information is presented in Figures 8 and 9. Here, the crack depth,

as determined from DCPD measurements, is shown as a function of cycles. In Figure 8, results are presented for the pipe/plate, T-plate and tubular joint, tested at similar stress ranges; 240, 250 and 260 MPa respectively. In each case, results for probes close to the center or hot-spot of the specimen are presented.

Differences in the fatigue behavior of this pipe/plate and this tubular joint, for crack depths to 0.6T, can be attributed to differences in aspect ratio development and the ratio of membrane to bending stress. The aspect ratio for the pipe/plate crack was consistently higher than for the tubular throughout this period. This, in combination with the slightly lower applied stress and the absence of membrane stress, resulted in lower crack growth rates in the pipe/plate.

In the pipe/plate, beyond 0.6 T, the crack begins to slow down and eventually curve toward the plate centre, under the weld toe. This behavior has been observed in fatigue tests of T-tubular joints, tested in axial loading [13]. It is believed that this slowing of the crack growth and subsequent curvature is due to a build-up of compressive stresses in the ligament, due to the cracked geometry. Although this type of curvature has been observed in fatigued tubular joints, it is quite severe in the pipe/plate. This may be due to the absence of any significant membrane stress. After about 0.9T, this curvature becomes so severe in the pipe/plate that the crack is eventually propagating parallel to the bottom surface of the plate. Break-through of the wall occurs eventually by shearing of the ligament. Since this crack front curvature unnecessarily complicates a fracture mechanics analysis, the useful life of a pipe/plate specimen is defined as 0.8T, i.e. at the onset of crack plane curvature.

Also shown in Figure 8 is the crack growth behavior for a 26 mm thick T-plate tested at 250 MPa. Crack coalescence in this T-plate was such that an edge crack formed at about 0.2T. By comparison, crack coalescence in the tubular quickly produced a single crack of very low aspect ratio. These quite different mechanisms led to very similar crack growth behavior. The difference in overall life is due to a shorter initiation and small crack growth period in the T-plate.

In Figure 9, crack growth behavior in the pipe/plate, tested at 160 MPa, is compared with a 26 mm thick T-plate, tested at 150 MPa. The difference in total life is actually quite small. However, if the initiation phases are subtracted, it can be seen that the propagation life for the pipe/plate is significantly longer than that for the T-plate. For the T-plate, beyond about 0.2T, there is a rapid acceleration in crack growth rate as the crack reaches the free edges.

4.3 Stress Intensity Factor Calibrations

A useful method for presenting the above results is to look at the crack growth rates as a function of crack depth. These can be used to calculate empirical stress intensity factors which are then presented in normalized form. This eliminates the initiation period and allows direct comparison of tests performed at different stress levels. It must be recognized that stress distribution will still influence the results, in particular the membrane/bending components are not distinguished. Also, due to the uncertainty associated with the measurement of small cracks, say less than 0.2T, the stress intensity correction facors only indicate trends in this region.

The crack depth information, presented in Figures 8 and 9, was differentiated using a sliding 7-point parabolic curve fitting routine as outlined in ASTM E 647-78T to obtain crack growth rate information. Stress intensity factors were then calculated using the Paris relation with exponent, m=3, and a constant, $C=5.36\times10^{-12}$ [14]. Here, crack growth rates are in m/cycle and stress intensity factors in $MPa\sqrt{m}$. These empirical Stress Intensity Factors (SIF's) have been normalized with respect to the SIF in an infinite plate with a through thickness centre crack, length 2a, subjected to a uniform stress field. This uniform stress field corresponds to the hot-spot stress in each case.

The two results for the pipe/plate show a clear difference during coalescence. This can be attributed to differences in aspect ratio development. In the high-stress test, early crack growth was dominated by a single high aspect ratio crack. This resulted in lower SIF's and slower relative crack growth. For deeper cracks, greater than 0.4T, there is a tendency for the two pipe/plate curves to converge as the aspect ratios converge.

Only the 150 MPa data is shown for the T-plates. The increase in SIF beyond 0.2T clearly indicates the effect when the crack reaches the free edge. Results from CANMET, presented in [5], showed that the centreline crack depth was 0.5T or greater before the crack had reached the free edge in some 26 mm thick specimens. This is not always true since the dominant semi-elliptic crack may occur near a free edge. For the two T-plate specimens discussed herein, tested at the University of Waterloo, the PD results indi-

cate that the crack had reached one free edge by about 0.2T.

In the tubular joint, for very small cracks, the stress intensity correction factor appears to increase sharply at about 0.08T. While it must be emphasized that the crack depth information from which this plot has been derived is much less reliable for such small cracks, it is possible that this increase in crack growth rate results from rapid coalescence with a nearby, more dominant crack. Beyond 0.1T, the tubular joint SIF's are consistently higher than those for the pipe/plate. This can be attributed to the earlier coalescence in the tubular which resulted in a very low aspect ratio crack. As this crack grows, the aspect ratio tends toward the same value as the pipe/plate. However, at the same time, the influence of the membrane component of stress increases in the tubular, keeping the crack growth rates higher.

Also shown in figure 10 are bounds for empirically derived stress intensity correction factors due to Dover [15]. These results were obtained for several types of tubular joints tested under variable amplitude loading. The lower bound corresponds to a T-joint tested in out-of-plane bending while the upper bound corresponds to either Y- or K-joints in axial loading. No results for a simple T-joint in in-plane bending were presented in [15]. It is clear that the trends of the pipe/plate results agree very well with tubular results obtained by Dover. However, significant differences exist between Dover's results and those for our unstiffened tubular, which was tested in in-plane bending. This difference may exist because of early coalescence and a higher membrane component in our tubular.

5. DISCUSSION

Results for T-plate specimens have clearly shown a free edge effect. Due to lower residual stresses at the plate edges, there is a tendency for the cracks to initiate and grow away from these edges. This has an influence on the resulting crack shape development. When the crack reaches the edges of the specimen there is a rapid increase in crack growth rate and a rapid end to the specimen life. The crack will contact the free edge sooner if the dominant semi-elliptic crack forms away from the centreline. In a freely corroding seawater environment there are far more initiation sites, crack coalescence occurs faster [5], and therefore the crack reaches the edges sooner. Thus T-plate joints may show an exaggerated influence of seawater on fatigue life. The absence of free edges makes the pipe/plate particularly attractive for studying the influence of seawater on fatigue crack growth behavior.

A comparison of the stress distribution in the pipe/plate, subjected to bending, with stress distributions in an unstiffened tubular joint subjected to in-plane bending, axial, and out-of-plane bending loading, shows that, statically, the pipe/plate is a reasonable representation of a tubular joint. In simple terms, it can be argued that the pipe/plate, as presently configured, simulates low β-ratio tubular joints subjected to a stress distribution between that for in-plane bending, and axial or out-of-plane bending loading.

Fatigue tests on two pipe/plate specimens in air gave crack shape developments similar to those reported by others [1] for tubular joints. Differences in fatigue behavior between the pipe/plate specimens and the unstiffened tubular, discussed herein, are explainable in terms of differences in aspect ratio development and the absence of membrane stress in the pipe/plate.

For the pipe/plate and the unstiffened tubular joint there is a tendency for multiple cracks to coalesce into a single semi-elliptic crack after about 0.2T. In the two pipe/plate specimens, despite very dissimilar early growth behavior, the coalesced cracks followed the same aspect ratio development. This suggests that the specimen geometry and the stress distribution along the weld toe are very significant factors influencing the development of deeper cracks. This hypothesis is supported by the results from the tubular, where the aspect ratio development can be explained in terms of the stress distribution along the weld toe.

The deep crack region, 0.2T to T, although relatively short in terms of overall fatigue life, is particularly relevant for the case of cracks detected in service. It must be emphasized however, that initiation and small crack growth, up to coalescence, represent the majority of the life in the specimens tested. Thus, for the purposes of design or fracture mechanics modelling, the early crack growth and coalescence phase must be carefully studied. This will prove difficult due to its highly variable nature. The results presented herein serve to emphasize that the stress distribution along the weld toe has a significant effect on early crack shape development. This must be considered in any fracture mechanics model which considers coalescence.

6. CONCLUSIONS

Monitoring of crack initiation and propagation in two pipe-to-plate specimens in air indicates that this type of specimen is a reasonable model of a low β-ratio tubular joint. It is much more suitable than the usual T-plate specimens for studies of the influence of seawater on fatigue crack propagation.

7. ACKNOWLEDGEMENTS

This research was funded by the Physical Metallurgy Research Laboratories of the Canada Centre for Minerals and Energy Technology. The authors wish to particularly thank M.J. Pates, formerly of AMCA International presently of ARCTEC Canada Ltd. for his contribution. Our present understanding of the DCPD crack monitoring system, particularly calibration, is largely a result of the efforts of R. Yee. The results for the tubular joint were provided by J. Forbes. A scholarship from the National Sciences and Engineering Research Council supported S. Lambert throughout this work.

8. REFERENCES

[1] Bignonnet, A., Lieurade, H.P., Sixou, Y., and Lebrur, J.L.: "Experimental Study of Fatigue Crack Propagation in Welded Tubular Connections", Second International Conference on Fatigue and Fatigue Thresholds, 3-7 September 1984, Birmingham, U.K. 1505-1513.

[2] Wylde, J.G. and McDonald, A.M.: "Modes of Fatigue Crack Development and Stiffness Measurement in Welded Tubular Joints", Fatigue in Offshore Structural Steels, Proceedings of a conference organized by the Institute of Civil Engineers, London, 24-25 February 1981.

[3] Wilson, T.J. and Dover, W.D.: "Corrosion Fatigue of Tubular Welded Joints", Ibid 1, 1495-1504.

[4] Vosikovsky, O., Bell, R., Burns, D.J. and Mohaupt, U.H.: "Fracture Mechanics Assessment of Fatigue Life of Welded Plate T-Joints Including Thickness Effect", Proc. of 4th international Conference on Behavior of Offshore Structures, J.A. Battjes ed., Elsevier Science Publishers B.V., Amsterdam 1985, 453-464.

[5] Mohaupt, U.H., Burns, D.J., Kalbfleisch, J.G., and Bell, R.: "Fatigue Crack Development and Thickness Effects in Welded Plate to Plate Connections", Paper TS 3, Proc. of this Intnl. Offshore Conf., Steel in Marine Structures, Delft, 1987.

[6] Vosikovsky, O., Bell, R., Burns, D.J. and Mohaupt, U.H.: "Effects of Cathodic Protection and Thickness on Corrosion Fatigue Life of Welded Plate T-Joints", Ibid 5.

[7] Bell, R., Vosikovsky, O., Burns, D.J. and Mohaupt, U.H.: "A Fracture Mechanics Model for Life Prediction of Welded Plate Joints", Ibid 5.

[8] Forbes, J., "Fatigue Tests of Tubular Joint 1", Progress report submitted to CANMET.

[9] "Background to New Fatigue Design Guidance for Steel Welded Joints in Offshore Structures", U.K. Department of Energy, HMSO, 1984.

[10] Clayton, A.M.: "Stresses in Tubular Joints", Interim Technical Report, UKOSRP 1/04, May 1981.

[11] Knott, J.F.: "The Use of Analogue and Mapping Techniques With Particular Reference to Short Cracks", The Measure ment of Crack Length and Shape Duriing Fracture and Fatigue, Ed. C.J. Beevers, EMAS, 1980.

[12] Yee, R.D., Lambert, S.B., Mohaupt, U.H. and Burns, D.J.: "Detection and Sizing of Fatigue Cracks at Weld Toes Using a DCPD technique", to be published 1987/88.

[13] von Delft, D.R.V., Dijkston, O.D. and Snijder, H.H.: "The Calculation of Fatigue Crack Growth in Welded Tubular Joints Using Fracture Mechanics", Offshore Technology Conference, Paper 5352, Houston, May 1986.

[14] Berge, S.: "Effect of Plate Thickness in Fatigue Design of Welded Structures", Offshore Technology Conference, Paper 4829, Houston, May 1984.

[15] Dover, W.D. and Dharmavasan, S.: "Fatigue Fracture Mechanics Analysis of T and Y Joints", Offshore Technology Conference, 3-6 May 1982, OTC 4404.

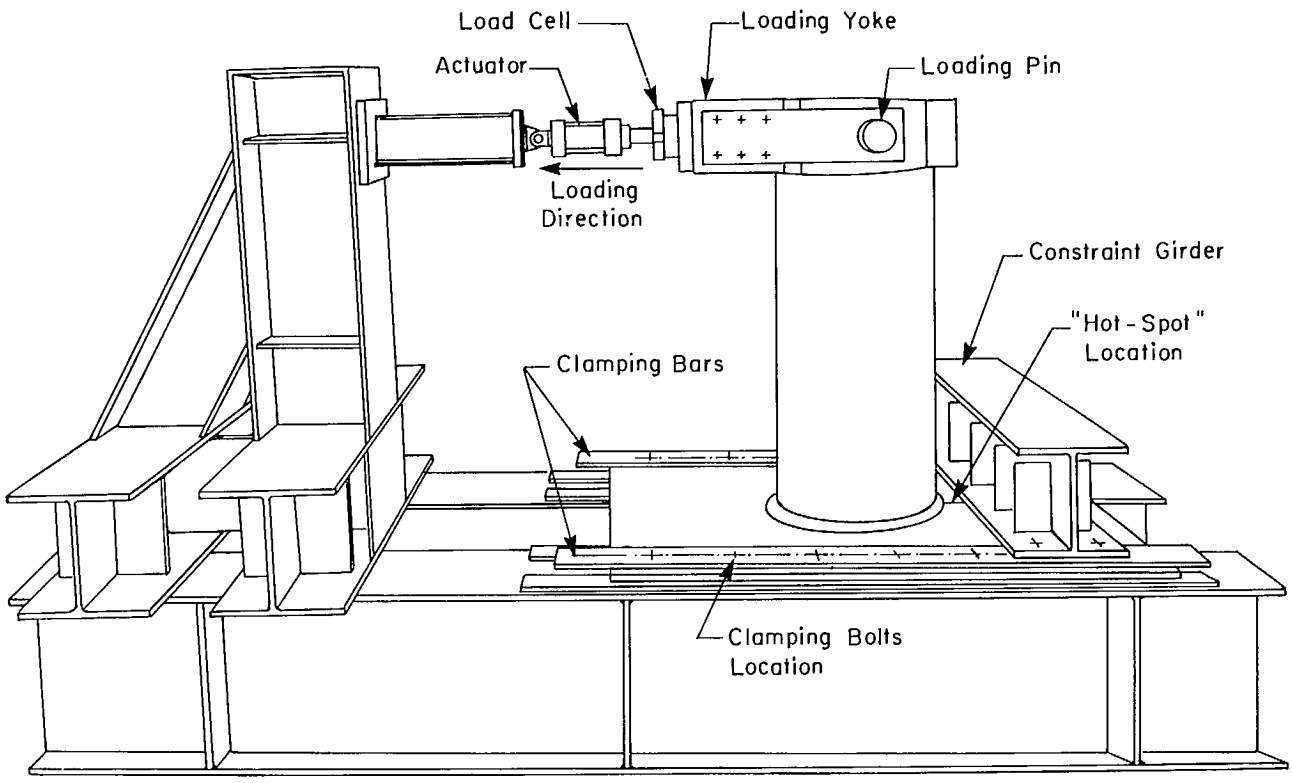

Figure 1 : Test rig for pipe/plate specimens

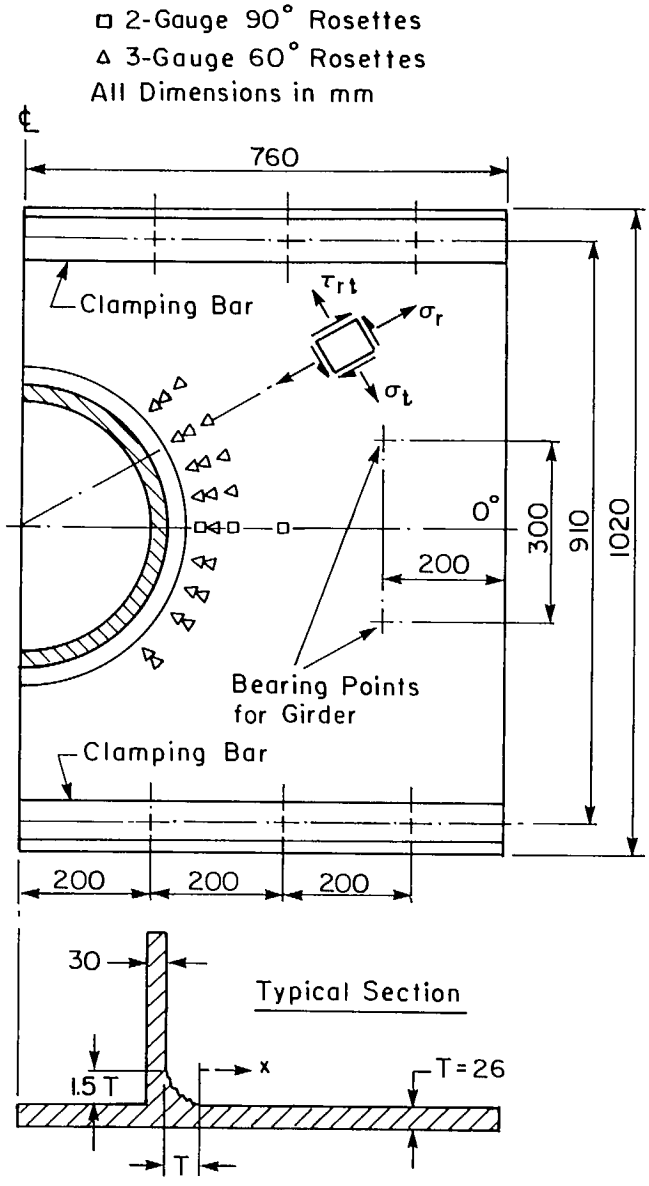

Figure 2 : Restraint and strain gauge positions

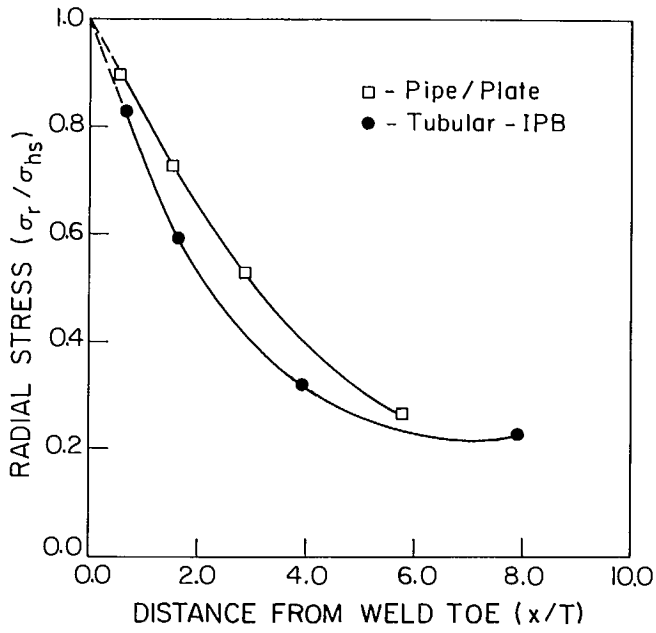

Figure 3 : Comparison of radial stress distributions used to define hot-spot stresses

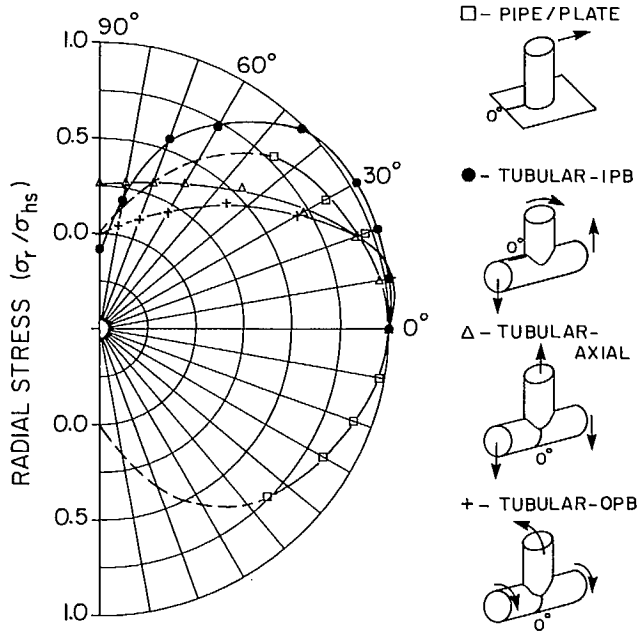

Figure 4 : Normalized radial stress distributions for pipe/plate and three tubular loading modes.

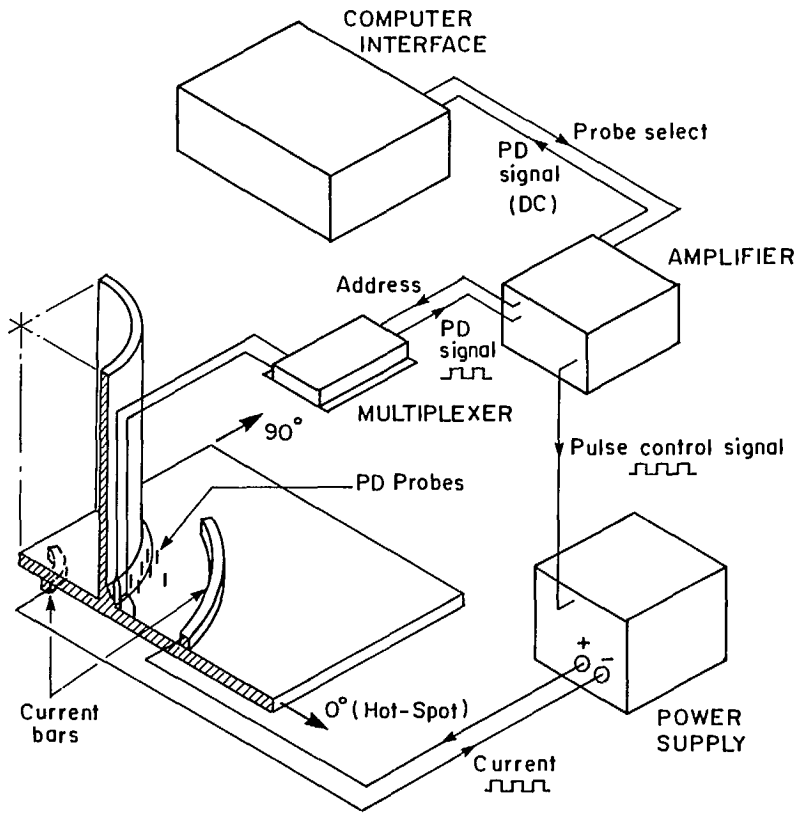

Figure 5 : DCPD system for pipe/plate tests

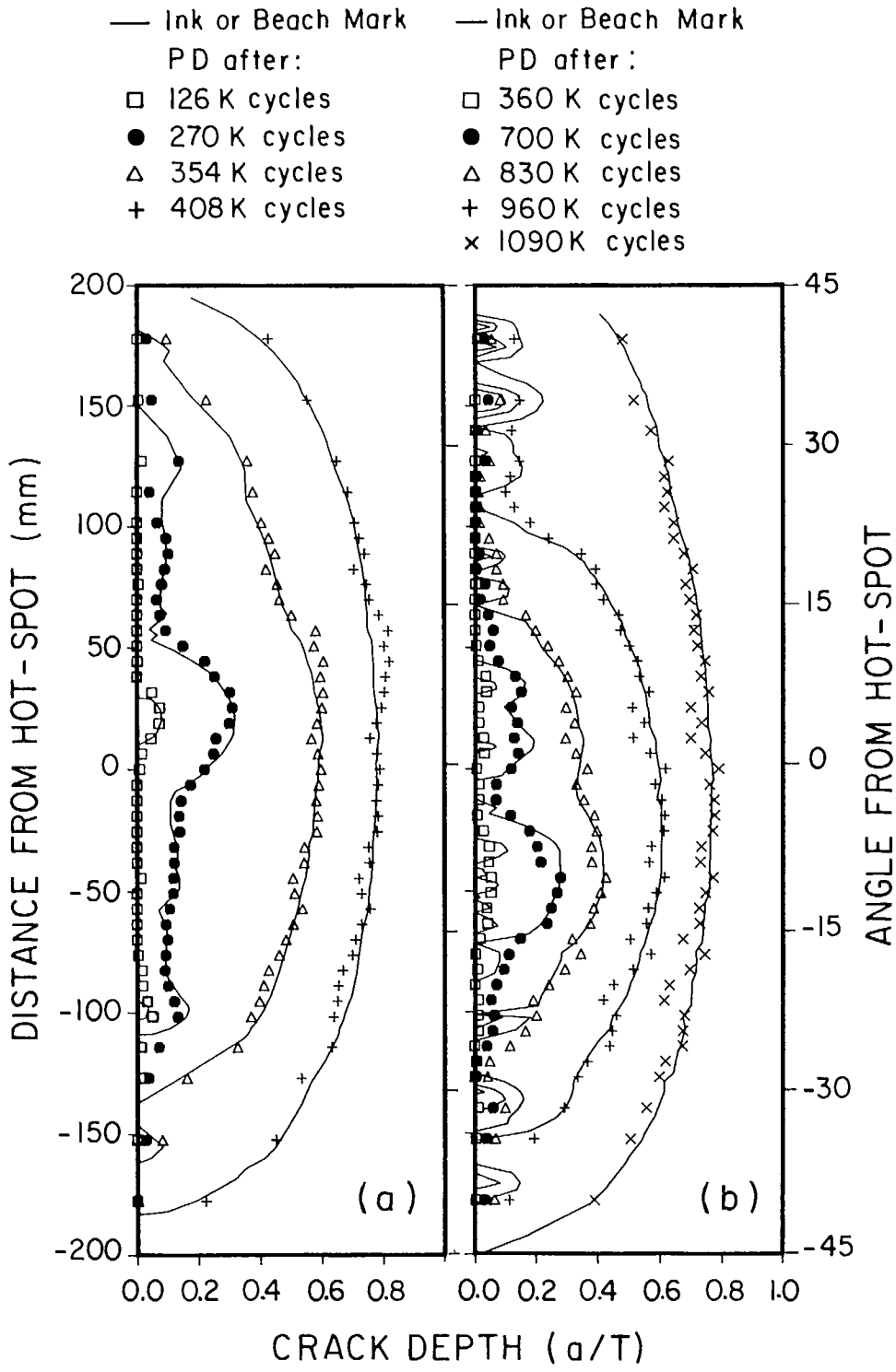

Figure 6 : Comparison of beachmarks and PD predictions for pipe/plates subjected to a) 240 MPa and b) 160 MPa hot-spot stress

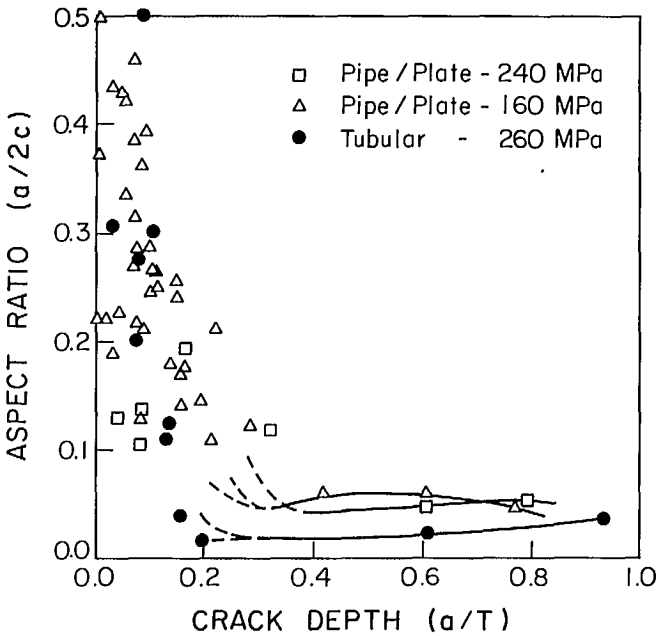

Figure 7 : Variation of aspect ratio with crack depth.

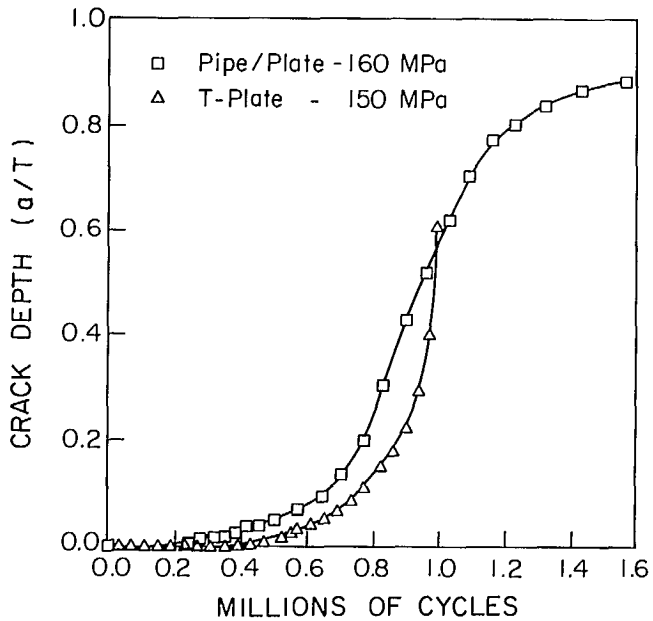

Figure 9 : Increase in crack depth during cycling of pipe/plate and T-plate joints

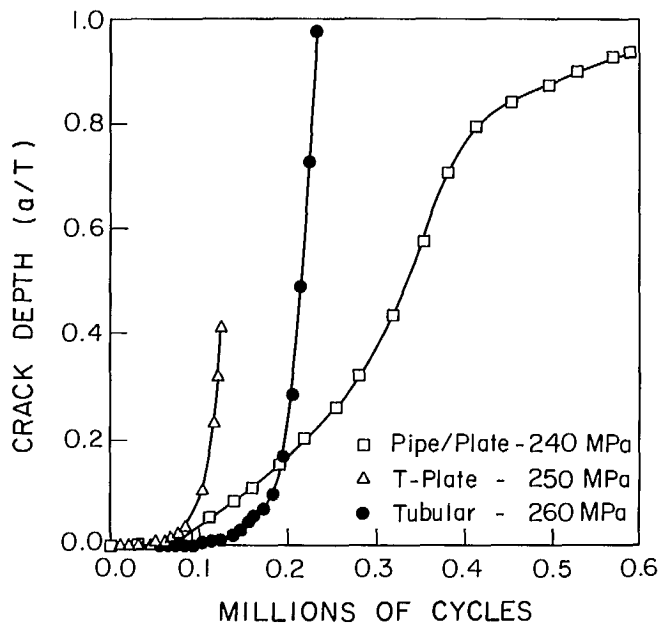

Figure 8 : Increase in crack depth during cycling of pipe/plate, T-plate and T-tubular joints

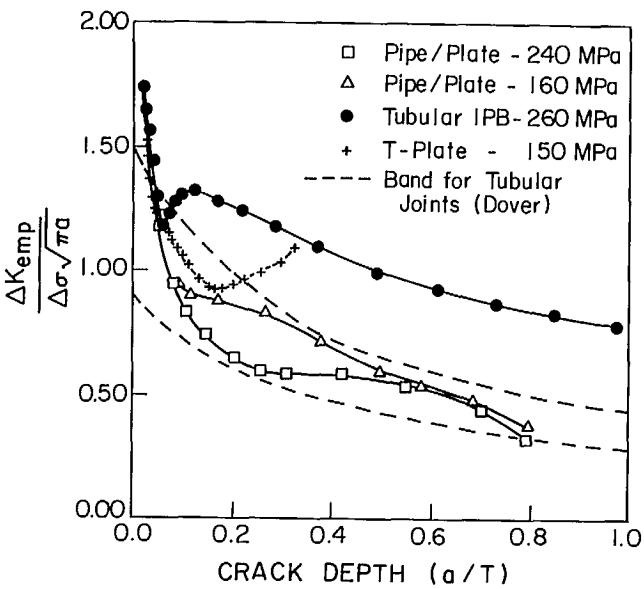

Figure 10 : Comparison of empirical stress intensity correction factors for pipe/plate, T-plate and tubular joints